2014

MULTIDIMENSIONAL OPTIMAL DROOP CONTROL FOR WIND RESOURCES IN DC MICROGRIDS

Kaitlyn J. Bunker
Michigan Technological University

MULTIDIMENSIONAL OPTIMAL DROOP CONTROL FOR WIND RESOURCES IN DC MICROGRIDS

By

Kaitlyn J. Bunker

A DISSERTATION

Submitted in partial fulfillment of the requirements for the degree of

DOCTOR OF PHILOSOPHY

In Electrical Engineering

MICHIGAN TECHNOLOGICAL UNIVERSITY

2014

This dissertation has been approved in partial fulfillment of the requirements for the Degree of DOCTOR OF PHILOSOPHY in Electrical Engineering.

Department of Electrical and Computer Engineering

Dissertation Advisor: *Dr. Wayne W. Weaver*

Committee Member: *Dr. Leonard J. Bohmann*

Committee Member: *Dr. Lucia Gauchia*

Committee Member: *Dr. Gordon G. Parker*

Department Chair: *Dr. Daniel R. Fuhrmann*

To my family

Contents

List of Figures

List of Tables

Acknowledgments

I would like to thank my advisor, Dr. Wayne W. Weaver, for his constant support and guidance. I would also like to thank my committee members, Dr. Leonard J. Bohmann, Dr. Lucia Gauchia, and Dr. Gordon G. Parker for their time and feedback.

Thank you also to my family and friends for their continued encouragement and support, and especially to my husband Kris.

The work in this dissertation was funded by a National Science Foundation Graduate Research Fellowship (DGE-1051031), and by the U.S. Army Research Laboratory (W911NF-13-2-0024).

Abstract

Two important and upcoming technologies, microgrids and electricity generation from wind resources, are increasingly being combined. Various control strategies can be implemented, and droop control provides a simple option without requiring communication between microgrid components. Eliminating the single source of potential failure around the communication system is especially important in remote, islanded microgrids, which are considered in this work. However, traditional droop control does not allow the microgrid to utilize much of the power available from the wind. This dissertation presents a novel droop control strategy, which implements a droop surface in higher dimension than the traditional strategy. The droop control relationship then depends on two variables: the dc microgrid bus voltage, and the wind speed at the current time. An approach for optimizing this droop control surface in order to meet a given objective, for example utilizing all of the power available from a wind resource, is proposed and demonstrated.

Various cases are used to test the proposed optimal high dimension droop control method, and demonstrate its function. First, the use of linear multidimensional droop control without optimization is demonstrated through simulation. Next, an optimal high dimension droop control surface is implemented with a simple dc microgrid containing two sources and one load. Various cases for changing load and wind speed are investigated using simulation and hardware-in-the-loop techniques. Optimal multidimensional droop control

is demonstrated with a wind resource in a full dc microgrid example, containing an energy storage device as well as multiple sources and loads. Finally, the optimal high dimension droop control method is applied with a solar resource, and using a load model developed for a military patrol base application. The operation of the proposed control is again investigated using simulation and hardware-in-the-loop techniques.

Chapter 1

Introduction

1.1 Wind Energy

The use of wind to generate electricity has become more and more common in recent years. As we strive for a sustainable future, using renewable energy sources like the wind is one way to help preserve our planet for future generations. Wind power provides a clean, sustainable energy source for generating electricity. Wind and other sources of renewable energy are often used as distributed resources and are increasingly being applied in connection with microgrids [1]. Advantages of using distributed generation sources like wind include cost and energy savings, since distributed sources in microgrids are located physically closer to load centers than traditional power plants tend to be. Distributed

sources like the wind can also provide power more easily to rural or remote locations [2]. Distributed sources are a good fit with the relatively new power system topology of microgrids.

1.2 Microgrids

Microgrids are small-scale power systems that are able to operate with a connection to the main power grid, but can also operate in islanded mode [3]. This capability to run separately can be especially beneficial during a blackout on the main grid, since the microgrid is able to continue operation. Microgrids can also enable a more efficient and reliable power system, since generated electricity does not have to travel long distances through transmission lines to reach consumers [4].

The size of microgrids can vary greatly, from single homes or buildings to corporate campuses or whole towns. Microgrids can be used in military applications on forward operating bases, and could also be mobile, such as an electric naval ship. Power electronics are an important part of connecting distributed generation with microgrids [5]. While ac [6], [7] and dc [8], [9] microgrids have been studied, this dissertation will focus on a dc microgrid example. The use of renewable sources and power electronics provides a good fit for a dc microgrid architecture [10]. A review of existing microgrids and test systems is presented in [11].

1.3 Droop Control

Droop is commonly chosen as the control method for power systems, including microgrids. The main benefit of droop control is that communication between sources and loads is not required [12]. This advantage alleviates some of the challenges related to implementing a communication system in microgrids [13] and eliminates a single source of failure. Avoiding the need for communication between system components increases the reliability of the microgrid. Reliability is an important consideration as microgrids continue to be implemented [14].

In a dc distribution system, each source is given a droop setting so that the power supplied from that source is proportional to the total load in the system. All of the sources and loads are connected to a common bus, so variation in the load causes changes in the bus voltage. In a system with a common dc bus, the bus voltage is always the same for all sources. Using different droop settings for each can allow the different sources to supply more or less power as the bus voltage varies [12].

1.4 Motivation

The advantage of using some type of droop control in a microgrid is the simplicity, and the fact that communication between the system components is not necessary. However, when implementing droop control with wind resources in microgrids, a large disadvantage is the fact that the wind speed is not considered - during times of higher wind speed, more power is available from the wind that is not utilized with traditional droop control. While previous research has shown possibilities for modifying droop control for wind resources, these still do not allow the wind speed to be taken into account.

This dissertation presents an improved method for applying droop control with wind resources in dc microgrids, using multiple dimensions. The power supplied from each source still depends on the bus voltage, as in traditional droop control. Adding a third dimension allows the power supplied from a wind resource to also depend on the wind speed at the current time. Using a high dimension droop control strategy allows much more of the available power from the wind to be utilized, while retaining the main advantages of using a droop control technique.

1.5 Dissertation Organization

Chapter 2 will provide a detailed background on the use of droop control with wind resources, as well as methods proposed by other researchers to improve upon the traditional method. The motivation behind this dissertation will be further explained, in terms of both improvements to traditional linear droop control, and of specific microgrid applications where this work would provide a benefit.

In Chapter 3, general methods that are used throughout the dissertation will be described. The use of average mode modeling of power electronics will be explained, along with the approach of modeling a variable voltage source behind a resistance with droop control. The equipment and procedure for hardware-in-the-loop (HIL) experiments will also be described.

Chapter 4 will focus on the change to high dimension droop control. An example dc microgrid is modeled, and the operation is simulated first using traditional linear droop control, and again using high dimension droop control. The results are compared, and show that much more of the available wind power is utilized when high dimension droop control is introduced. This chapter also includes discussion of one method for choosing the optimal orientation of the plane for high dimension droop control.

Chapter 5 will show a method of optimizing a droop control relationship to meet a given

objective. An example is demonstrated for a dc microgrid, first using two dimensions. The method is then expanded to higher dimensions, and again demonstrated through simulation and using hardware-in-the-loop. The results for three cases are compared: traditional linear droop control (line), high dimension linear droop control (plane), and high dimension optimal droop control (surface).

The work shown in Chapter 6 will be an extension of the work shown in Chapter 5. Here, the optimal high dimension droop control method will be implemented with a full microgrid example containing energy storage. Next, an example dc microgrid for a military application will be used to demonstrate the use of an optimal high dimension droop control surface for a solar resource. Simulation and hardware-in-the-loop results will be presented.

Chapter 7 summarizes the primary achievements of this work, including the two main new research contributions. Possible avenues for future research in related areas are suggested.

Chapter 2

Background

The main motivation of this dissertation is to improve upon the droop control concept when used with wind resources in microgrids to maximize renewable resource use, while retaining the advantages of traditional droop control. This chapter provides background on previous work to address this motivation, as well as on potential applications of this research.

2.1 Droop Control with Microgrids

Various control strategies for microgrids have been investigated, including droop control [15] [16] [17]. Droop control has been applied with both ac and dc microgrids. One main

benefit of choosing this type of control is the decentralized nature, as demonstrated by previous research [18]. In an ac microgrid, droop control can be used to take advantage of this benefit [19], and to improve upon traditional droop control when the inverter impedance is complex [20]. In a dc microgrid, voltage control is an important challenge, and previous research has demonstrated the use of droop control to maintain system voltage while also allowing for load sharing [21], and to achieve precise control of power flow [22].

Traditional dc droop control is implemented as shown in Fig. 2.1, where two sources are connected with a dc microgrid. They share the same bus voltage, shown in the figure as 290 V. Each source has been given a linear droop setting with a different slope, so that as the bus voltage changes, the reference current for each source also changes with respect to that linear relationship. In this example, when the load in the system increases and the bus voltage decreases, source 2 will provide more additional power than source 1, since the droop relationship for source 2 has a steeper slope. Both sources would adjust their output to meet the change in load, without sharing any information with each other or the with the rest of the system.

Adjustments to traditional droop control have been proposed to achieve better operation when applied with microgrids. The traditional ac droop control relationships can be written

$$f_0 = f_n - m_p P \tag{2.1}$$

$$V_0 = V_n - n_q Q \tag{2.2}$$

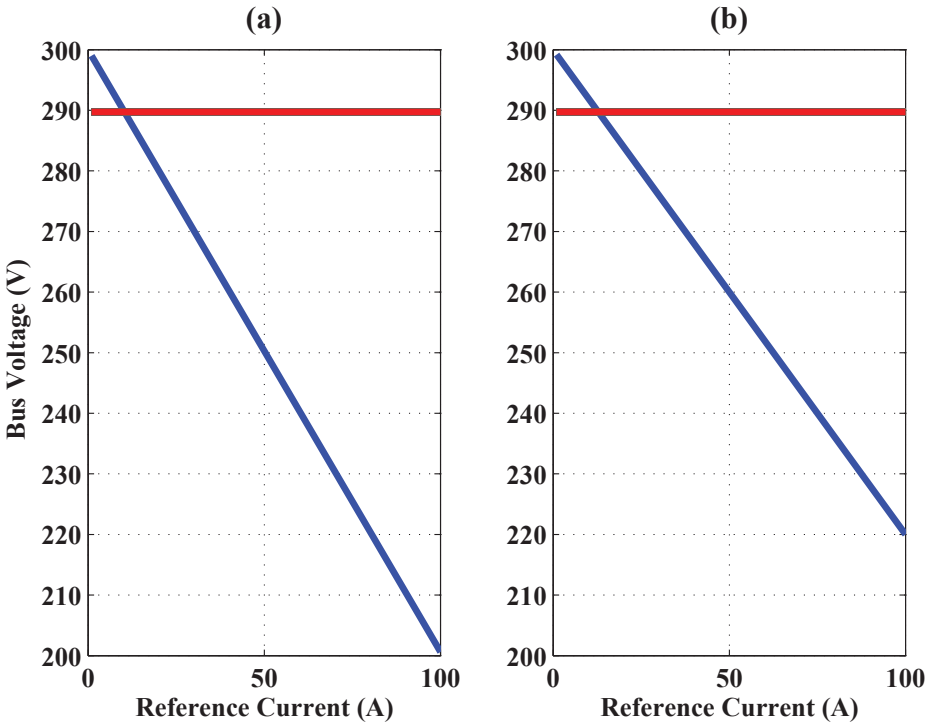

Figure 2.1: Traditional implementation of dc droop control for (a) source 1 and (b) source 2.

where f_0 and V_0 are the current operating frequency and voltage, and P and Q are the current real and reactive power supplied by the source. The other variables are constants that define the linear droop control relationship; f_n and V_n are the nominal values of frequency and voltage that define the intercept of the lines, while m_p and n_q are the droop gains that define the slope of the lines.

Luo et al. propose an offset P' be added to the linear droop setting for sources connected

to the dc bus in a microgrid, expanding the traditional droop control equations to

$$f_0 = f_n - m_p(P + P') \tag{2.3}$$

$$V_0 = V_n - n_q(Q + Q') \tag{2.4}$$

which allows the inverter to better balance its active output power with the input power from the source [23].

One concern when using droop control with microgrids is maintaining stability, especially in remote or islanded microgrids that do not have the large electricity grid to keep the operation of the system stable [24]. Barklund et al. have demonstrated the importance of choosing droop coefficients that will not cause instability, and a method for choosing them. This work focused on finding a range of droop control settings that will ensure stability for a linear system, and showed that while larger droop gains can improve the load sharing between sources, they also decrease the stability margin for the microgrid [25]. A trade-off can be considered between choosing droop settings that allow for optimal load sharing, and settings that ensure stability [26]. Mohamed and El-Saadany have further considered this trade-off when the system has a complex impedance [27]. An alternative droop control method was proposed, where the traditional ac droop control relationships in (2.1) and (2.2)

are expanded to include derivative terms, as

$$f_0 = f_n - m_p P - m_d \frac{d\delta}{dt} \tag{2.5}$$

$$V_0 = V_n - n_q Q - n_d \frac{d\delta}{dt} \tag{2.6}$$

where m_p and n_q are traditional ac droop gains, and m_d and n_d are additional droop gains for the change in the power angle δ [28]. Results from this research show that this approach improves the load sharing between various resources in the microgrid. Adapting droop control to ensure load sharing in a microgrid was also studied in [29].

An additional challenge with some microgrids is their ability to operate either in connection with the main electricity grid, or disconnected from the grid in an islanded mode. Nagliero et al. have presented a study of droop control with wind resources in a microgrid, and two droop settings are recommended: one for grid-connected operation and one for islanded microgrid operation [30]. Additional previous research has examined the transition between grid-connected and islanded modes, while using droop control [31] [32].

As previously discussed, one advantage to droop control is the lack of communication required between system components. However, including some communication links where they are available can improve the overall operation of the microgrid. Gao et al. have demonstrated that the inclusion of some shared information can enhance droop control [33], and another study had all sources reporting information to a centralized microgrid

control center [34]. Additional research has focused on hierarchical control of microgrids, with multiple levels of control that in some cases rely on communication links [35]. This dissertation research has focused on microgrids where a communication link is unavailable, or where it is undesirable to include communication capabilities.

2.2 Droop Control with Wind

Droop control has also been implemented with wind resources in microgrids [36]. While new challenges are presented when connecting wind resources in a microgrid setting [37], adding energy storage and applying an alternative droop control method has been demonstrated as one method for reducing these challenges [38].

Using droop control with wind resources has been demonstrated as beneficial for various types of wind turbines. For example, Fazeli et al. showed the use of droop control with doubly-fed induction generator (DFIG) wind turbines to supply constant power to the connected grid [39]. Other previous research has shown the use of droop control to allow for voltage sag ridethrough with permanent magnet synchronous generator (PMSG) wind turbines [40]. Several previous studies have been conducted for offshore wind farms [41], including investigating methods for choosing the optimal droop gains for offshore wind scenarios [42] [43].

To improve frequency regulation of wind turbines in ac systems, another approach which gives lower droop settings to those sources with higher power margins is proposed [44]. In a grid-connected setting, wind resources can be utilized with droop control for active power control, and are often more flexible than traditional generation sources [45]. Diaz et al. have shown modeling of the available wind resources, and calculation of the capacity factor for a droop-regulated microgrid containing wind [46].

Successful implementation of droop control with wind resources in a standalone dc microgrid has been demonstrated [47]. For an ac microgrid, previous research has suggested including H^{∞} control to improve the performance of traditional droop control and reduce errors based on measurement noise [48].

The challenges encountered in using droop control with wind resources due to the variable nature of wind are clear [49]. When using traditional linear droop control, appropriate droop control settings that allow for load sharing while also utilizing energy from the wind are difficult to find. This dissertation will present an alternative droop control method to address these challenges.

2.3 Optimization

An additional consideration is the optimization of the control or operation of a microgrid system to meet a given objective. Previous studies have designed control methods to find the time-optimal response [50], or the cost-optimal response as the load changes [51]. Other research has focused on game theory as an alternative to droop control, and used optimal control methods to maintain overall efficiency and stability [52] [53]. Reducing the effect of transients was also the objective in the optimal control design in [54].

Other research has focused on a system that contains both ac and dc sections. The optimal dc droop gain was found in order to maintain stability in the ac portion of the system [55]. An alternative optimal droop control method has been proposed by Rokrok and Golshan, where the voltage reference for each source is drooped as a function of the active and reactive power outputs of that source [56]. In dc microgrids, optimal control techniques have been applied to predetermine optimal switching surfaces for various transient events [57], as well as to control the operation of a battery energy storage system connected with the system [58].

This research will use optimal control techniques to find a droop control relationship to best meet a given objective. The main focus is wind resources, with an objective of utilizing all of the power available from the wind. Chapter 6 will expand this concept to other types

of sources, finding an optimal droop control relationship to meet an objective for a solar resource.

2.4 Applications

2.4.1 Remote Microgrids

One application for this research is remote microgrids, which are not located near the main electrical grid, and therefore operate as standalone systems. These microgrids may also be located in countries that do not have a centralized electricity grid system, or on physical island communities [59]. In some cases, these communities have relied on diesel generation; the addition of renewable resources and control methods such as droop control can reduce their consumption of diesel fuel and their carbon emissions [60].

Various types of resources can be combined in a remote microgrid, and previous research has been conducted on both wind-diesel systems [61] and PV-diesel systems [62]. Specific examples of remote microgrids have been studied and demonstrated in Northern Canada [63], the Maldives [64], and in other places around the world. Methods for regulating the frequency of a remote ac microgrid using solar [65] and wind [66] have been presented.

2.4.2 Islanded Microgrids

Alternatively, some microgrids have the option to operate while connected with the grid, or in a separate, islanded mode [67]. This dissertation work can be applied with a microgrid that is operating as an island. Stability is important regardless of the operation mode, but becomes especially important in islanded microgrids [68].

An example of a dc microgrid including energy storage and using droop control was presented in [69]. The use of droop control has been studied in islanded microgrids [70]. No previous research which expands droop control to higher dimensions has been found.

2.4.3 Military Microgrids

Another key application of this research is for microgrids used by the military. Research has been conducted on the topic of implementing microgrids at fixed military installations within the United States [71] [72]. This dissertation will focus on the application of microgrid technologies in overseas military operations. Specific examples include forward operating bases (FOB), observation posts (OP), and patrol bases (PB) [73]. These may be permanent or temporary bases used by the military while on assignment in foreign countries. Chapter 6 will include a demonstration of a PB with a size of 20-40 people, so this type of microgrid will be considered here.

There are several additional challenges when considering microgrids for military applications. First, the PBs may be somewhat temporary, so equipment that can be easily transported to the location, then moved to future locations is important to consider. Reliability is especially important in military microgrids, since many lives depend on the consistent operation of the electrical equipment at the PB [74]. Minimizing the use of fuel is also critical, as transporting fuel to the PB can cost $400 per gallon [75], and can be dangerous, resulting in the loss of one life for every 24 fuel convoys in Iraq and Afghanistan in 2007 [76].

Including renewable resources can help reduce the amount of fuel needed, and energy storage can be included to increase the reliability of the system. Assessing the amount of storage needed for energy surety has been previously studied [77] [78]. Using the improved droop control methods presented in this dissertation can allow a military microgrid to utilize as much renewable resources as possible, without relying on a communication link between the microgrid components - this eliminates the electrical system communications as a single source of failure that would be especially vulnerable in a military setting.

Chapter 3

Methods

This chapter will describe general methods that are used throughout the rest of the dissertation. The modeling of power electronics will be discussed first, including details on switching, average-mode, and simplified models. Details on the equipment and setup for hardware-in-the-loop experiments will follow.

3.1 Power Electronics Modeling

This dissertation will use dc-dc converters to connect various components to a dc microgrid. A buck (step-down) converter is shown in Fig. 3.1.

In order to avoid violating basic circuit voltage and current laws, either switch q_1 or switch

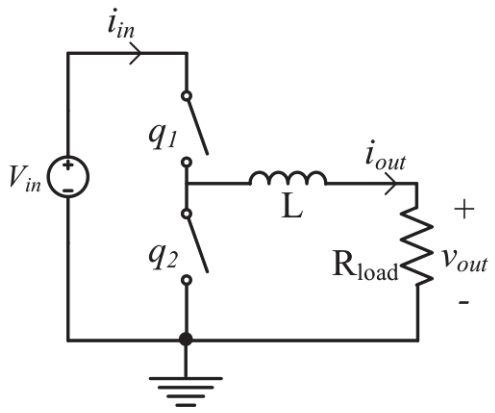

Figure 3.1: Buck (step down) dc-dc converter model.

q_2 must be closed at all times - both cannot be closed or open at the same time. This means that

$$q_1 = 1 - q_2 \tag{3.1}$$

when the converter is operating in continuous current mode, with the current i_{out} always greater than zero. When q_2 is closed, energy from the inductor is used to supply the load R_{load}. If the inductor L is small, this energy may become exhausted quickly, and the current i_{out} becomes zero. With this zero current, the switch q_2, which is practically implemented using a diode, will turn off before switch q_1 turns on. This creates a period of time where both switches are turned off, and equation (3.1) is no longer valid. The converter is then operating in discontinuous current mode [79]. In this research, the inductor sizes will be chosen large enough to maintain operation in continuous current mode, so that equation (3.1) is used.

In continuous current mode, when switch q_1 is closed, the output voltage is equal to the input voltage. When switch q_1 is open, the output voltage is equal to zero. Therefore, we can write

$$v_{out}(t) = q_1 V_{in}. \tag{3.2}$$

3.1.1 Average Mode

Using average mode for power electronics converters allows a simpler model to be used, where the detailed switching is not included [80].

The average value of the output voltage can be found

$$< v_{out} >= \frac{1}{T} \int_0^T q_1(t) V_{in} dt \tag{3.3}$$

where T is the switching time period. Since V_{in} is a constant, it can be moved outside of the integral,

$$< v_{out} >= \frac{V_{in}}{T} \int_0^T q_1(t) dt. \tag{3.4}$$

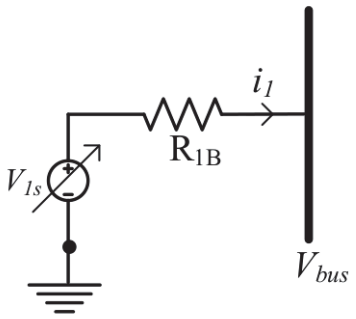

Figure 3.2: Variable voltage source model used in developing droop control relationships.

This results in an average output voltage of

$$< v_{out} >= D_1 V_{in} \tag{3.5}$$

where D_1 is the duty ratio for switch q_1, and represents the percentage of each switching period that the switch is closed [79]. This average mode model for dc-dc converters will be utilized throughout this dissertation.

3.1.2 Droop Control Model

An additional modeling approach will be used for dc sources connected through a power electronics converter to the microgrid, and controlled using droop control, which will be presented in Ch. 5. Fig. 3.2 shows this model, where a variable voltage source is connected through a resistor to the microgrid dc bus.

This equivalent approach allows the converter model to be simplified to only a variable output voltage, without including the actual switching, or an average model of the switching, in the simulation. This approach will be used in this dissertation as a preliminary method for modeling the system and designing droop control algorithms. Average mode modeling for power electronics will then be simulated, and full switching models will be implemented using hardware-in-the-loop.

3.2 Hardware-in-the-Loop Experimental Setup

In order to verify the simulation results obtained in this dissertation, the same microgrids will be implemented using a hardware-in-the-loop (HIL) approach. This allows the system to be emulated in software, and connected with real world hardware in real time [81]. Using an HIL approach allows the system to be built and tested virtually with new proposed control methods, while interfacing with real hardware [82].

For each case, the same component values were implemented in simulation, and in a Typhoon HIL600 unit. The HIL experimental apparatus is shown in Fig. 3.3. The Typhoon HIL600 has 16 channels of $\pm 5\ V$ analog output (AO) that can be mapped to data points in the HIL circuit. The microgrid control board then offsets and scales these signals to $0\ V$ to $+3.3\ V$ that are read by the 12-bit analog to digital converters on all three DSPs. For the different microgrid examples presented in this dissertation, 5-7 channels of analog signals

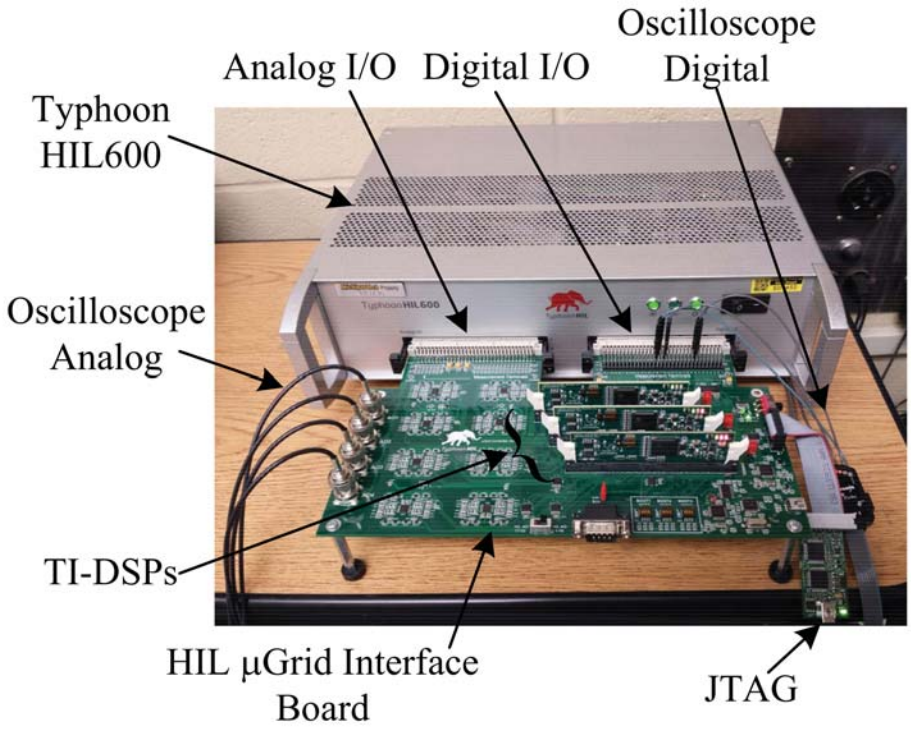

Figure 3.3: Typhoon HIL600 with microgrid control board and three TI-F28335 DSP ControlCARDs (Photo courtesy of Wayne Weaver).

Table 3.1
Hardware-in-the-loop analog output configuration

AO Channel	Model Parameter	Scaling
1	V_{bus}	$100\ V\ per\ 1\ V_{dc}$
2	I_1	$10\ A\ per\ 1\ V_{dc}$
3	I_2	$10\ A\ per\ 1\ V_{dc}$
4	I_3	$10\ A\ per\ 1\ V_{dc}$
5	$V_{1,ref}$	$100\ V\ per\ 1\ V_{dc}$
6	$V_{2,ref}$	$100\ V\ per\ 1\ V_{dc}$
7	$V_{3,ref}$	$100\ V\ per\ 1\ V_{dc}$

are needed to implement the proposed control. The analog signals and the scaling from the HIL are shown in Table 3.1.

The microgrid control board has BNC connectors linked with the first four analog output

channels that are convenient to connect to an oscilloscope. For this work, these were used to view the first four signals in Table 3.1, and capture the results in oscilloscope traces.

The controller for each source was implemented on a separate Texas Instruments F28335 DSP ContolCARD [83] programmed through the Embedded Coder toolbox in MATLAB/Simulink. By using separate control cards for each of the sources, decentralized control is ensured; each source uses only local information, and the proposed control method does not require a communication link between the sources and/or the other components in the microgrid. Optimal control of a dc microgrid has been tested using a hardware-in-the-loop approach in previous work [84].

Chapter 4

Multidimensional Droop Control

This chapter will develop and demonstrate a high dimension droop control method. First, state space models for each of the basic microgrid components (sources, energy storage devices, and loads) will be presented. Control methods for each type of component will be discussed, including traditional linear droop control, and the proposed high dimension droop control for wind resources. Optimal selection of the high dimension droop plane will be discussed. Next, an example dc microgrid will be implemented in simulation, and the results compared for both traditional and high dimension droop control.

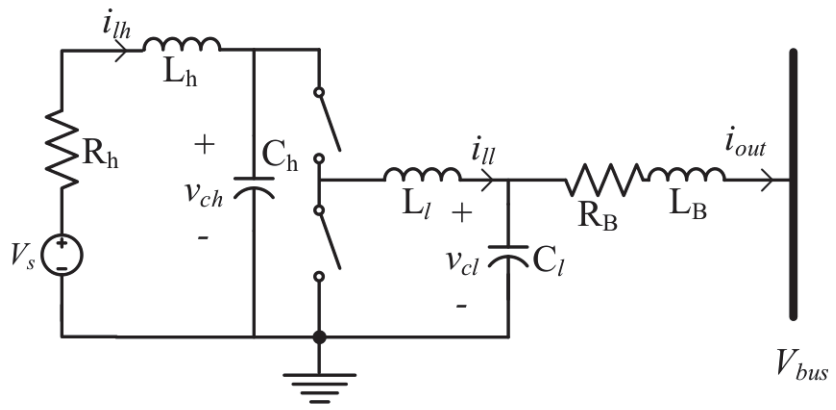

Figure 4.1: General model for microgrid sources.

4.1 Microgrid Modeling and Control

This section will present the model and control method proposed for general microgrid components, including conventional sources, wind sources, energy storage devices, variable loads, and constant impedance loads. All power electronics will be modeled using average mode methods [80], as described in Ch. 3.

4.1.1 Sources

In this dissertation, microgrid sources are modeled with buck converters which step the high voltage of the sources down to match the bus voltage. Fig. 4.1 shows the buck converter model for each source.

The model for each source contains five states

$$\frac{dv_{ch}}{dt}C_h = i_{lh} - Di_{ll} \tag{4.1}$$

$$\frac{di_{ll}}{dt}L_l = Dv_{ch} - v_{cl} \tag{4.2}$$

$$\frac{dv_{cl}}{dt}C_l = i_{ll} - i_{out} \tag{4.3}$$

$$\frac{di_{lh}}{dt}L_h = V_s - R_h i_{lh} - v_{ch} \tag{4.4}$$

$$\frac{di_{out}}{dt}L_B = v_{cl} - R_B i_{out} - V_{bus} \tag{4.5}$$

where D is the duty cycle for switch 1 in average mode. The proposed control methods for both conventional and wind sources are discussed in the next section.

4.1.1.1 Conventional Sources

For conventional sources, traditional dc voltage droop control is used. In traditional droop control for a dc system, the power supplied from each source changes as the bus voltage changes, with movement along a line with a chosen slope. The equation for the reference current from a source is

$$i_{ref} = \frac{V_{ref} - V_{bus}}{R_d} \tag{4.6}$$

where V_{ref} is the desired bus voltage, and R_d is the droop setting which represents a virtual series line resistance.

To implement droop control, two additional states are added. The first compares the current command from (4.6) to the actual output current of the source,

$$\frac{derror_1}{dt} = i_{ref} - i_{out}. \tag{4.7}$$

The second compares the voltage command to the actual voltage at the output of the converter,

$$\frac{derror_2}{dt} = v_{cl,ref} - v_{cl}. \tag{4.8}$$

A proportional-integral (PI) control loop can then be implemented to replace $v_{cl,ref}$ in (4.8)

$$v_{cl,ref} = k_{pi}(i_{ref} - i_{out}) + k_{ii}error_1. \tag{4.9}$$

A second PI control loop is then implemented to replace the average value of the duty cycle, D, and allow the converter to track the reference voltage,

$$D = k_{pv}(v_{cl,ref} - v_{cl}) + k_{iv}error_2. \tag{4.10}$$

Fig. 4.2 shows the traditional linear droop control implemented for conventional sources.

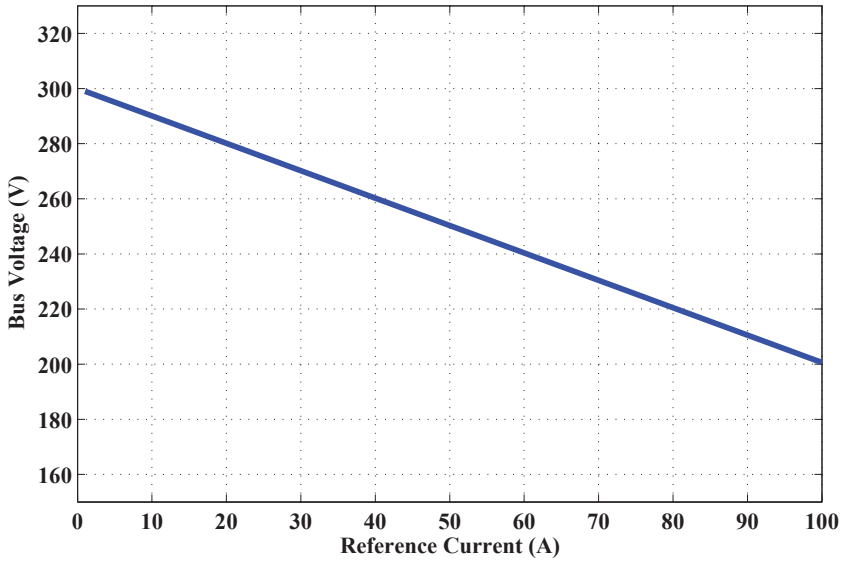

Figure 4.2: Traditional, 2D droop settings for implementing droop control.

4.1.1.2 Wind Sources

For wind sources, the linear droop control presented above is expanded into three dimensions to create a droop surface as shown in Fig. 4.3. Variation in bus voltage still causes adjustments in power supplied from the source. However, variation in wind speed also causes changes in power supplied. The reference current for a source is now determined by a plane,

$$i_{ref} = \frac{V_{ref} - V_{bus}}{R_{d1}} + \frac{v_w}{R_{d2}} \tag{4.11}$$

where v_w is the wind speed, and R_{d1} and R_{d2} represent the droop settings in two dimensions. R_{d1} is with respect to voltage and R_{d2} is with respect to wind speed. In Fig. 4.3, the two

droop settings are 10.8 for R_{d1}, and 0.28 for R_{d2}. The selection of these droop control parameters will be discussed in section 4.3.

This multidimensional approach allows more power from the wind to be utilized, since the current reference increases with wind speed. In this chapter, a linear relationship is used to build a plane in three dimensions for the droop surface. This is a first step for this high dimension droop control approach; further chapters will investigate nonlinear relationships between reference current and both bus voltage and wind speed.

This modified droop control can be implemented in the same way as traditional droop control. The complete state model of the wind source and controller is

$$\frac{dv_{ch}}{dt}C_h = i_{lh} - (k_{pv}[k_{pi}(\frac{V_{ref}-V_{bus}}{R_{d1}} + \frac{v_w}{R_{d2}} - i_{out}) + k_{ii}error_1 - v_{cl}] + k_{iv}error_2)i_{ll} \tag{4.12}$$

$$\frac{di_{ll}}{dt}L_l = (k_{pv}[k_{pi}(\frac{V_{ref}-V_{bus}}{R_{d1}} + \frac{v_w}{R_{d2}} - i_{out}) + k_{ii}error_1 - v_{cl}] + k_{iv}error_2)v_{ch} - v_{cl} \tag{4.13}$$

$$\frac{dv_{cl}}{dt}C_l = i_{ll} - i_{out} \tag{4.14}$$

$$\frac{di_{lh}}{dt}L_h = V_s - R_h i_{lh} - v_{ch} \tag{4.15}$$

$$\frac{di_{out}}{dt}L_B = v_{cl} - R_B i_{out} - V_{bus} \tag{4.16}$$

$$\frac{derror_1}{dt} = \frac{V_{ref}-V_{bus}}{R_{d1}} + \frac{v_w}{R_{d2}} - i_{out} \tag{4.17}$$

$$\frac{derror_2}{dt} = k_{pi}(\frac{V_{ref}-V_{bus}}{R_{d1}} + \frac{v_w}{R_{d2}} - i_{out}) + k_{ii}error_1 - v_{cl}. \tag{4.18}$$

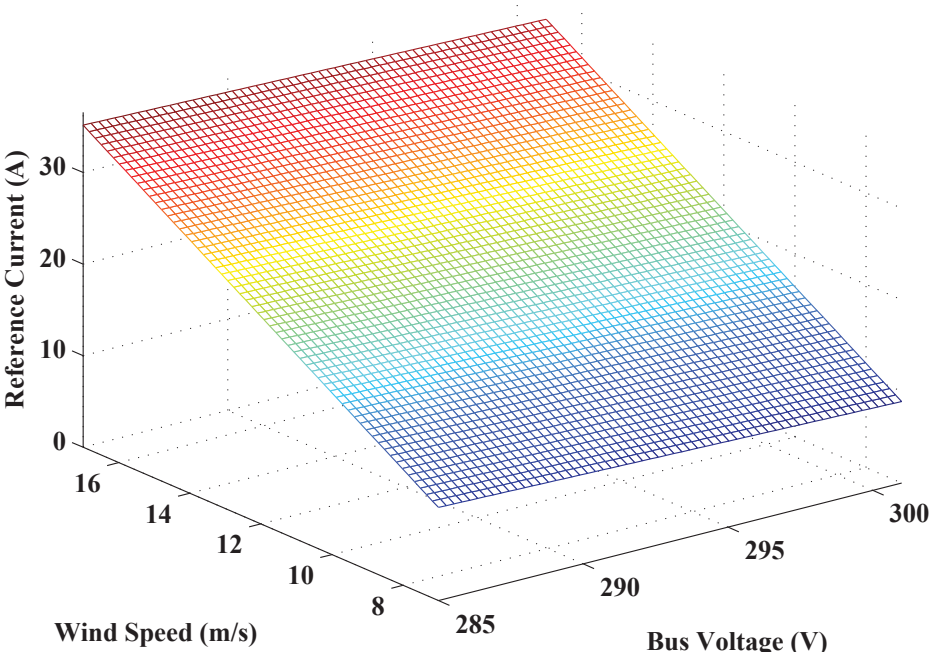

Figure 4.3: Plot of 3D surface for implementing high dimension droop control for wind sources.

For each of the sources, the numeric values of the various circuit parameters are shown in Table 4.1.

In order to analyze the stability of the system with the proposed multidimensional droop controller, the Jacobian matrix was formed by calculating the partial derivative of each state equation with respect to each of the states. The seven states in (4.12) - (4.18) can be numbered 1-7; the states are then x_1-x_7, and the state equations can be called f_1-f_7. The

Table 4.1
Source 1 and Source 2 parameter values.

Source 1				**Source 2**		
Component	**Value**	**Unit**		**Component**	**Value**	**Unit**
V_h	400	V		V_h	380	V
R_h	0.2	Ω		R_h	0.2	Ω
C_h	0.2	mF		C_h	0.2	mF
L_h	1.5	mH		L_h	1.5	mH
C_l	0.08	F		C_l	0.08	F
L_l	5	mH		L_l	5	mH
R_B	0.1	Ω		R_B	0.23	Ω
L_B	1.2	mH		L_B	0.8	mH
V_{ref}	300	V		V_{ref}	300	V
R_d	0.9			R_d	0.8	
k_{pi}	1			k_{pi}	1	
k_{ii}	10			k_{ii}	10	
k_{pv}	1			k_{pv}	1	
k_{iv}	10			k_{iv}	10	

Jacobian matrix is then formed

$$J = \begin{pmatrix} \delta_{x_1} f_1 & \delta_{x_2} f_1 & \cdots & \delta_{x_7} f_1 \\ \delta_{x_1} f_2 & \delta_{x_2} f_2 & \cdots & \delta_{x_7} f_2 \\ \vdots & \vdots & \ddots & \vdots \\ \delta_{x_1} f_7 & \delta_{x_2} f_7 & \cdots & \delta_{x_7} f_7 \end{pmatrix}. \tag{4.19}$$

The numeric values in Table 4.1 were included, and a reasonable operating point of 295 V for the bus voltage, and 8 m/s for the wind speed was chosen. The equilibrium point where all state equations are equal to zero was found using these numeric values. The eigenvalues

Table 4.2
Eigenvalues for source and controller state model.

-57.26 + 1970.61j
-57.26 - 1970.61j
-20.04 + 138.91j
-20.04 - 138.91j
-54.25
-6.85
-0.97

of the completed Jacobian matrix were then calculated at this equilibrium point, and are shown in Table 4.2. Since all of the eigenvalues have negative real parts, the stability of the source model with the proposed controller is confirmed for this equilibrium point [85]. The eigenvalues remain negative when bus voltage and wind speed are varied within reasonable ranges.

4.1.2 Energy Storage Devices

Microgrids often contain energy storage devices, to balance the power supplied from the sources and demanded from the loads while operating in islanded mode [86]. As the microgrid concept is increasingly implemented, the importance of energy storage becomes clear. One of the key benefits of microgirds is their capability to operate in islanded mode, disconnected from the main electricity grid. This is especially important during times of disturbance on the main grid, which would disrupt electricity service to many customers. With a microgrid, the option to operate as an island allows many of those customers to continue with uninterrupted electricity. Microgrids also provide the capability to supply

power to critical loads, for example providing power to hospitals during a natural disaster that causes a blackout on the electricity grid [87].

In both of these cases, the fact that there are nearby distributed generation sources allows the microgrid to continue operating while the main electricity grid is not. When some of those distributed sources are renewable energy options with variable resources, such as sunlight or wind, it is difficult to predict how much electric power the microgrid can supply, and when. The addition of some form of energy storage alleviates this concern, allowing excess energy produced to be stored, and used as needed [88]. The importance of including energy storage when wind sources are included in the system is detailed in [89]. Since energy storage is a key part of a successful microgrid, it is important to ensure that any proposed control design for a microgrid component would function well alongside an energy storage device. Therefore, energy storage is included in the sample microgrid used in simulation to test the proposed high dimension droop control for wind resources.

While many options are available for energy storage in microgrids, in this dissertation a battery is simulated. The battery model used is based on the FreedomCAR design [90]. Fig. 4.4 shows the battery model, with the bi-directional dc-dc buck converter as the interface to the microgrid dc bus.

The model for the energy storage system is similar to the model for each source. There are

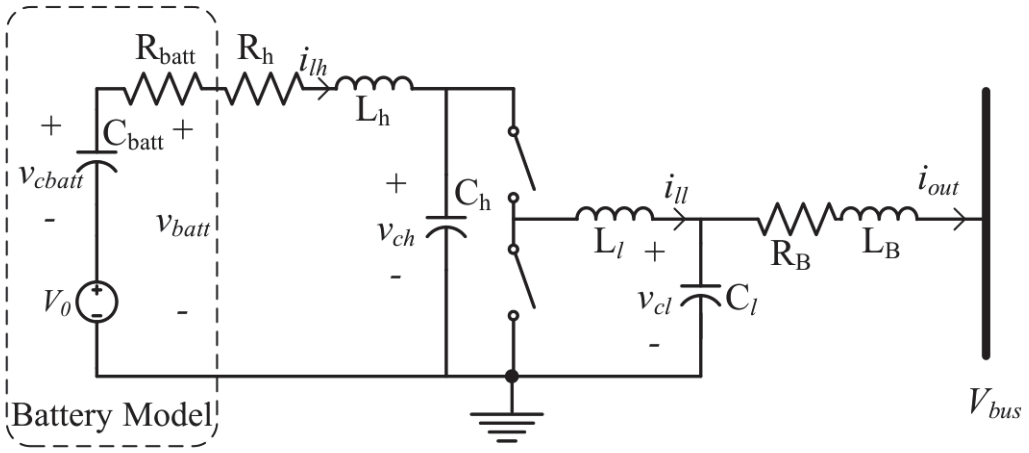

Figure 4.4: General model for microgrid energy storage devices.

again five states for the converter, with an additional state for the battery defined as

$$\frac{dv_{ch}}{dt}C_h = i_{lh} - Di_{ll} \tag{4.20}$$

$$\frac{di_{ll}}{dt}L_l = Dv_{ch} - v_{cl} \tag{4.21}$$

$$\frac{dv_{cl}}{dt}C_l = i_{ll} - i_{out} \tag{4.22}$$

$$\frac{di_{lh}}{dt}L_h = v_{batt} - R_h i_{lh} - v_{ch} \tag{4.23}$$

$$\frac{di_{out}}{dt}L_B = v_{cl} - R_B i_{out} - V_{bus} \tag{4.24}$$

$$\frac{dv_{cbatt}}{dt}C_{batt} = i_{lh}. \tag{4.25}$$

Defining the equations in this way results in a positive current i_{out} when the battery is discharging, or supplying power to the microgrid. The current i_{out} is negative when the battery is charging, or absorbing power from the microgrid.

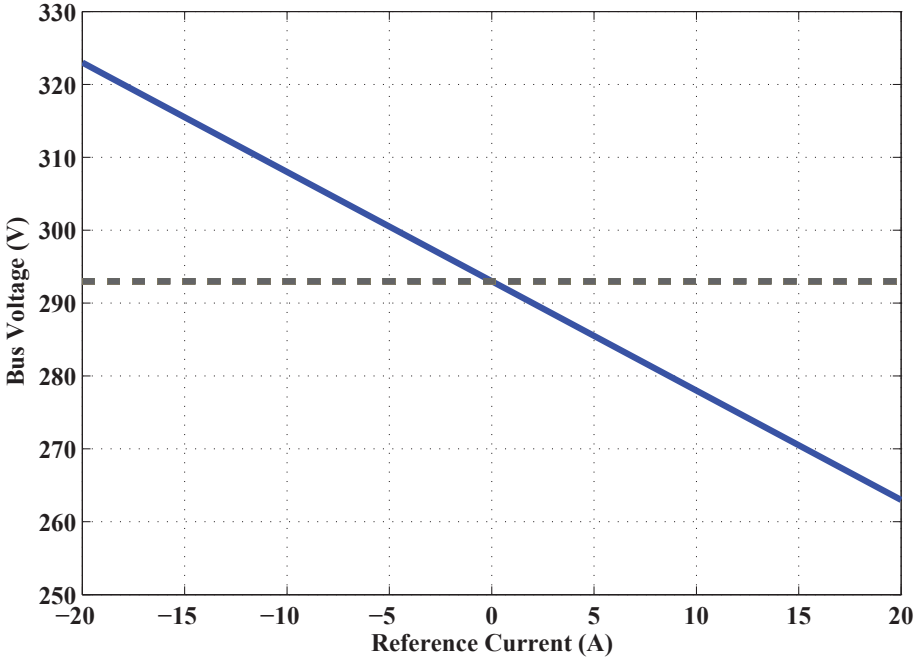

Figure 4.5: Droop control for microgrid energy storage: battery charges when bus voltage is above the reference value, and discharges when bus voltage is below the reference value.

Droop control can be implemented for the energy storage in a similar manner as for the traditional source, as in (4.6)-(4.10). When the bus voltage is above the reference value the battery absorbs current and charges. When the bus voltage is below this reference, the battery discharges. Fig. 4.5 shows the droop control as implemented for the battery in this simulated microgrid.

This simple control implementation will allow the system to operate without a communication link necessary between the energy storage system and the rest of the microgrid. More complex control designs could be implemented to schedule the charging of the battery, however, this is beyond the scope of this research.

Table 4.3
Energy storage parameter values.

Component	Value	Unit
C_h	1	mF
L_h	0.2	mH
C_l	0.08	F
L_l	1	mH
R_B	1	Ω
L_B	1.2	mH
C_{batt}	10	mF
R_{batt}	0.001	Ω
V_{ref}	293	V
R_d	1.5	
k_{pi}	1	
k_{ii}	10	
k_{pv}	1	
k_{iv}	10	

The numeric values used in the energy storage model are shown in Table 4.3.

4.1.3 Loads

In this dissertation, two general types of loads are considered: constant impedance loads, and variable impedance loads. The modeling approach for both load types is discussed here. The resistive load model used here is similar to an actual lighting type load.

4.1.3.1 Variable Loads

The general load is modeled with a buck converter, to step the bus voltage down to the level of the load. Fig. 4.6 shows the buck converter model for each load. The model for each load contains four states, with equations defined as

$$\frac{dv_{ch}}{dt}C_h = i_{in} - Di_{ll} \tag{4.26}$$

$$\frac{di_{ll}}{dt}L_l = Dv_{ch} - v_{cl} \tag{4.27}$$

$$\frac{dv_{cl}}{dt}C_l = i_{ll} - \frac{v_{cl}}{R_{load}} \tag{4.28}$$

$$\frac{di_{in}}{dt}L_h = V_{bus} - R_h i_{in} - v_{ch}. \tag{4.29}$$

The numeric values used for the variable load parameters are shown in Table 4.4. A PI controller can be implemented to keep the load at a desired nominal voltage. This adds one state to the model,

$$\frac{derror}{dt} = V_{nom} - v_{cl}. \tag{4.30}$$

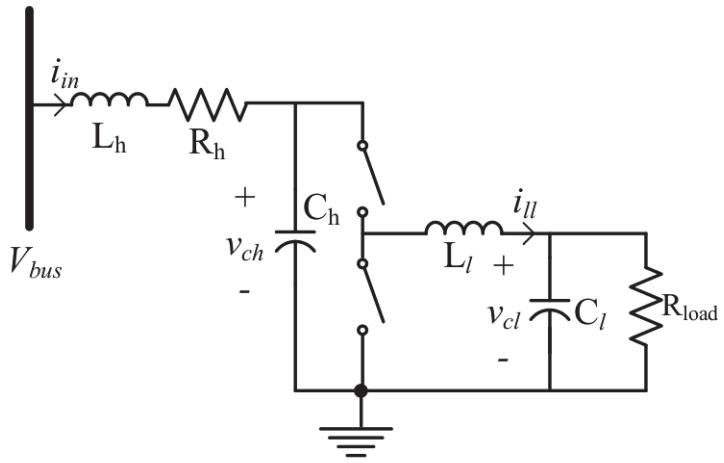

Figure 4.6: General model for microgrid variable loads.

Table 4.4
Variable load parameter values.

Component	Value	Unit
V_{nom}	200	V
R_h	0.2	Ω
C_h	20	μF
L_h	0.15	mH
C_l	0.8	mF
L_l	7.5	mH
k_{pl}	1	
k_{il}	10	

The duty cycle D can then be replaced with the PI controller, such that

$$D = k_{pl}(V_{nom} - v_{cl}) + k_{il} error. \tag{4.31}$$

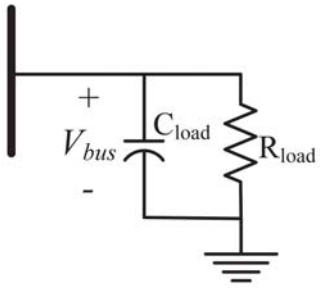

Figure 4.7: General model for microgrid loads with constant impedance.

Table 4.5
Constant load parameter values.

Component	Value	Unit
C_{load}	1	mF
R_{load}	30	Ω

4.1.3.2 Constant Impedance Loads

Fig. 4.7 shows the model used for constant impedance loads. There is just one state for the constant impedance load model,

$$\frac{dV_{bus}}{dt}C_{load} = \Sigma i_{sources} - \Sigma i_{loads} + \Sigma i_{storage} - \frac{V_{bus}}{R_{load}} \tag{4.32}$$

where the currents from the sources, energy storage devices, and other loads are summed together.

The numeric values used for the constant load parameters are shown in Table 4.5.

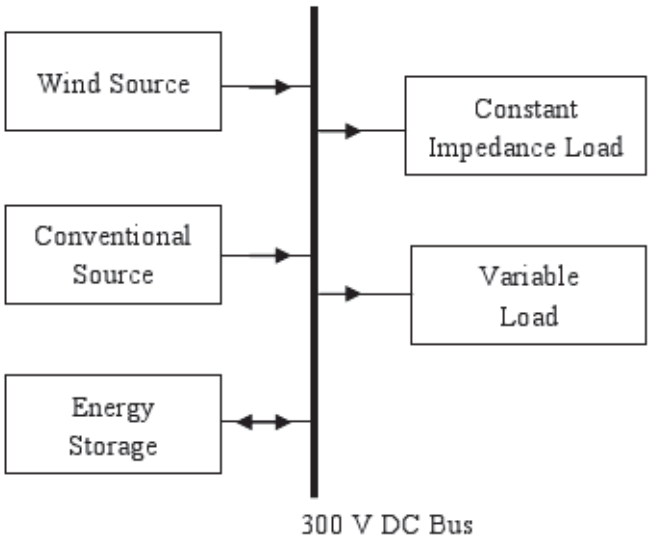

Figure 4.8: One-line diagram of example dc microgrid used in simulation.

4.2 Example Microgrid

The microgrid system used in this dissertation is on the scale of a home or other building, and is shown in Fig. 4.8. The wind source is a small-scale wind turbine, while the conventional source is a liquid-fuel generator. The constant impedance load has an impedance which remains the same throughout the simulation, while the variable load changes with time. A timeframe of one day is simulated, and a load profile throughout the day was chosen by scaling actual data from an existing power system [91]. A wind speed profile for the day was approximated by calculating an average of daily wind speed measurements [92]. The load and wind speed profiles used for this 24 hour simulation period are shown in Fig. 4.9. The wind source is based on a 12 kW wind turbine, with a power curve as shown in Fig. 4.10 [93].

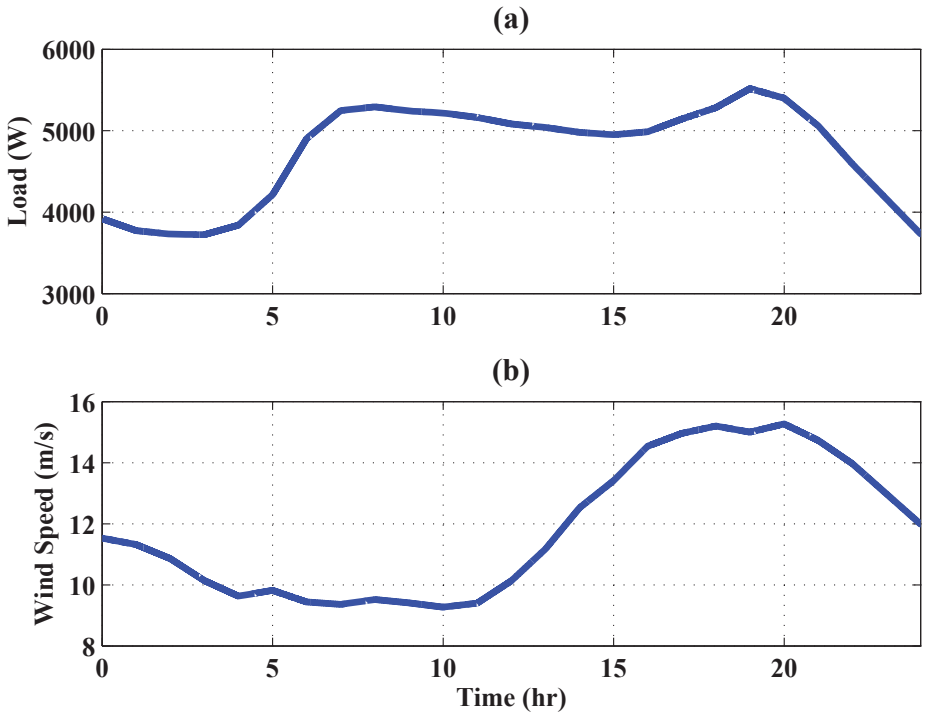

Figure 4.9: (a) Load and (b) wind speed profiles for simulated 24 hour period.

4.3 Selection of Planar Droop Surface

With the proposed high dimension droop control, the control designer has an additional component to choose, since there are droop constants in two dimensions instead of just one. Choosing different values for these parameters changes the orientation of the droop plane, and the operation of the system. One method for choosing the optimal droop constants is presented here.

The amount of power available from the wind but unused by the microgrid can be summed

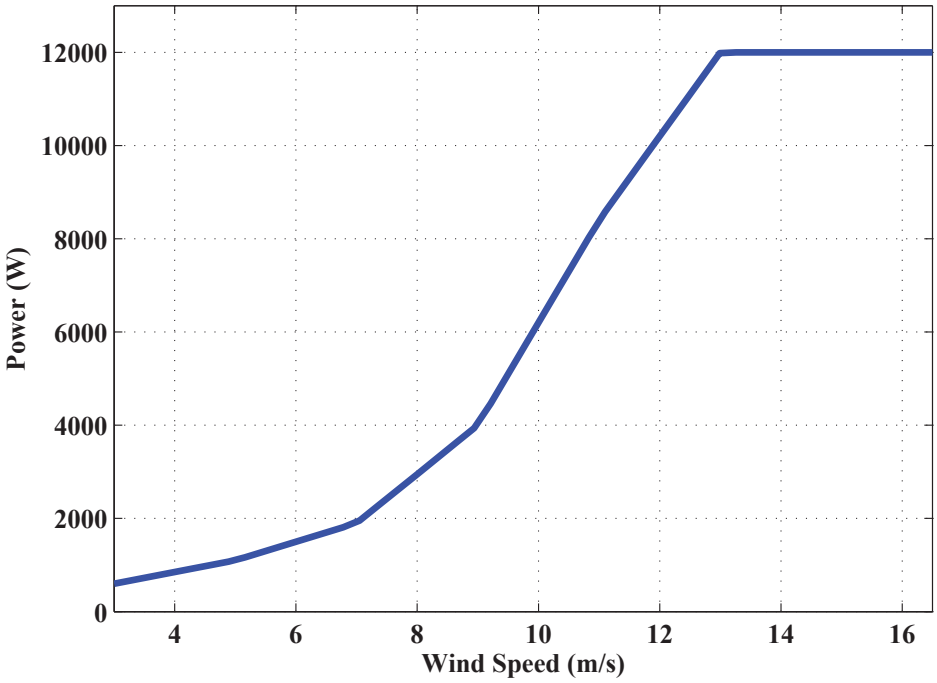

Figure 4.10: Power curve for 12 kW wind turbine.

over a given time period as

$$P_u = \int (P_a - P)dt \tag{4.33}$$

where P_a is the power available from the wind and P is the power generated by the wind source (power utilized from the wind). The power available from the wind P_a was determined using the wind speed profile shown in Fig. 4.9b and the wind turbine power curve shown in Fig. 4.10.

It is likely that there are some constraints on the microgrid operation. For example, it may be undesirable to allow the conventional source to stop providing any power, so there is a

minimum output power that should be maintained from this source. There is likely also a limit to the charging current for the battery. Additionally, while the bus voltage should vary, a constraint can be added to choose a droop control plane that keeps V_{bus} within +/- 5% of the nominal value. These constraints can be written as

$$500 \leq i_{out,2} V_{bus} \ (W) \tag{4.34}$$

$$-10 \leq i_{lh,batt} \leq 10 \ (A) \tag{4.35}$$

$$285 \leq V_{bus} \leq 315 \ (V) \tag{4.36}$$

There are multiple options for solving the optimization problem presented above. One method is the minimum principle, which involves adding a co-state variable for each state and creating a Hamiltonian function, as described in [94]. Many other approaches to numerical optimization have been developed [95]. A simple approach to minimizing (4.33) was used here, and is described below.

The slope of the droop surface in each direction was varied at discrete intervals, with the constraints in (4.34)-(4.36) included: a 500 W minimum output from the conventional source, a 10 A maximum charging current for the battery, and a $+/-$ 5% bound around 300 V for bus voltage. Fig. 4.11 shows the cost plotted with respect to both of the slopes, with the minimum cost point given the constraints shown. While the cost values below the solid line continue to get smaller, using a droop surface with those slopes causes the bus

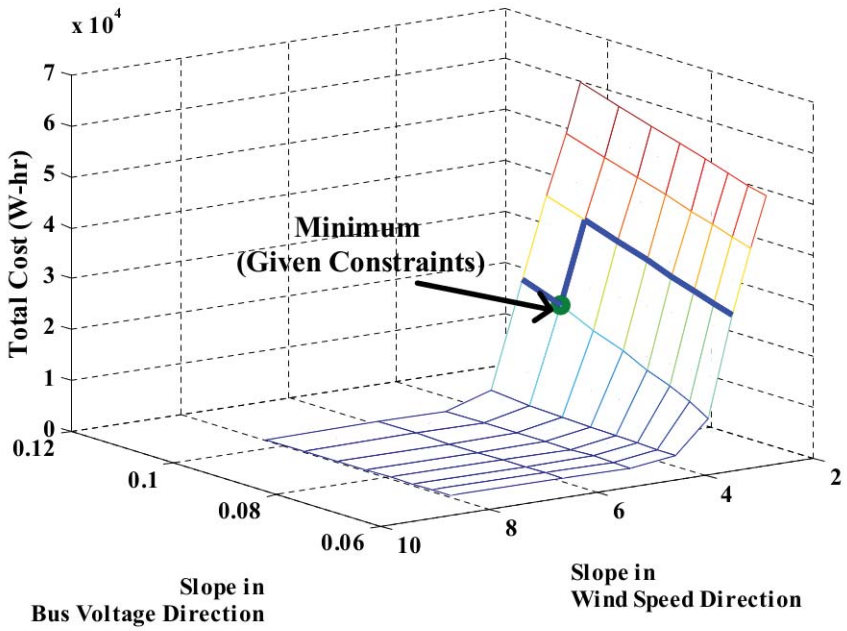

Figure 4.11: Cost from (4.33) with varying slopes in wind speed and bus voltage directions, including constraint conditions. Minimum cost point given constraints is shown.

voltage to leave the +/- 5% bound around 300 V.

The cost equation is summing the unused power over a time period, resulting in a measure of unused energy in Watt-hours. For this scenario, the optimal droop plane that meets the three constraints results in 22,762 W-hr of unused energy.

The method presented here is effective for finding the optimal droop control plane for a specific scenario, using the load and wind speed profiles over a 24 hour period shown in Fig. 4.9. The next chapter will present a more generalized method for determining an optimal droop surface for all scenarios.

Table 4.6
Constraints considered in simulated microgrid.

Component	Parameter	Constraint
Conventional Source	Minimum Power Output	500 W
Battery	Maximum Charging Current	-10 A
Microgrid	Bus Voltage	+/- 5%

4.4 Simulation Results

To test the proposed droop control scheme, the example microgrid described above was modeled using MATLAB/Simulink. The system was first simulated using a traditional droop control technique for both the conventional and wind sources, with droop settings similar to Fig. 4.2.

Next, the system was simulated using the proposed multidimensional droop surface for the wind source, with a traditional droop setting for the conventional source. The optimal droop surface was chosen as described above, with the constraints shown in Table 4.6. The resulting slopes are $\frac{1}{R_{d1}} = 0.0926$ in the bus voltage direction, and $\frac{1}{R_{d2}} = 3.5714$ in the wind speed direction. The droop surface for the wind source is shown in Fig. 4.12, along with the source's movement on the surface during the simulation. The points marked A, B, and C provide a reference for the plot of the source's output with respect to time, which will be shown in Fig. 4.15.

The power from each source for the two cases is shown in Fig. 4.13. The power available

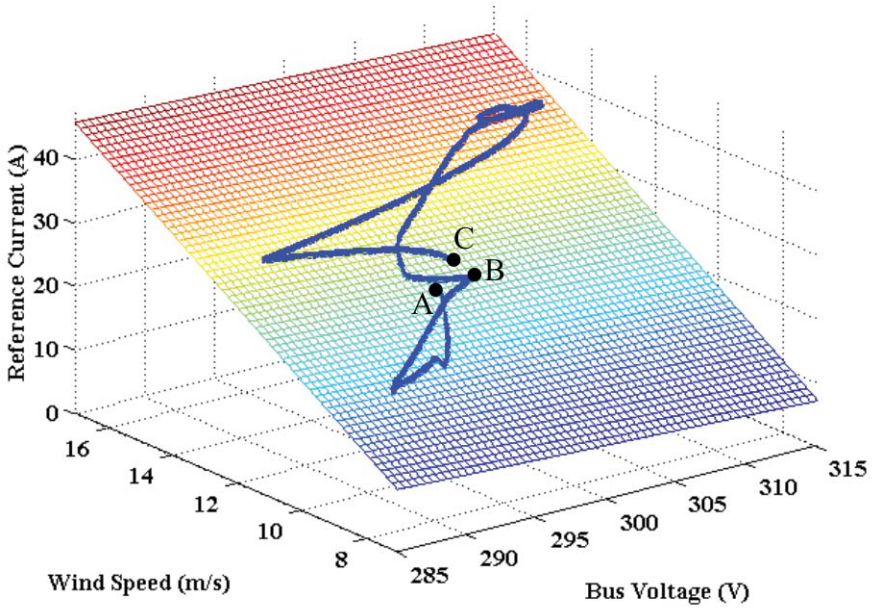

Figure 4.12: Plot of 3D droop surface for wind source.

from the wind is included, and it is clear that using the planar droop surface allows more of the available wind power to be utilized (and requires less liquid fuel).

A summary of the simulation results using traditional droop control is shown in Fig. 4.14, and Fig. 4.15 shows a summary of the simulation results using high dimension droop control. The points marked A, B, and C provide a reference back to the plot of the source's movement along the droop control plane, shown in Fig. 4.12. The power supplied by each source, consumed by each load, and supplied from the battery are shown in both cases. For this example scenario, the battery is supplying power to the system when traditional droop control is used. When high dimension droop control is implemented instead, the battery is able to charge during times of high wind and/or low load. The battery reverses its power

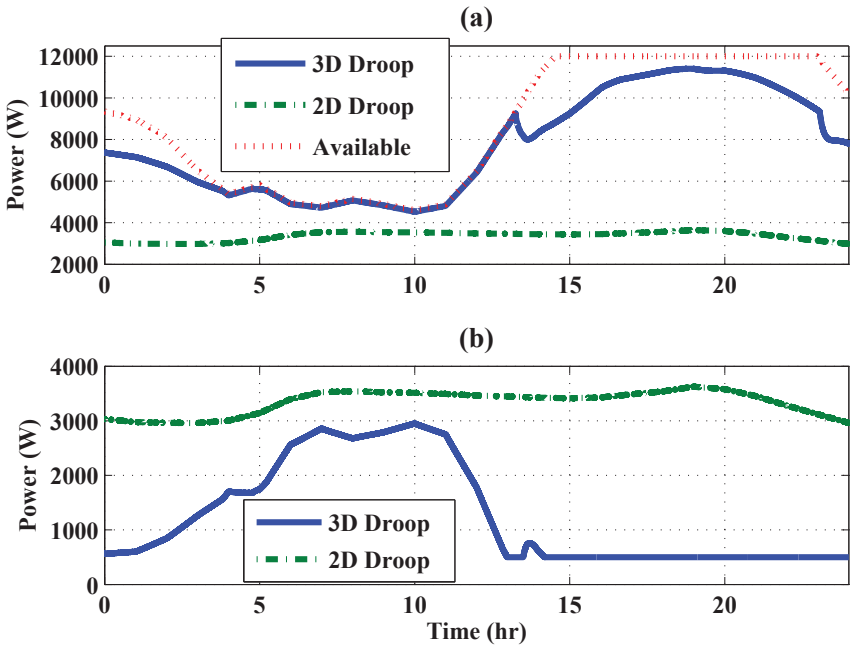

Figure 4.13: Power supplied from (a) wind source and (b) conventional source using 2D and 3D droop. Power available from the wind is also shown.

flow and supplies power during the morning hours, when the load is increased but the wind speed has dropped.

The microgrid bus voltage for each simulation is shown in Fig. 4.16. When high dimension droop control is used, the bus voltage varies more than in the traditional droop case. This is one trade-off that must be considered when choosing the droop surface. In this example with high dimension droop, more power from the wind is utilized and the bus voltage still remains within +/- 5% of the nominal value of 300 V.

The cost was calculated for each simulation using (4.33), and the results are shown in Table 4.7. The cost is reduced significantly when the multidimensional droop surface is

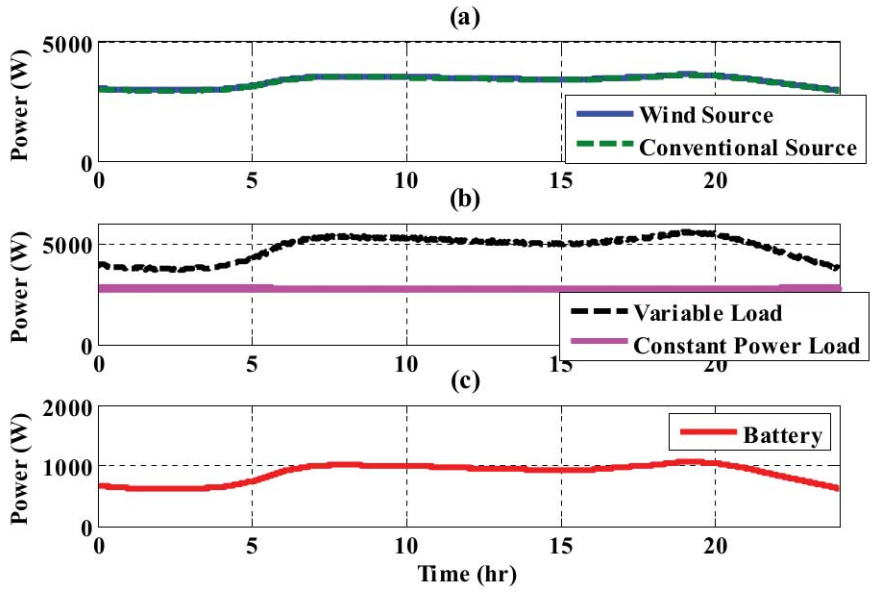

Figure 4.14: Simulation results using traditional droop control: (a) power supplied by each source, (b) power consumed by each load, and (c) power supplied by the battery.

Table 4.7
Comparison of unused energy from the wind for two droop control methods.

Control Strategy	Unused Energy (W-hr)
Traditional 2D Droop	127,610
High Dimension Droop	22,762

used instead of traditional droop control, even when realistic constraints on the system are considered.

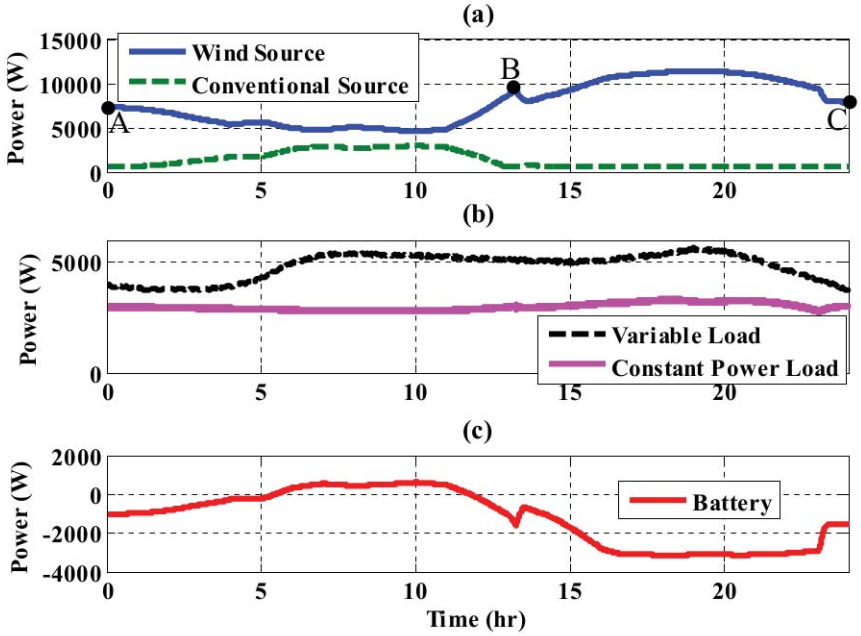

Figure 4.15: Simulation results using high dimension droop control: (a) power supplied by each source, (b) power consumed by each load, and (c) power supplied by the battery.

4.5 High Dimension Droop Control Conclusions

The results presented in this chapter show that using a multidimensional droop surface to control a wind turbine connected with a dc microgrid allows the wind speed at the current time to be considered as a part of the control. This new proposed control method retains the simplicity of traditional droop, while allowing more of the available power from the wind to be utilized.

The proposed high dimension droop control for wind resources was demonstrated here in

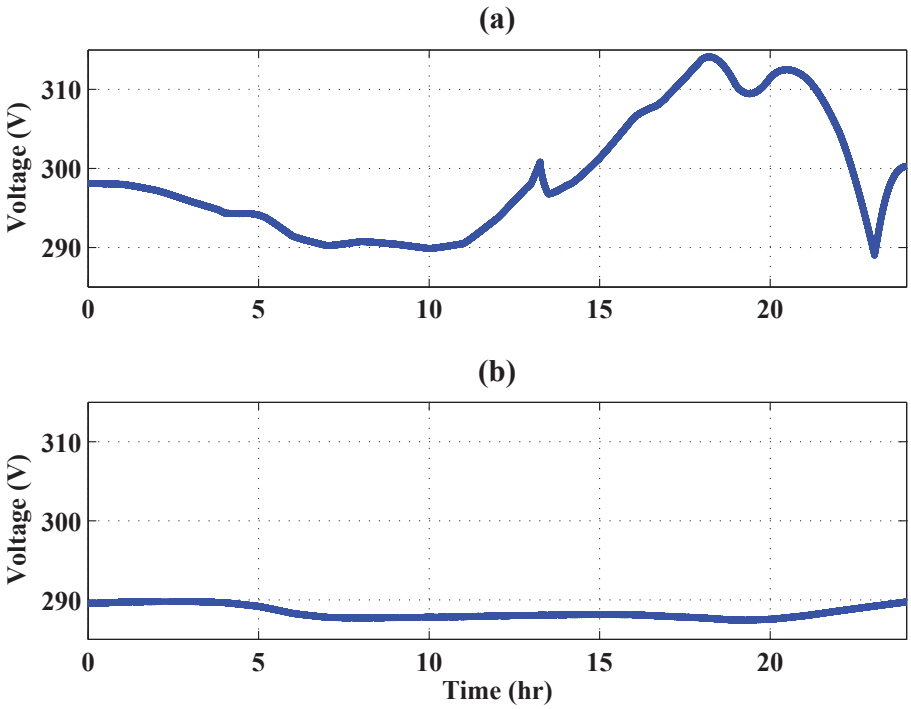

Figure 4.16: Microgrid bus voltage with (a) high dimension droop control and (b) traditional droop control.

a simulation of a small microgrid, with a size representing a home or other small building. Actual wind speed and load profile data was used to ensure a realistic simulation of the microgrid over a 24 hour period.

As discussed, energy storage is a key factor in a microgrid containing renewable resources such as wind. The results presented here show that the proposed high dimension droop control for wind resources works well in conjunction with an energy storage system. In times of high wind, energy is stored in the battery, and that energy is used to supply the microgrid in times of lower wind speed. This is accomplished without the need for communication between the wind source and the battery, resulting in a simple and reliable

control strategy for a dc microgrid.

However, the work presented in this chapter is confined to using a linear droop control surface (plane) in three dimensions. The optimal plane was found for average profiles of changing load and wind speed over a 24 hour period. Since both load and wind speed can vary and be uncertain, further chapters will present a method for optimizing a droop surface for general operation of a microgrid system, rather than a specific case.

Chapter 5

Multidimensional Optimal Droop Control

This chapter presents a method of optimizing the droop control strategy for a source in order to meet a given objective. First, an example using two dimensional droop control will be demonstrated. Next, the method will be expanded to the high dimension droop control proposed in Ch. 4. Simulation and hardware-in-the-loop testing will compare the use of traditional droop control (line), high dimension droop control (plane), and optimal high dimension droop control (surface) for a wind source connected to a sample microgrid.

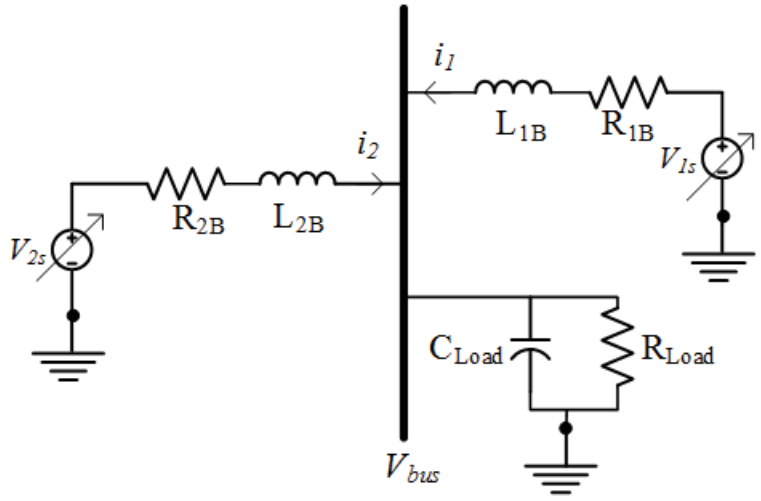

Figure 5.1: Simple microgrid example with two sources and one load.

5.1 Microgrid Modeling and Control

Fig. 5.1 shows the sample microgrid system used in this chapter. This system can be defined using five state equations: one for the current from each source, one for the droop controller for each source, and one for the bus voltage.

$$\frac{di_1}{dt}L_{1B} = V_{1s} - V_{bus} - R_{1B}i_1 \tag{5.1}$$

$$\frac{di_{error,1}}{dt} = i_{ref1} - i_1 \tag{5.2}$$

$$\frac{di_2}{dt}L_{2B} = V_{2s} - V_{bus} - R_{2B}i_2 \tag{5.3}$$

$$\frac{di_{error,2}}{dt} = i_{ref2} - i_2 \tag{5.4}$$

$$\frac{dV_{bus}}{dt}C_{load} = i_1 - i_2 - \frac{V_{bus}}{R_{load}}. \tag{5.5}$$

Table 5.1
Microgrid parameter values.

Component	Value	Unit
R_{1B}	0.1	Ω
L_{1B}	1	mH
R_{2B}	0.2	Ω
L_{2B}	2	mH
C_{load}	1	mF
V_{ref}	100	V
R_d	1	
k_p	1	
k_i	10	

Proportional-integral control loops can then be implemented to replace V_{1s} and V_{2s} as

$$V_{1s} = k_p(i_{ref1} - i_1) + k_i i_{error,1} \tag{5.6}$$

$$V_{2s} = k_p(i_{ref2} - i_2) + k_i i_{error,2}. \tag{5.7}$$

For Source 2, traditional linear droop control will be implemented, where

$$i_{ref2} = \frac{V_{ref} - V_{bus}}{R_d}. \tag{5.8}$$

For Source 1, the reference current is left as a variable, i_{ref1}. The following section will show a method to find the optimal i^*_{ref1} as a function of bus voltage to meet a given objective.

The numeric values used for this microgrid model are shown in Table 5.1.

5.2 Example in Two Dimensions

5.2.1 Optimization of Droop Control

With the system model defined, this section will describe a method to find an optimal droop control relationship between reference current and bus voltage to meet a given objective [96]. First, the state equation model of the system is solved to find the steady-state result, since droop control allows the system to move between stable steady-state points [12].

$$i_{1,ss} = i_{ref1} \tag{5.9}$$

$$i_{error,1,ss} = \frac{R_{1B} i_{ref1}(R_d + R_{load}) + R_{load}(R_d i_{ref1} + V_{ref})}{k_i(R_d + R_{load})} \tag{5.10}$$

$$i_{2,ss} = -\frac{R_{load} i_{ref1} - V_{ref}}{R_d + R_{load}} \tag{5.11}$$

$$i_{error,2,ss} = \frac{R_{load}(R_d i_{ref1} + V_{ref}) + R_{2B}(-R_{load} i_{ref1} + V_{ref})}{k_i(R_d + R_{load})} \tag{5.12}$$

$$V_{bus,ss} = \frac{R_{load}(R_d i_{ref1} + V_{ref})}{R_d + R_{load}}. \tag{5.13}$$

In this steady-state result, most of the quantities are constant system parameters, or constant control values that can be chosen. The only remaining quantity that can vary is the load resistance R_{load}. Since we are looking for u as a function of V_{bus}, we can use (5.13) to solve

for the load resistance:

$$R_{load} = \frac{R_d V_{bus,ss}}{R_d i_{ref1} - V_{bus,ss} + V_{ref}}. \tag{5.14}$$

We can calculate the power supplied by Source 1 in steady state, use (5.14) to replace R_{load}, and simplify the result

$$\begin{aligned} P_{1,ss} &= V_{1s,ss} i_{1,ss} && (5.15)\\ &= \frac{-1}{R_d + \frac{R_d V_{bus,ss}}{R_d i_{ref1} - V_{bus,ss} + V_{ref}}} [i_{ref1}(-R_{1B} R_d i_{ref1} - \frac{R_{1B} R_d i_{ref1} V_{bus,ss}}{R_d i_{ref1} - V_{bus,ss} + V_{ref}} - \\ &\quad \frac{R_d^2 i_{ref1} V_{bus,ss}}{R_d i_{ref1} - V_{bus,ss} + V_{ref}} - \frac{R_d V_{bus,ss} V_{ref}}{R_d i_{ref1} - V_{bus,ss} + V_{ref}})] && (5.16)\\ &= i_{ref1}(R_{1B} i_{ref1} + V_{bus,ss}). && (5.17) \end{aligned}$$

With this steady-state power as a function of both i_{ref1} and V_{bus}, we can choose an objective function, and solve for i^*_{ref1} as a function of V_{bus} that optimally meets that objective. For example, choose an objective to have Source 1 output a constant power, regardless of how the load changes in the system,

$$J = (\hat{P} - P_{1,ss})^2 \tag{5.18}$$

where $\hat{P}$ is the desired power to be supplied from Source 1. The complete objective function

is then

$$J = (\hat{P} - i_{ref1}(R_{1B} i_{ref1} + V_{bus,ss}))^2. \tag{5.19}$$

Taking the derivative with respect to V_{bus} and setting the result equal to zero results in

$$0 = 2 i_{ref1}(-\hat{P} + i_{ref1}(R_{1B} i_{ref1} + V_{bus,ss})). \tag{5.20}$$

Solving for the optimal i^*_{ref1} gives the optimal relationship for reference current with respect to bus voltage, desired output power, and line resistance,

$$i^*_{ref1} = \frac{-V_{bus} + \sqrt{4\hat{P}R_{1B} + V^2_{bus}}}{2R_{1B}} \tag{5.21}$$

5.2.2 Step Change in Load

To test the proposed droop control scheme, the example microgrid described above was modeled using MATLAB/Simulink. The system was first simulated using a traditional droop control technique for both sources, then repeated using the optimal droop control relationship found above for Source 1, for various test cases. For this simulation, a more complete model of the microgrid was implemented, including the power electronic components that connect the sources to the bus. The source model is shown in Fig. 4.1. All

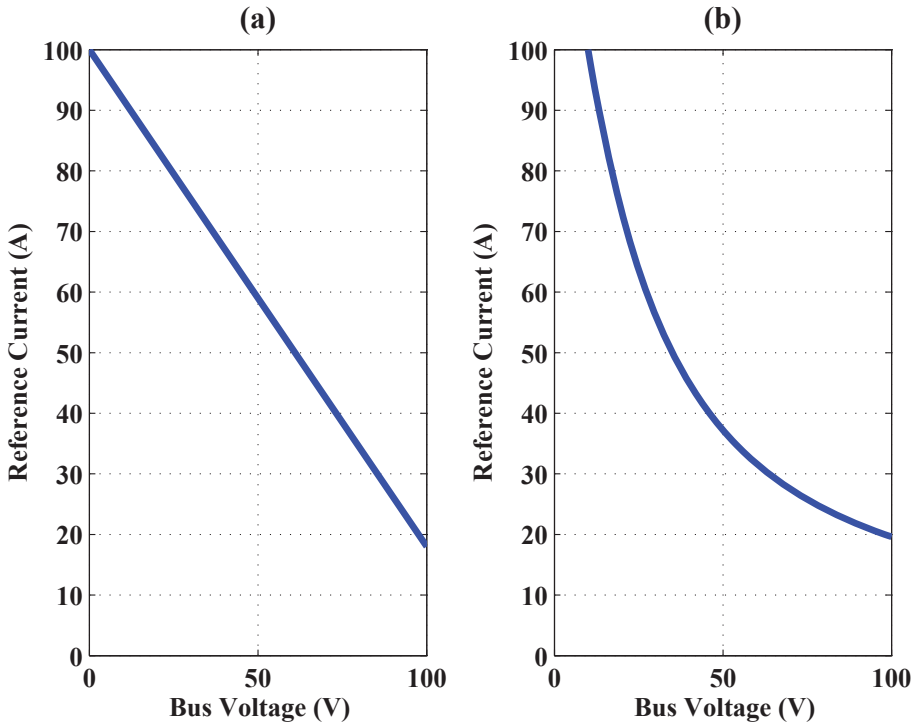

Figure 5.2: Droop control relationships: (a) traditional; (b) optimal.

power electronics are modeled using average mode methods [80], as described in Ch. 3.

For all test cases, a constant desried output of 2000 W from Source 1, and a line resistance R_{1B} of 0.1 Ω, are implemented in the optimal reference current relationship found in (5.21). Fig. 5.2 shows the traditional linear droop control used in the first simulation, and the optimal droop control that was implemented in the second simulation, for each case.

5.2.2.1 Simulation Results

For an initial test case, a step increase in load power was simulated (a step decrease in load resistance). The change in load resistance occurred at $t = 0$ during the simulation, and is

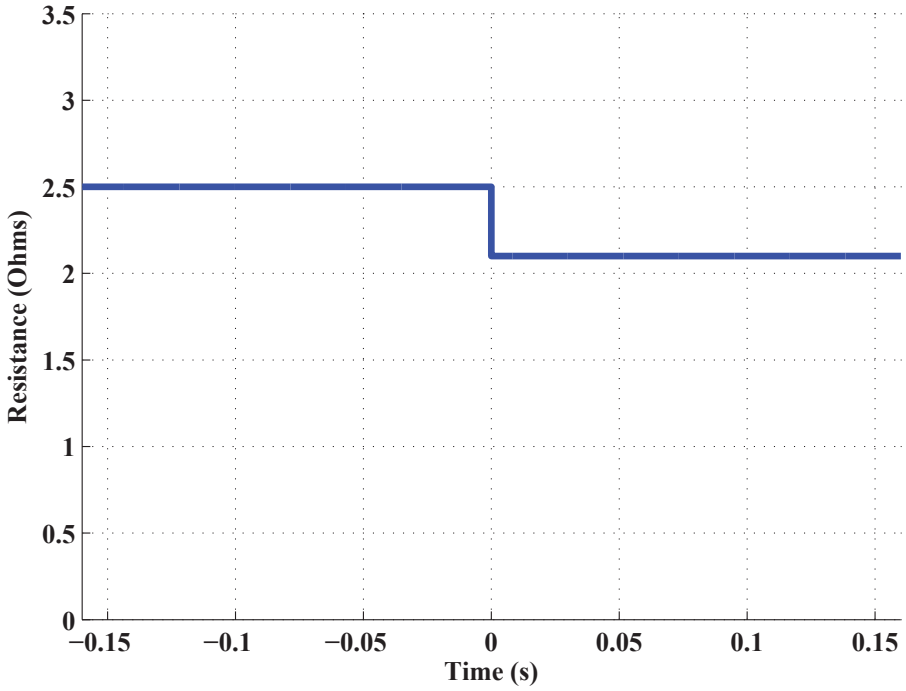

Figure 5.3: Step change in load implemented in both simulation and hardware-in-the-loop.

shown in Fig. 5.3.

Fig. 5.4 shows the power supplied by Sources 1 and 2 during this simulation, as the step change in load occurs. The results using traditional linear droop control are shown first, along with the results of using the optimal droop control relationship. With traditional droop control, both sources increase their output to share the increase in load. With this new droop control method, Source 1 continues to supply the desired constant 2000 W, while Source 2 increases its output to supply the increase in load.

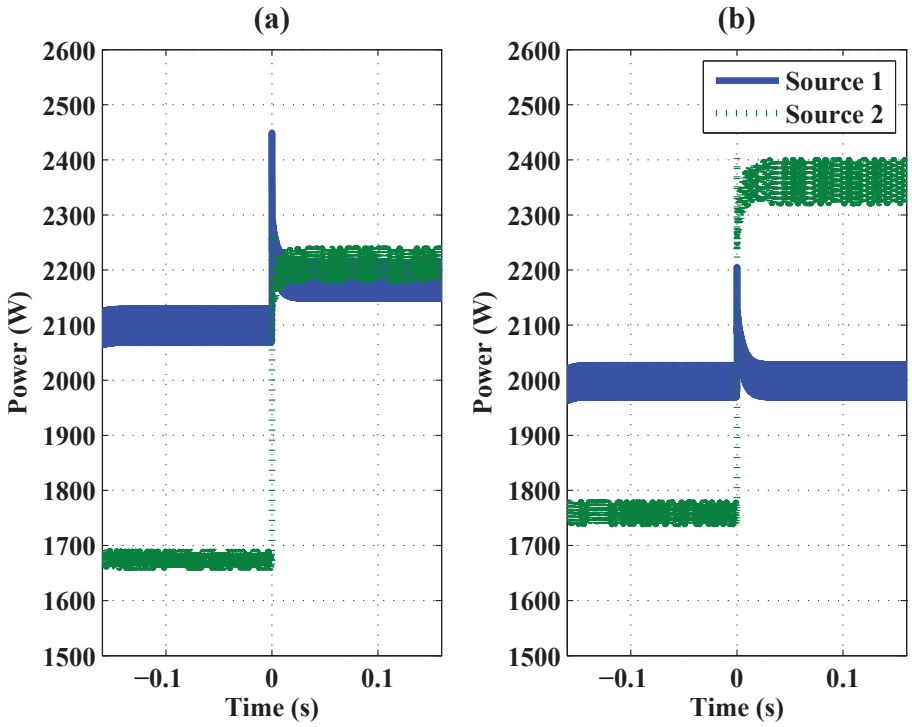

Figure 5.4: Simulation results for power supplied by Sources 1 and 2 with step change in load: (a) traditional; (b) optimal.

5.2.2.2 Hardware-in-the-Loop Results

In order to verify the simulation results presented in the previous section, the same example microgrid was implemented using a hardware-in-the-loop (HIL) approach, as described in Ch. 3. For the HIL experiment, all power electronics switching was included, along with parasitic inductances and capacitances. The circuit schematic used in the Typhoon software is shown in Fig. 5.5. The numeric parameter values are the same as those used in simulation, and shown in Tables 4.1 - 4.5.

First, traditional linear droop control was implemented for both sources, as in (5.8). The

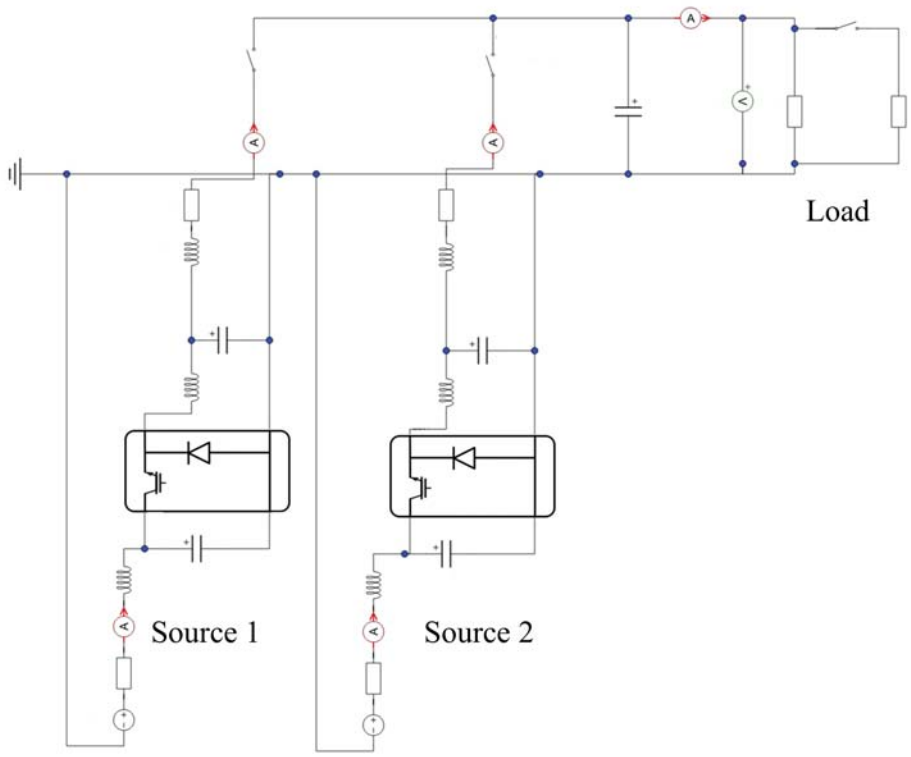

Figure 5.5: Hardware-in-the-loop schematic for small microgrid example.

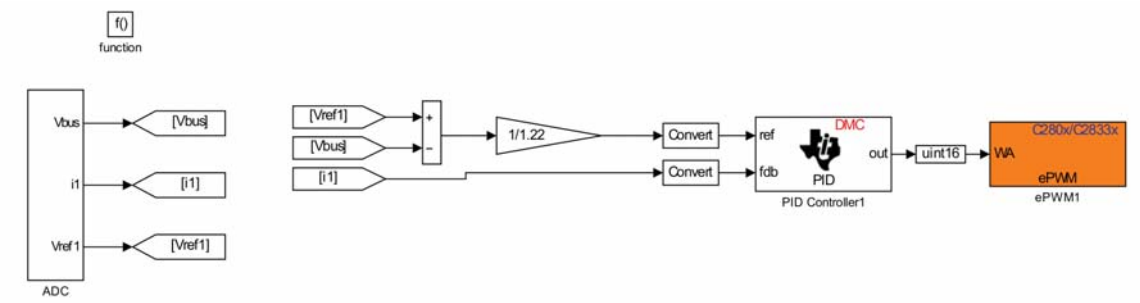

Figure 5.6: HIL controller for Source 1 - traditional droop.

controllers implemented for each of the two sources are shown in Figs. 5.6 and 5.7. As described in Ch. 3, the operation of each source is controlled by a separate Texas Instruments ControlCARD throuh the MATLAB/Simulink Embedded Coder.

The same step change in load that was used in the simulation was also implemented here.

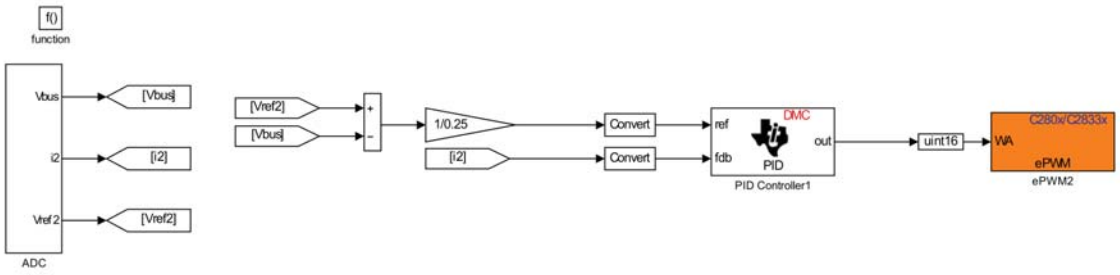

Figure 5.7: HIL controller for Source 2 - traditional droop.

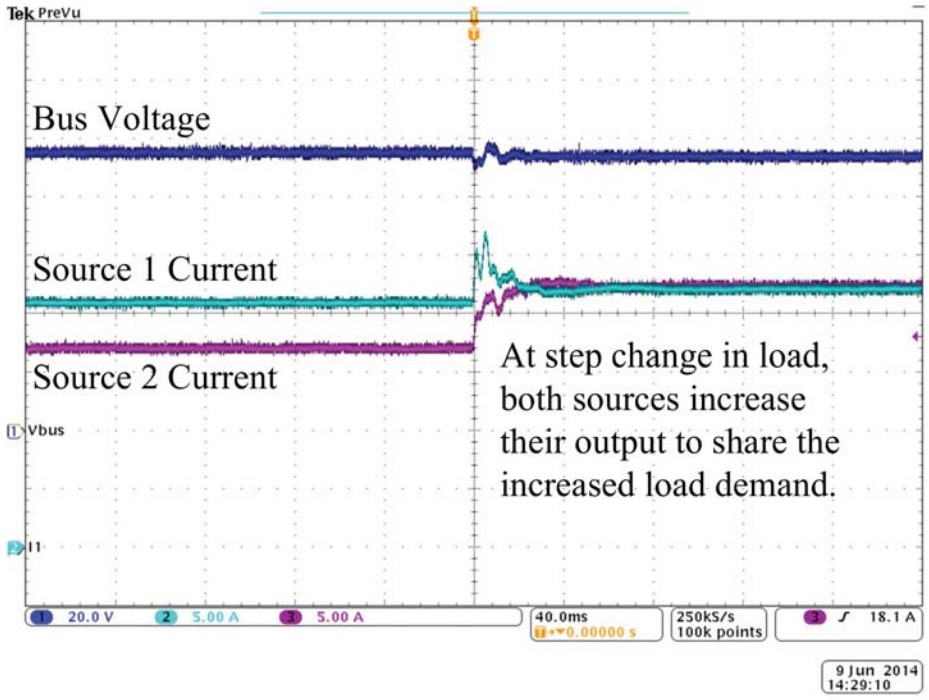

Figure 5.8: Hardware-in-the-loop results with traditional droop control during a step change in load: Ch1 Bus Voltage; Ch2 Source 1 Current; Ch3 Source 2 Current.

The results for the microgrid bus voltage, and the currents supplied by Source 1 and Source 2 are shown in Fig. 5.8. Both currents share the same zero point on the oscilloscope trace. As in the simulation results with traditional droop control, when a step increase in the load occurs, both sources increase their output and share the additional load.

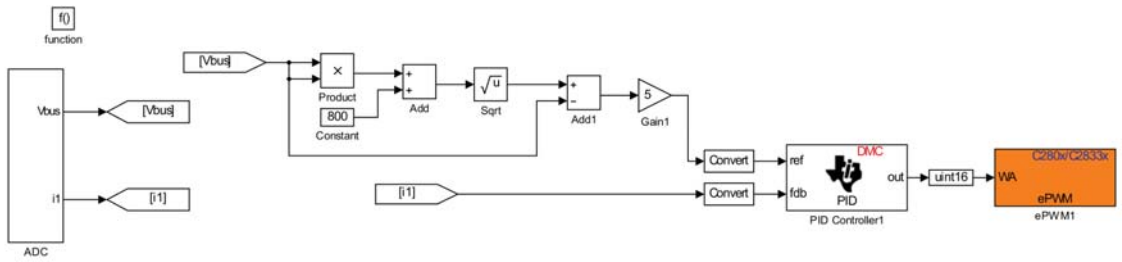

Figure 5.9: HIL controller for Source 1 - optimal droop.

Next, the optimal droop control relationship (5.21) was implemented with Source 1, while Source 2 continued to operate with traditional linear droop control. The new controller implemented for Source 1 is shown in Fig. 5.9.

The results of implementing the same step increase in load are shown in Fig. 5.10. As desired, the current supplied from Source 1 changes only slightly, so that Source 1 continues to output a nearly constant 2000 W. Source 2 supplies additional current in order to meet the increased load.

5.2.2.3 Comparison of Results

The data from the oscilloscope traces in Figs. 5.8 - 5.10 was imported and plotted using MATLAB, along with the simulation results presented earlier. This allows for a direct comparison for the same scenario that was both simulated and implemented using HIL.

Fig. 5.11 shows the microgrid bus voltage using traditional droop, and optimal droop control. The simulation and HIL results for each case are plotted together, and the average

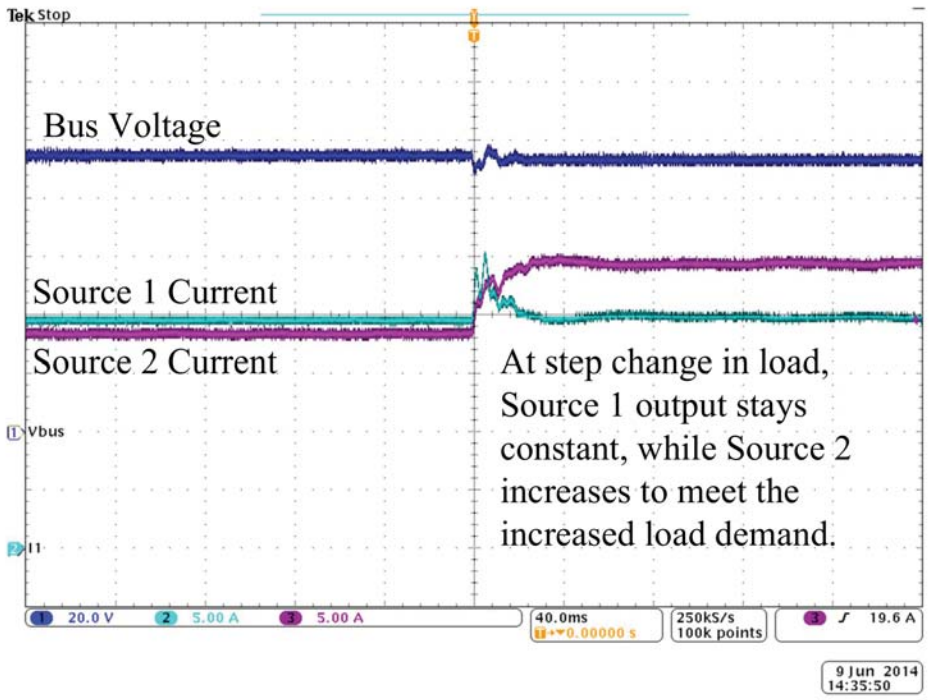

Figure 5.10: Hardware-in-the-loop results with optimal droop control during a step change in load: Ch1 Bus Voltage; Ch2 Source 1 Current; Ch3 Source 2 Current.

values match closely.

Figs. 5.12 and 5.13 show the current supplied by Source 1 and Source 2, respectively. Simulation and HIL results are plotted together for both traditional and optimal droop control. While the general shape of the current waveforms match for both simulation and HIL, there is a small error, especially for Source 1. Many factors may contribute to this difference, including the fact that the power electronics were simulated in average mode, while actual switching is emulated through the HIL.

Plotting the simulation and HIL results together in Figs. 5.11 - 5.13 shows that the HIL

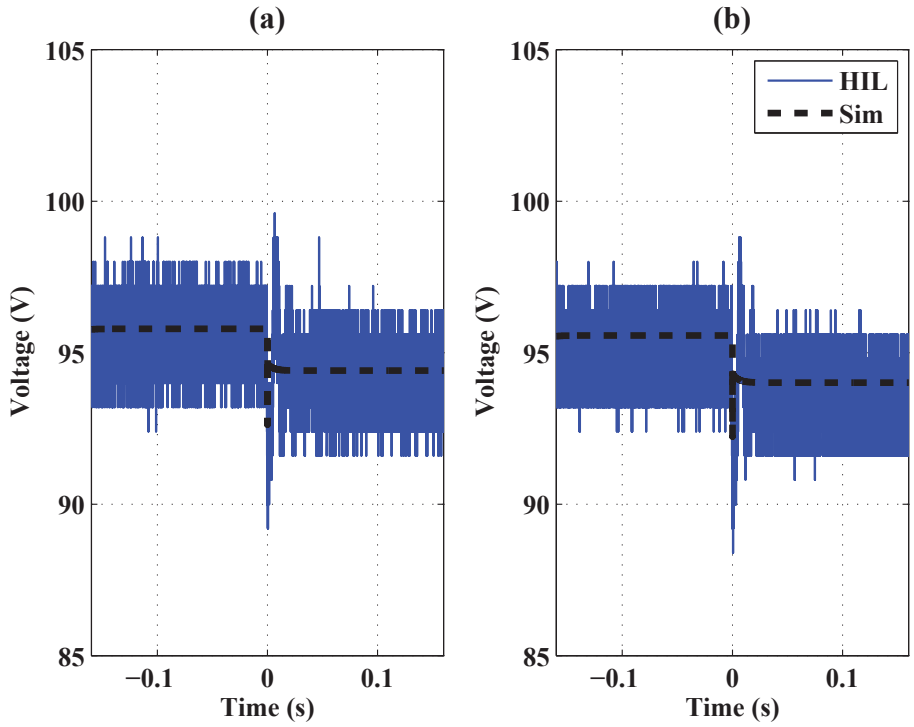

Figure 5.11: Simulation and hardware-in-the-loop results for bus voltage during a step change in load: (a) traditional; (b) optimal.

results validate the simulation using the proposed optimal droop control method. The advantage of using a HIL in the development and testing of this proposed control system is a substantial decrease in development time and cost. Since the controls have been thoroughly tested and verified with the HIL, the control algorithms in the TI ControlCARDs can be directly applied to a full hardware system with a high confidence.

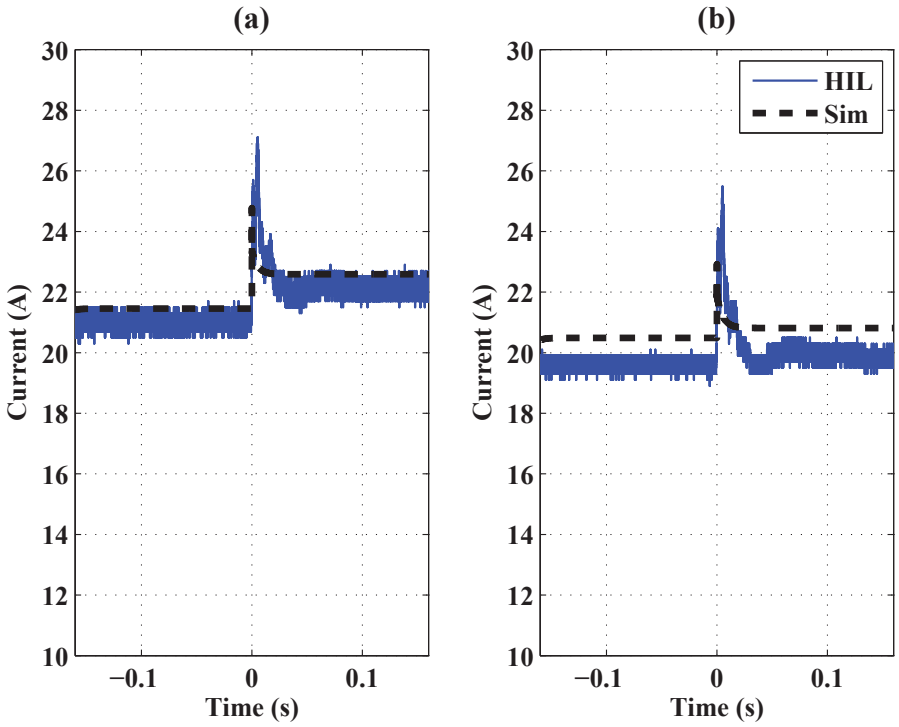

Figure 5.12: Simulation and hardware-in-the-loop results for Source 1 current during a step change in load: (a) traditional; (b) optimal.

5.2.3 Varying Load Profile

For a more realistic test case, a timeframe of one day was simulated, and a day long load profile was chosen by scaling actual data from an existing power system [91]. The load resistance profile over this 24 hour time period is shown in Fig. 5.14.

Fig. 5.15 shows the power supplied by Sources 1 and 2 over a 24 hour period with a varying load. The results using traditional linear droop control are shown first, along with the results of using the optimal droop control relationship. With this new droop control method, Source 1 supplies the desired constant power even as the load changes.

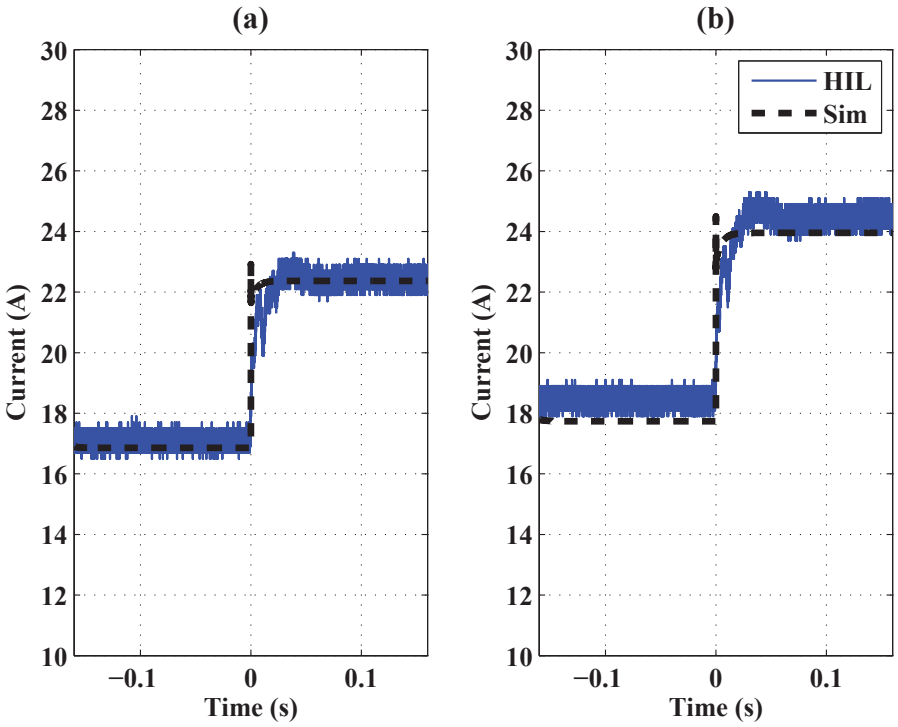

Figure 5.13: Simulation and hardware-in-the-loop results for Source 2 current during a step change in load: (a) traditional; (b) optimal.

The bus voltage during both simulations is shown in Fig. 5.16. The bus voltage follows a similar changing profile whether traditional or optimal droop control is implemented for Source 1, although it is slightly lower overall when optimal droop control is used.

5.3 Example in Three Dimensions

This section expands the planar optimization method described in Ch. 4 to find an optimal droop relationship in three dimensions, where the reference current for the source depends on both the bus voltage and the wind speed.

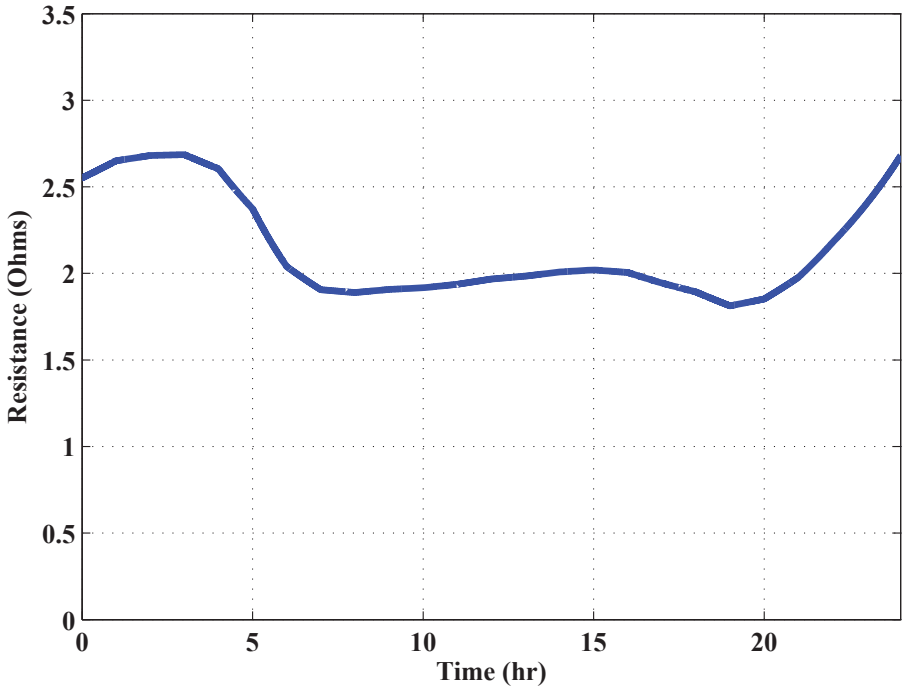

Figure 5.14: Simulated load profile over a 24 hour period.

5.3.1 Optimization of High Dimension Droop Control

The results in the previous section demonstrate an optimal droop relationship based on an objective of supplying constant power from a source. In this section, the objective will be for the source to meet a power amount that is changing over time. For example, for a wind resource, an objective could be to use all of the power available from the wind, based on the wind speed at the current time. In this case, $\hat{P}$ is a function of wind speed, rather than a constant. The optimal equation for reference current from (5.21) becomes

$$i^*_{ref1} = \frac{-V_{bus} + \sqrt{4\hat{P}(w)R_{1B} + V^2_{bus}}}{2R_{1B}} \tag{5.22}$$

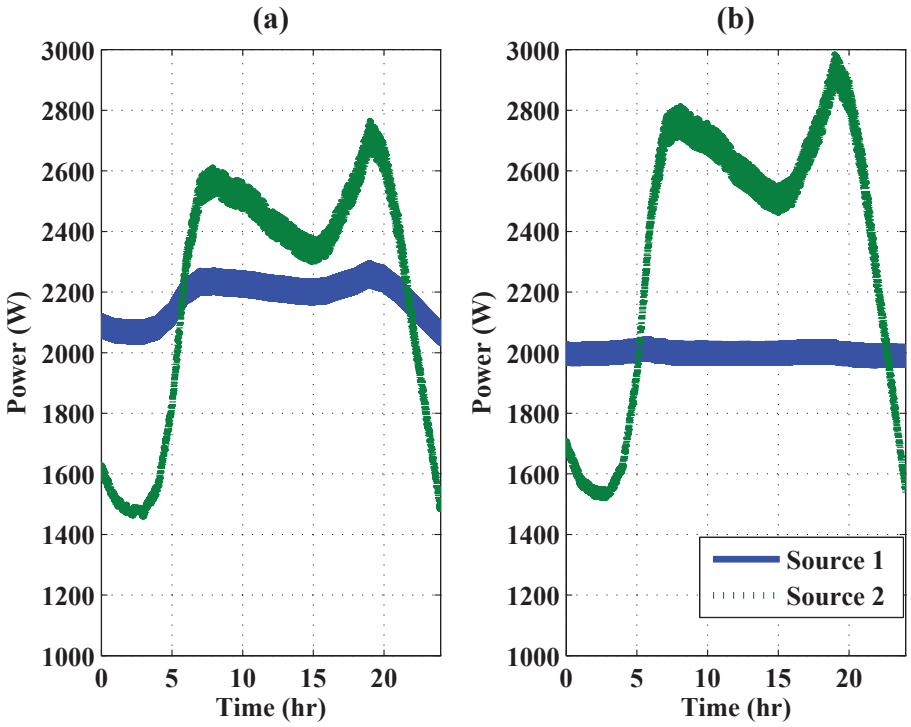

Figure 5.15: Simulation results for power supplied by Sources 1 and 2 with varying load: (a) traditional; (b) optimal.

where w is the wind speed.

For this example, a 2 kW wind turbine is simulated. The power curve for the turbine is shown in Fig. 5.17; this relationship is used to replace $\hat{P}(w)$ in (5.22).

5.3.2 Step Change in Wind

For an initial test case, a step change in wind speed from 10 m/s to 13 m/s was implemented in both simulation and hardware-in-the-loop. Fig. 5.18 shows this step change in wind speed, along with the associated step change in power available from the wind, based on

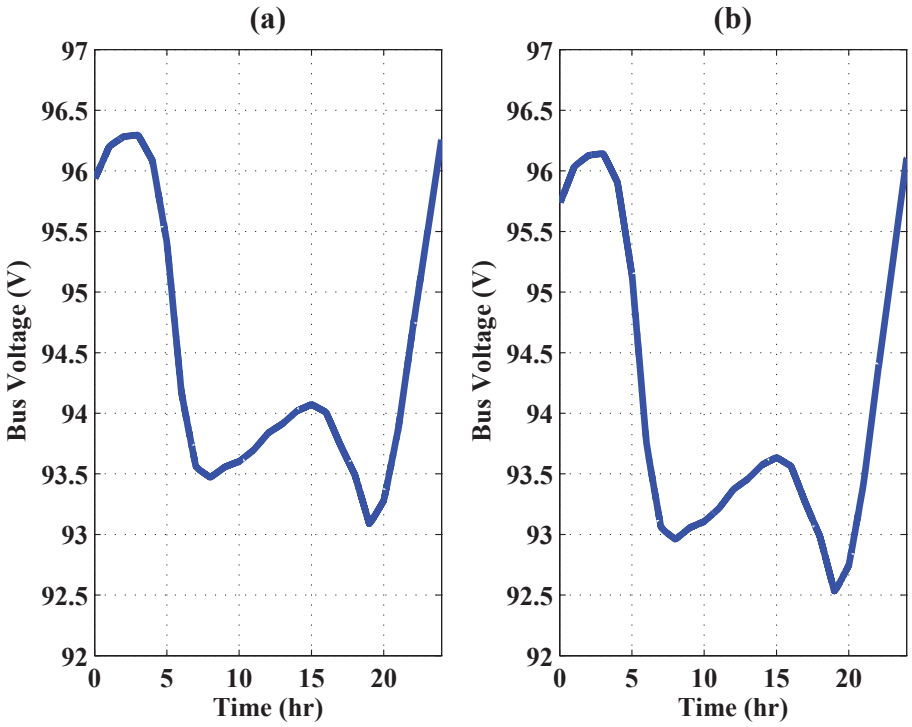

Figure 5.16: Simulation results for microgrid bus voltage with varying load: (a) traditional; (b) optimal.

Fig. 5.17.

5.3.2.1 Simulation Results

The system was simulated using the optimal high dimension droop control relationship found above in (5.22). Fig. 5.19 shows the power supplied by each source during the simulation. When the wind speed is increased at $t = 0$, the power supplied by Source 1 increases to match the new level of available power from the wind.

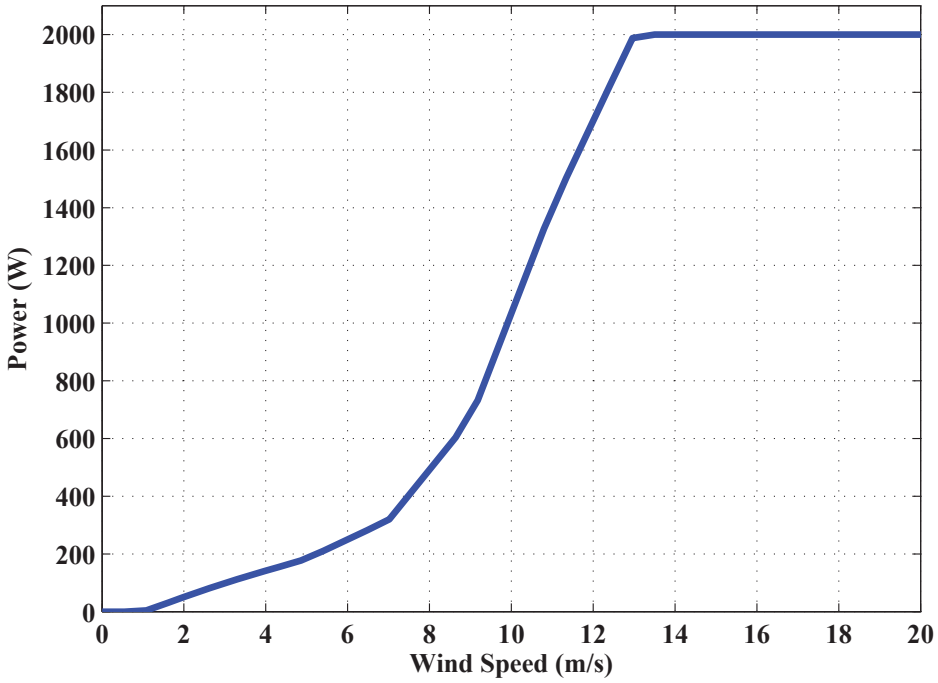

Figure 5.17: Power curve for 2 kW wind turbine.

5.3.2.2 Hardware-in-the-Loop Results

The optimal high dimension droop control relationship in (5.22) was implemented in hardware-in-the-loop in the same manner described in Ch. 3. The same step change in wind speed that was used in the simulation was also implemented here. The HIL schematic and traditional droop control implementation were the same as in Figs. 5.5 and 5.7. The optimal droop controller implemented for Source 1 is shown in Fig. 5.20.

The results for the microgrid bus voltage, and the currents supplied by Source 1 and Source 2 are shown in Fig. 5.21. Both currents share the same zero point on the oscilloscope trace.

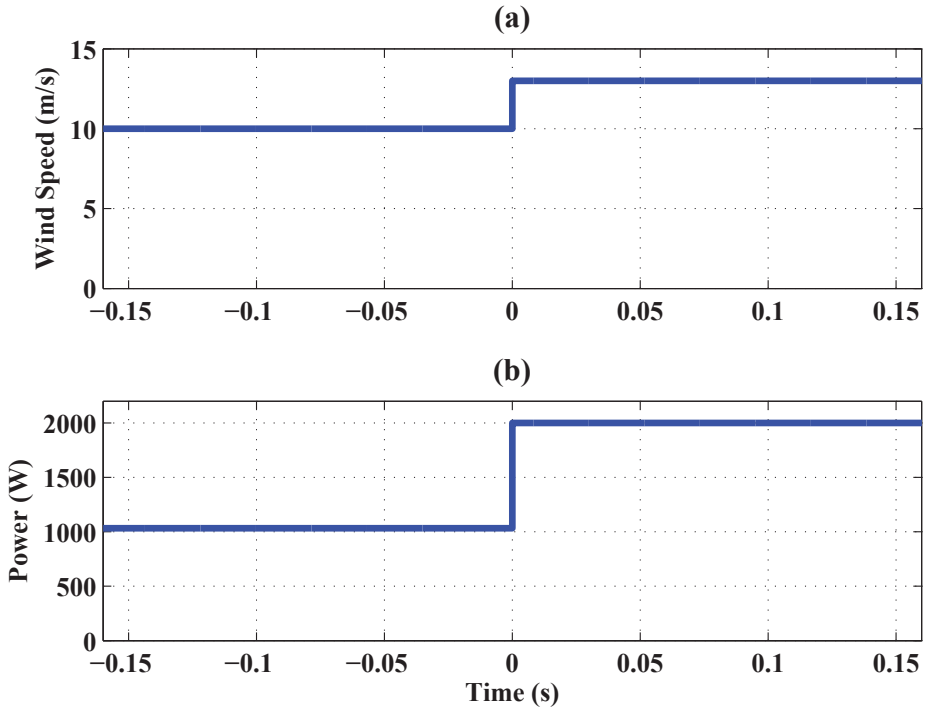

Figure 5.18: Step in change in (a) wind speed and (b) power available from the wind, implemented in both simulation and hardware-in-the-loop.

As in the simulation results with traditional droop control, when a step increase in the wind speed occurs, Source 1 increases its output based on the increased power available from the wind. Source 2 decreases its output so that the two sources together share the load, which is constant for this example.

5.3.2.3 Comparison of Results

The data from the oscilloscope traces in Fig. 5.21 was imported and plotted using MATLAB, along with the simulation results presented earlier. This allows for a direct comparison for the same scenario that was both simulated and implemented using HIL.

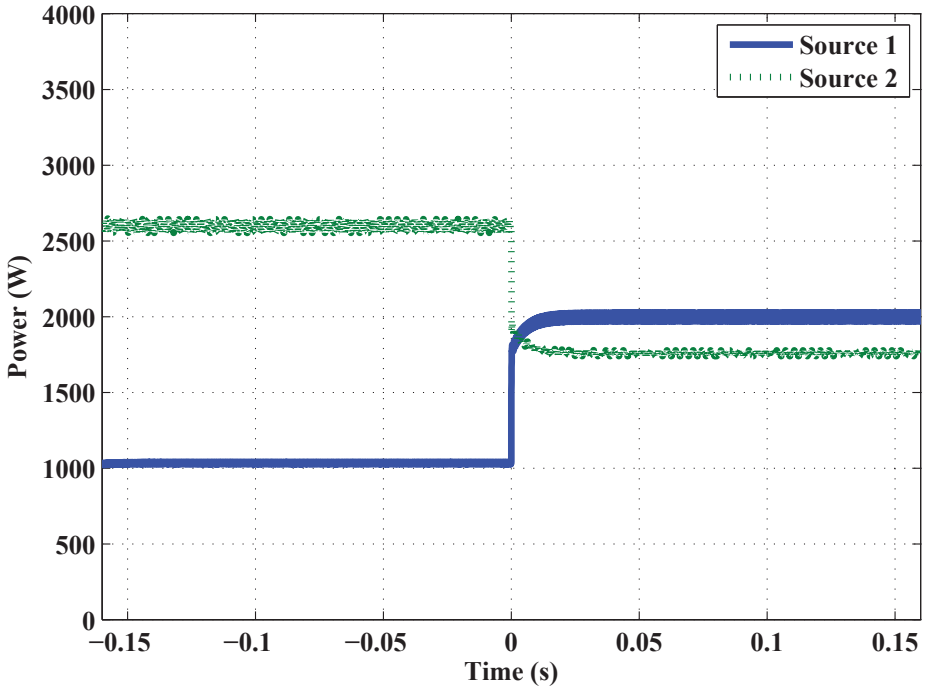

Figure 5.19: Simulation results for power supplied by Sources 1 and 2 during a step change in wind speed.

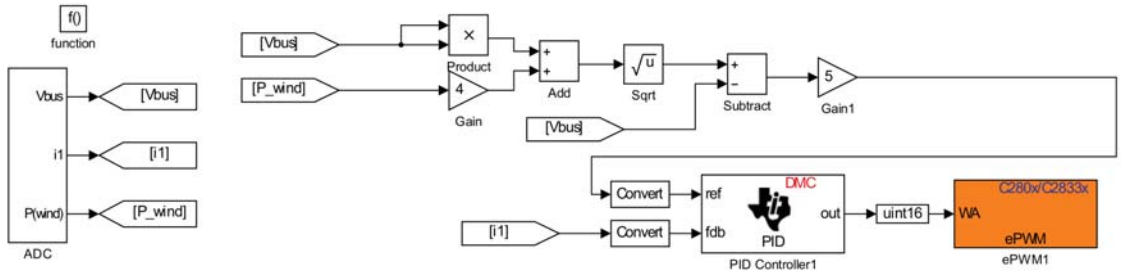

Figure 5.20: HIL controller for Source 1 - optimal high dimension droop.

Fig. 5.22 shows the microgrid bus voltage during the step change in wind speed. The simulation and HIL results are plotted together. While the general shape of the voltage waveforms match for both simulation and HIL, there is a small error. Many factors may contribute to this difference, including the fact that the power electronics were simulated in average mode, while actual switching is emulated through the HIL.

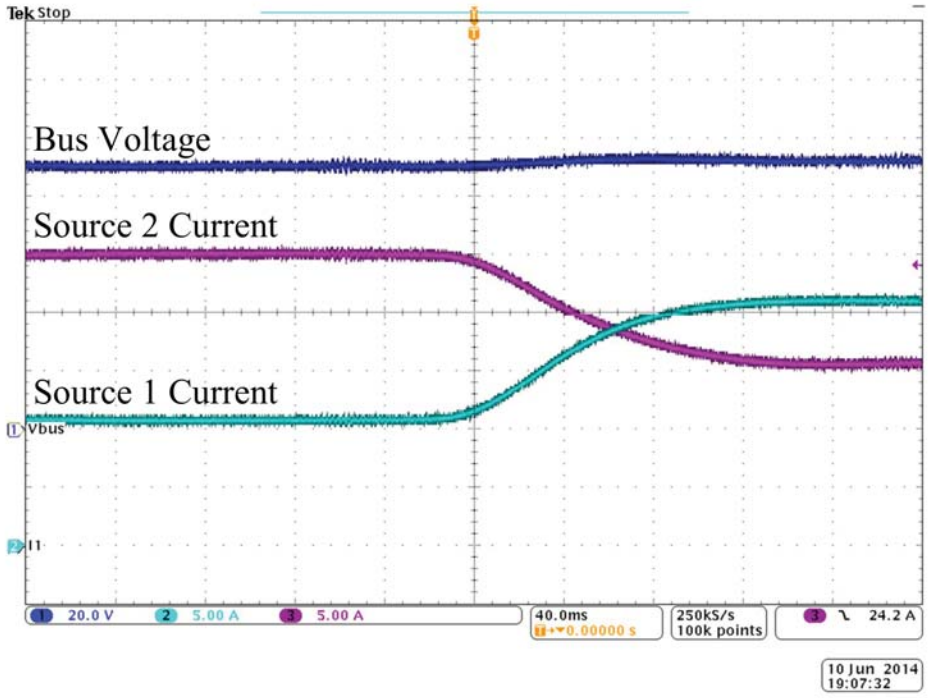

Figure 5.21: Hardware-in-the-loop results with optimal high dimension droop control during a step change in wind speed: Ch1 Bus Voltage; Ch2 Source 1 Current; Ch3 Source 2 Current.

Figs. 5.23 and 5.24 show the current supplied by Source 1 and Source 2, respectively. Simulation and HIL results are plotted together. The simulation and HIL steady-state values of current before and after the step change in wind speed match, however the two sets of results do not match during the transient event. This is due to the fact that different time constants were used in the simulation and HIL experiments. The proportional and integral gains for the PI controller in simulation and HIL were also not tuned for achieving a very fast transient response. Since the control methods proposed in this dissertation are designed for use over large time periods, the difference found between simulation and HIL results for this test of a very small time period was not a key concern for this research.

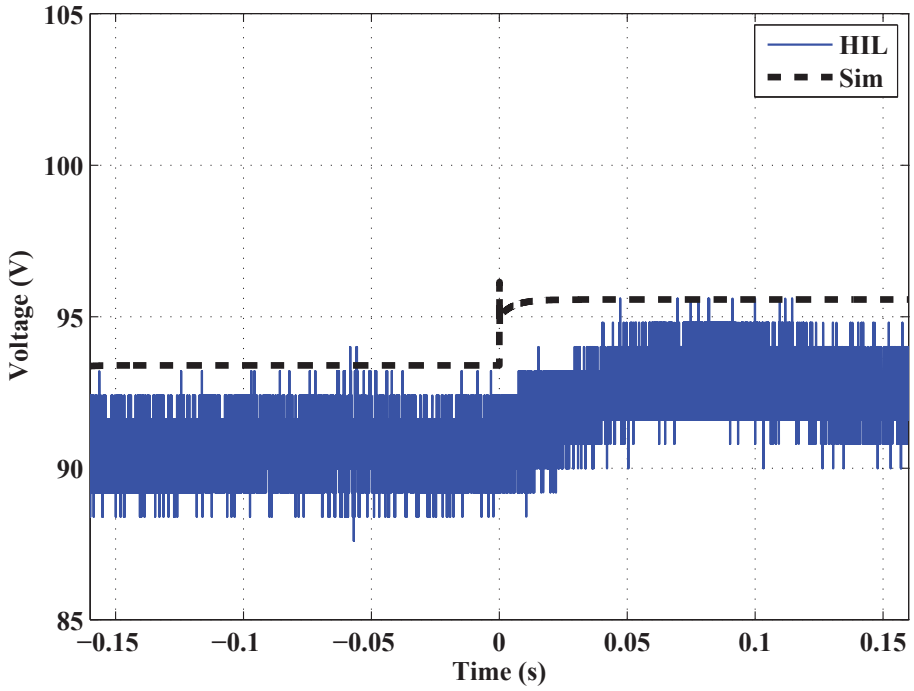

Figure 5.22: Simulation and hardware-in-the-loop results for bus voltage during a step change in wind speed.

5.3.3 Varying Wind and Load Profiles

The example microgrid shown in Fig. 5.1 was simulated using the same average load and wind speed profiles from Ch. 4, shown in Fig. 4.9. The system was simulated with three controllers: first using traditional linear droop control, then using the high dimension droop control method demonstrated in Ch. 4, and finally using the optimal high dimension droop control method described here. The results of the three simulations are presented and compared in this section.

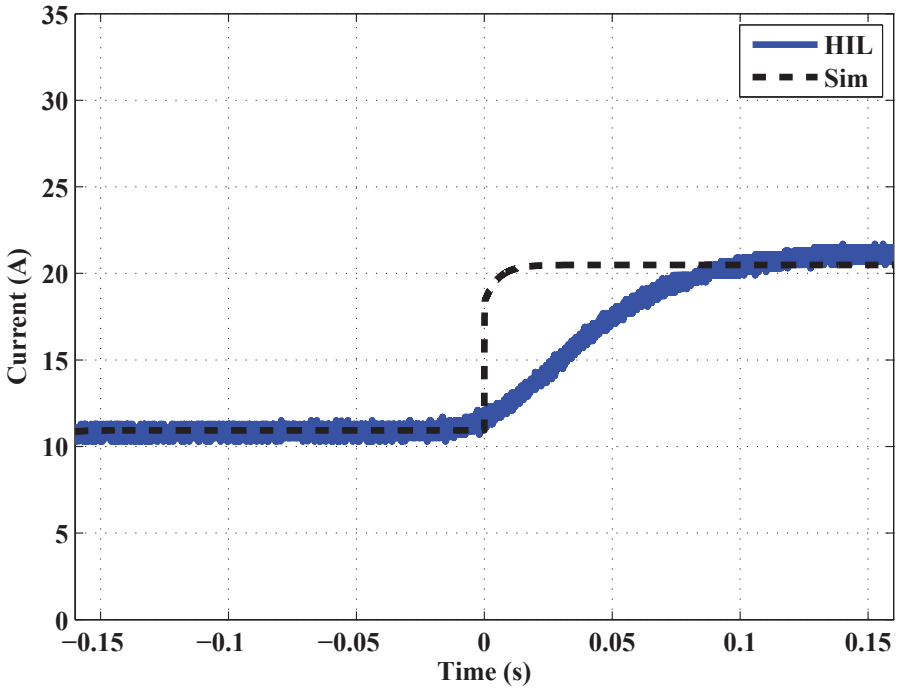

Figure 5.23: Simulation and hardware-in-the-loop results for Source 1 current during a step change in wind speed.

5.3.3.1 Traditional Droop Control

First, the system was simulated using a traditional linear droop control relationship as shown in Fig. 5.25. Fig. 5.26 shows both the power available from the wind, and the power utilized from the wind over the simulation. Much of the available wind power goes unused with this control method.

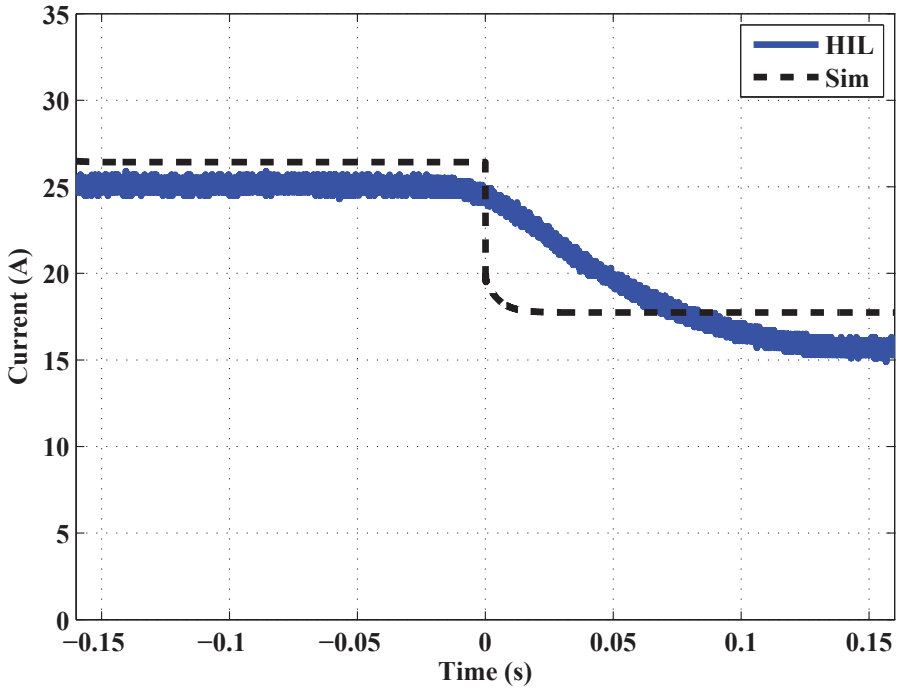

Figure 5.24: Simulation and hardware-in-the-loop results for Source 2 current during a step change in wind speed.

5.3.3.2 High Dimension Droop Control

Next, the system was simulated using a plane in three dimensions as the droop control relationship, shown in Fig. 5.27. Fig. 5.28 shows both the power available from the wind, and the power utilized from the wind over the simulation. More of the available wind power is utilized with this method, while the benefits of traditional droop control are maintained.

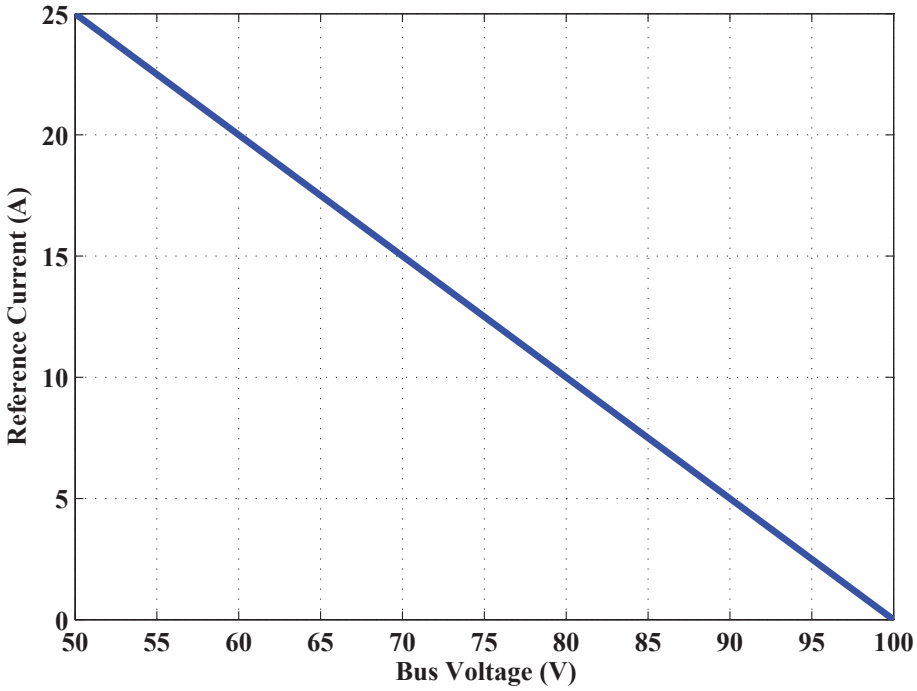

Figure 5.25: Traditional linear droop control for microgrid simulation.

5.3.3.3 Optimal High Dimension Droop Control

Finally, the system was simulated using the optimal droop relationship (5.22) to minimize the wasted power available from the wind, shown in Fig. 5.29. For wind speeds from 0 to 13 m/s, (5.22) defines the optimal droop surface shown in the figure. At wind speeds above 13 m/s, the wind turbine has reached its maximum power output of 12 kW, so $\hat{P}(w)$ becomes constant, and the surface no longer varies with wind speed.

Fig. 5.30 shows both the power available from the wind, and the power utilized from the wind over the simulation. The power used from the wind matches closely with the power

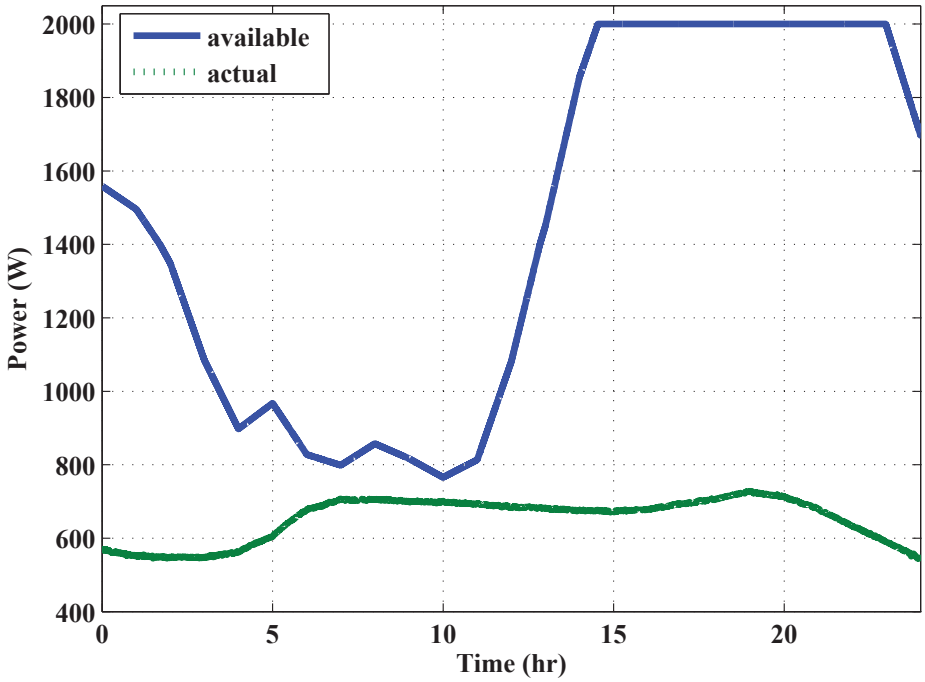

Figure 5.26: Power available and utilized from the wind using traditional linear droop control.

available, and very little available wind power is wasted. Again, the benefits of traditional droop control are maintained, and no communication link is needed between the wind resource and other components in the microgrid.

5.3.3.4 Comparison of Simulation Results

For each of the three simulation cases above, the unused power from the wind source was summed over the 24 hour simulation time period. A comparison of the amount of unused energy for each case is shown in Table 5.2. Using high dimension droop control (a plane) decreases the unused energy to almost half of that for traditional linear droop control. Using

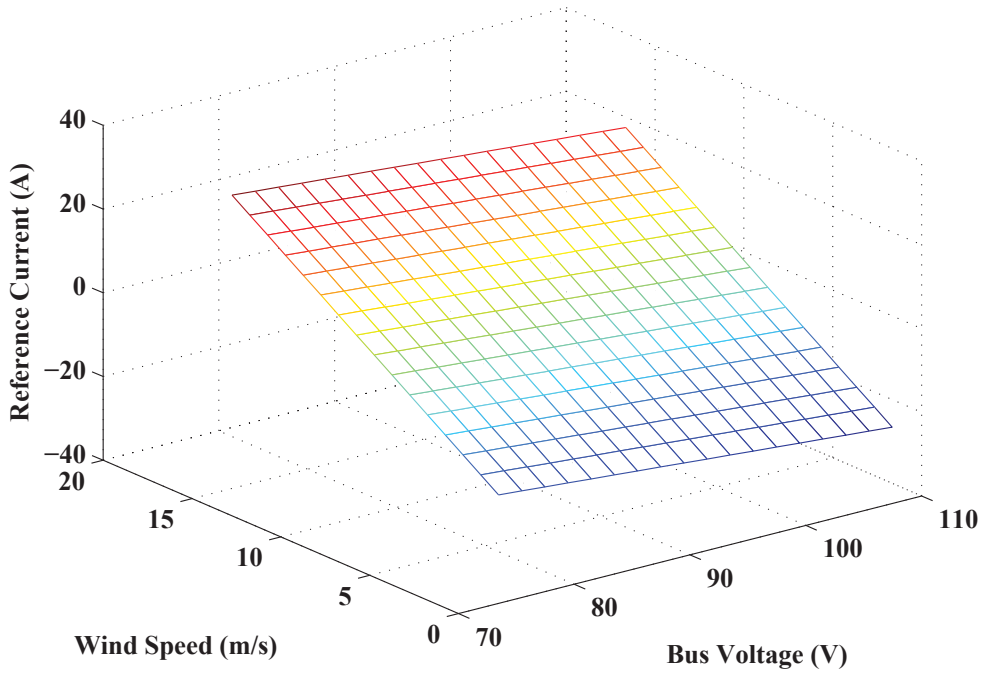

Figure 5.27: High dimension droop control for microgrid simulation.

Table 5.2
Comparison of unused energy from the wind for three droop control methods.

Droop Control Strategy	Reference Current Equation	Unused Energy (W-hr)
Linear	$i_{ref1} = \frac{V_{ref} - V_{bus}}{R_d}$	19,050
Planar	$i_{ref1} = \frac{V_{ref} - V_{bus}}{R_{d1}} + \frac{v_w}{R_{d2}}$	8,662
Optimal Surface	$i_{ref1} = \frac{-V_{bus} + \sqrt{4\hat{P}(w)R_{1B} + V_{bus}^2}}{2R_{1B}}$	279

the optimized droop surface for the wind source decreases the unused energy to nearly zero.

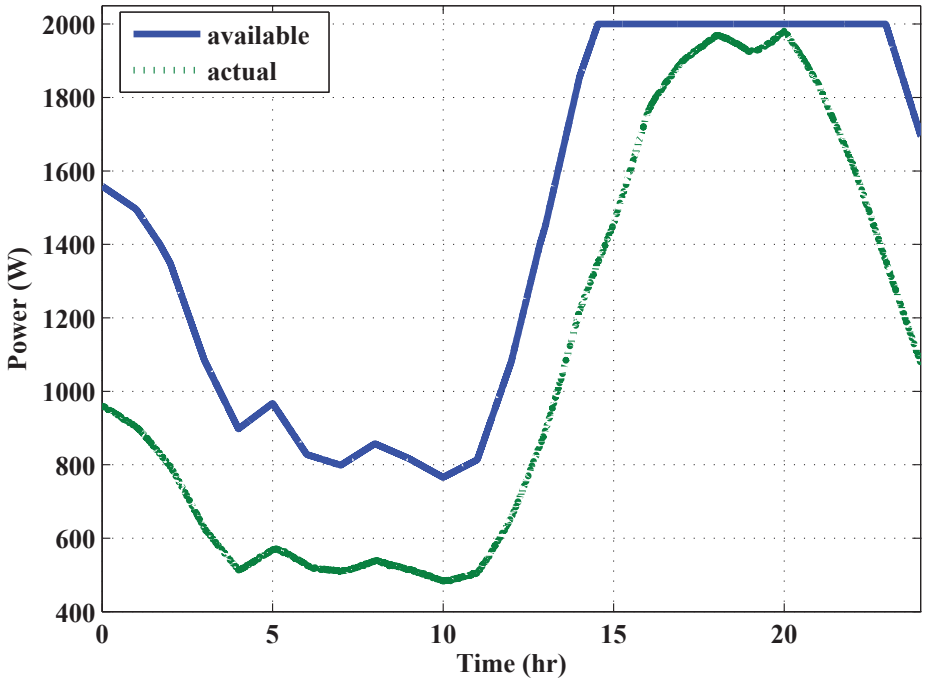

Figure 5.28: Power available and utilized from the wind using high dimension droop control.

5.4 Optimal High Dimension Droop Control Conclusions

The results presented in this chapter show that the droop control relationship for a source in a dc microgrid can be optimized to meet a given objective. An example microgrid was simulated and demonstrated through HIL, and the results show that a droop control relationship can be chosen to keep the power supplied by a source constant. The optimization method can then be expanded to multiple dimensions, and a droop control relationship can be chosen to allow the power supplied by a source to match the power available from the wind.

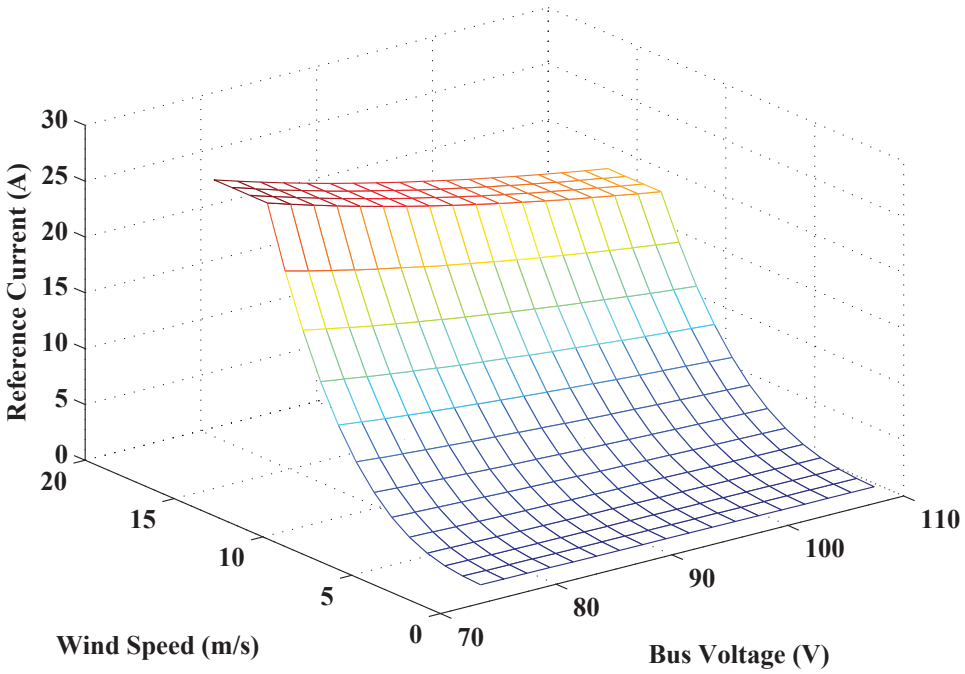

Figure 5.29: Optimal high dimension droop control for microgrid simulation.

This control method retains the advantages of traditional droop control, and does not require a communication link between the system components. It also allows all of the power available from the wind to be utilized, which is an improvement over traditional droop control, and over high dimension droop control using a plane. The droop control surface is optimized for general operation of the system - it is not necessary to know the expected wind speed and load profiles in order to determine the surface shape.

The work presented in this chapter is confined to a simple dc microgrid example with two sources and one load. The following chapter will implement the optimal high dimension droop control method in a more robust example system containing energy storage, and

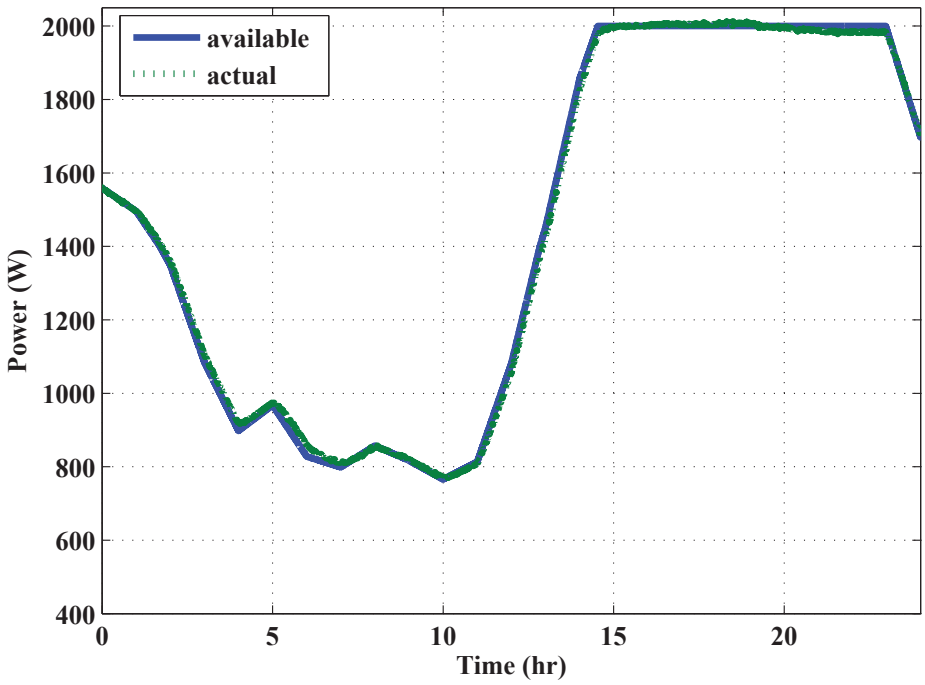

Figure 5.30: Power available and utilized from the wind using optimal high dimension droop control.

demonstrate its use in a military forward operating base application.

Chapter 6

Multidimensional Optimal Droop Control - Applications and Examples

The previous chapter presented a method for finding an optimal droop control surface in three dimensions to meet the objective of minimizing the unused energy from a wind resource. The method was demonstrated using a small example microgrid containing two sources and one load. This chapter will demonstrate the optimal high dimension droop control method for additional example microgrids, and for a military patrol base (PB) application.

6.1 Full Microgrid Example

The example microgrid from Chapter 4 is used in this chapter to demonstrate optimal high dimension droop control on a more complete example system. The details of the modeling method used for each component in the microgrid can be found in Chapter 4, and the full microgrid model is shown in Fig. 6.1. The numeric parameter values are the same as those used in 4, and shown in Tables 4.1 - 4.5.

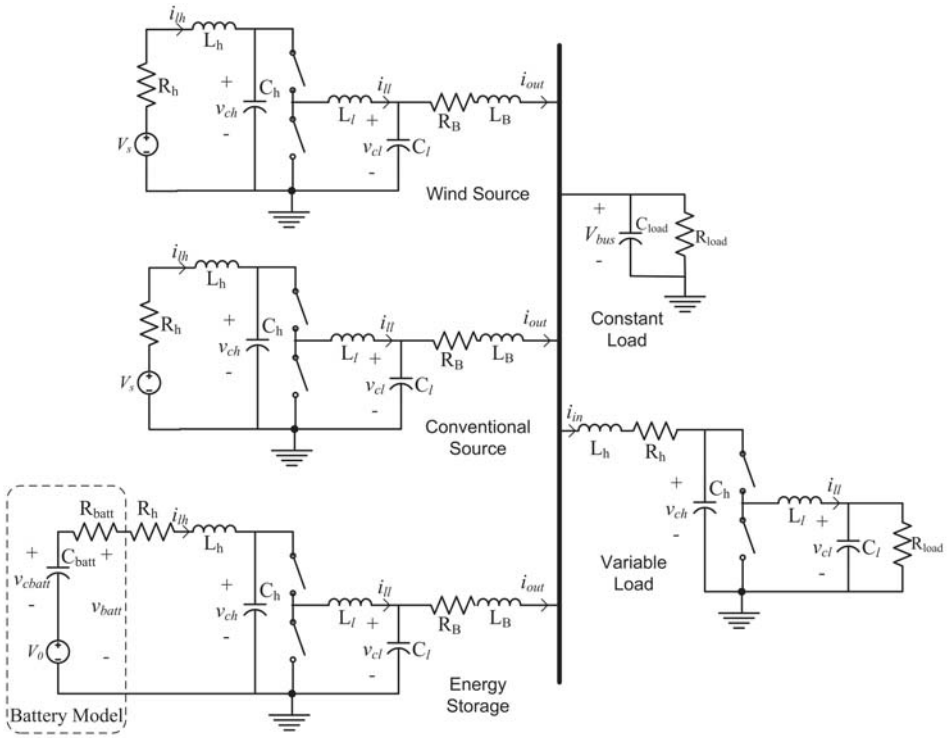

Figure 6.1: Example microgrid for demonstration of droop control methods.

6.1.1 Varying Wind and Load Profiles

The full example microgrid was simulated three times - first with traditional linear droop control, then with high dimension droop control using a plane, and finally with optimal high dimension droop control using a surface. The results using each type of control are presented in the following sections. The system was modeled for a 24 hour period, using the wind speed and load profiles shown in Fig. 6.2.

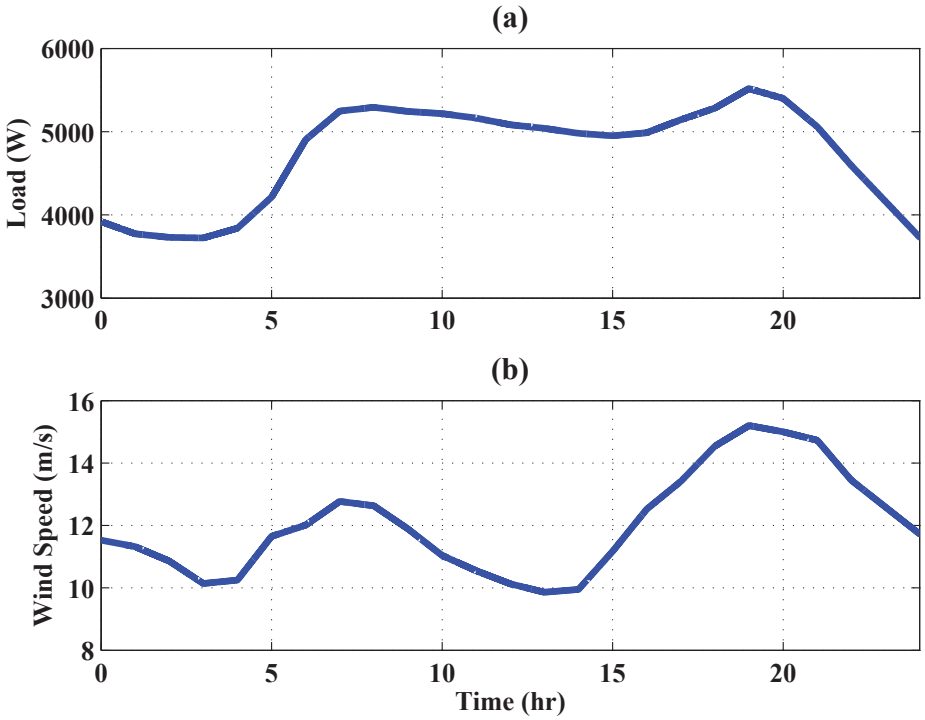

Figure 6.2: (a) Load and (b) wind speed profiles for simulated 24 hour period.

6.1.1.1 Traditional Droop Control

First, the system was simulated using traditional, linear droop control for both sources, and for the battery. The droop control relationships are shown in Fig. 6.3. The conventional source and the energy storage device will keep their same linear droop control settings for all three of the simulations.

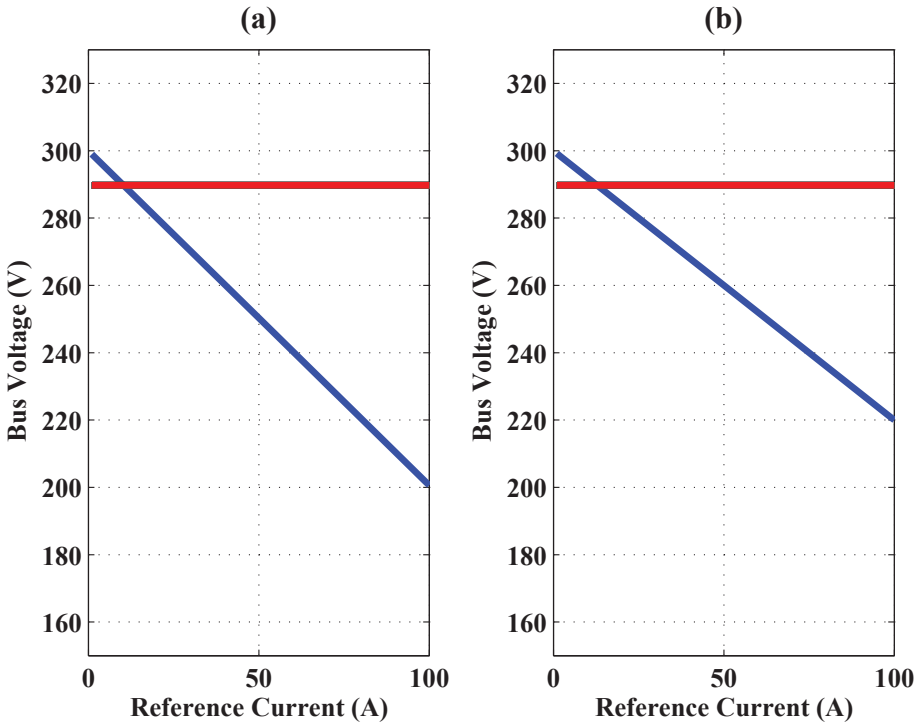

Figure 6.3: Linear droop control relationships for (a) wind source and (b) conventional source for first simulation.

The results of simulating the system are shown in Fig. 6.4. Both sources share the load, and the wind resource does not change its operation based on the wind speed. The battery is needed throughout the day to provide additional power to the system.

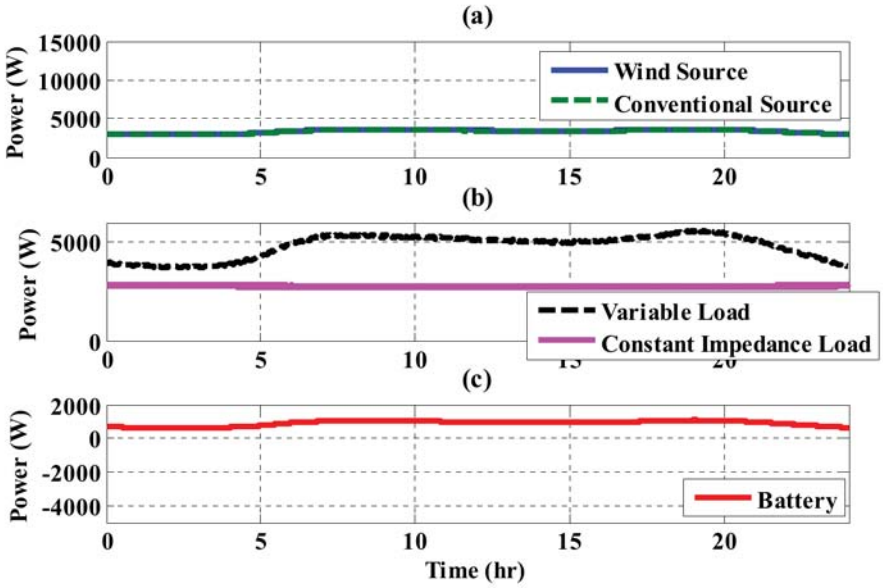

Figure 6.4: Simulation results using traditional droop control: (a) power supplied by each source, (b) power consumed by each load, and (c) power supplied by the battery.

6.1.1.2 High Dimension Droop Control

Next, the system was simulated using high dimension droop control for the wind resource. The droop control plane is shown in Fig. 6.5, along with the operation of the source during this simulation. The points marked D, E, and F provide a reference for the plot of the source's output with respect to time, which will be shown in Fig. 6.6.

The results of simulating the system are shown in Fig. 6.6. The points marked D, E, and F provide a reference back to the plot of the source's movement along the droop control plane, shown in Fig. 6.5. Both sources share the load, and the wind resource changes its

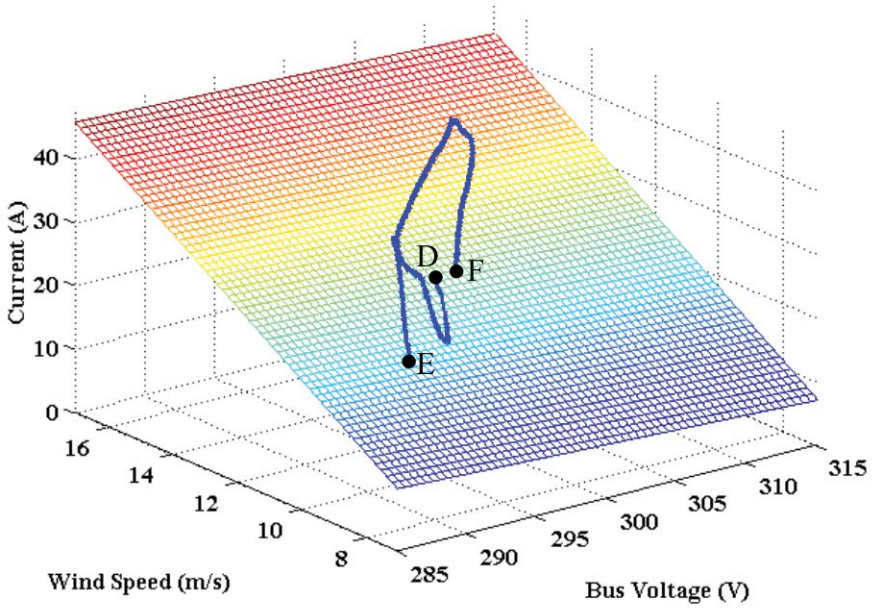

Figure 6.5: High dimension droop control relationship for second simulation.

operation some based on the wind speed. The conventional resource is needed during times of lower wind speed to ensure that the load is met. The battery is now able to charge during the times of higher wind speed.

6.1.1.3 Optimal High Dimension Droop Control

Finally, the system was simulated using optimal high dimension droop control for the wind resource. The method presented in Chapter 5 was used to find the optimal surface for a 12 kW wind turbine. The droop control surface is shown in Fig. 6.7, along with the operation

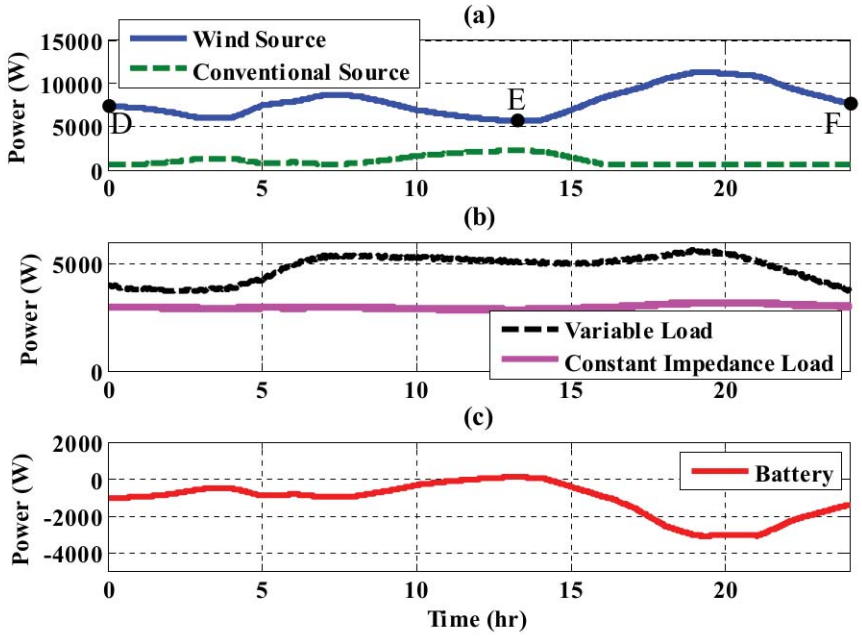

Figure 6.6: Simulation results using high dimension droop control: (a) power supplied by each source, (b) power consumed by each load, and (c) power supplied by the battery.

of the source during this simulation. The points marked G, H, and I provide a reference a reference for the plot of the source's output with respect to time, which will be shown in Fig. 6.8.

The results of simulating the system are shown in Fig. 6.8. The points marked G, H, and I provide a reference back to the plot of the source's movement along the droop control surface, shown in Fig. 6.7. Both sources share the load, and the wind resource changes its operation based on the wind speed. The conventional source outputs its minimum requirement of 500 W throughout the simulated day. The battery is able to charge for

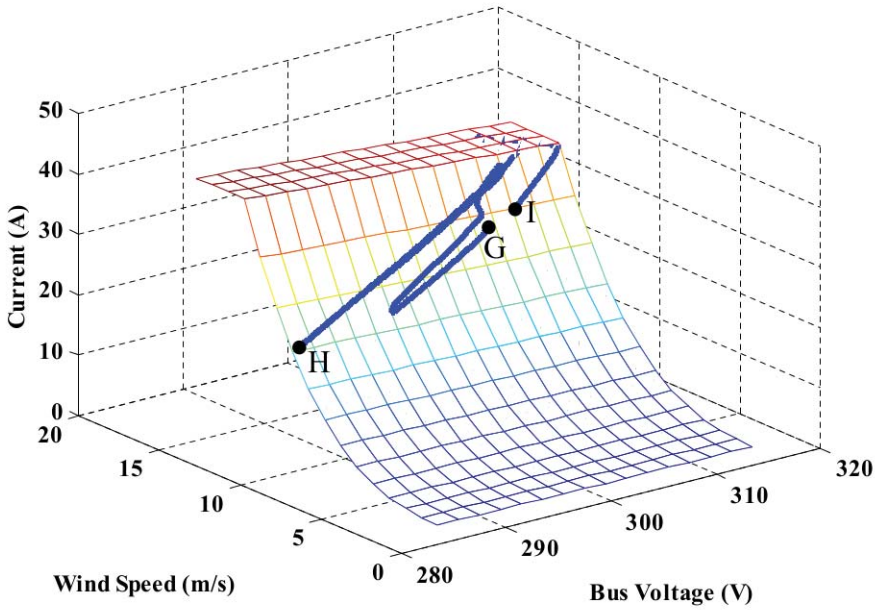

Figure 6.7: Optimal high dimension droop control relationship for third simulation.

most of the day, and supplies some power to the system when needed.

6.1.1.4 Comparison of Simulation Results

The power supplied from the two sources in each of the three simulations are compared in Fig. 6.9. Using high dimension droop control with a plane allows more of the energy from the wind to be utilized, while using an optimal high dimension droop control surface allows almost all of it to be utilized. This also requires the conventional source to be used less, resulting in fuel savings.

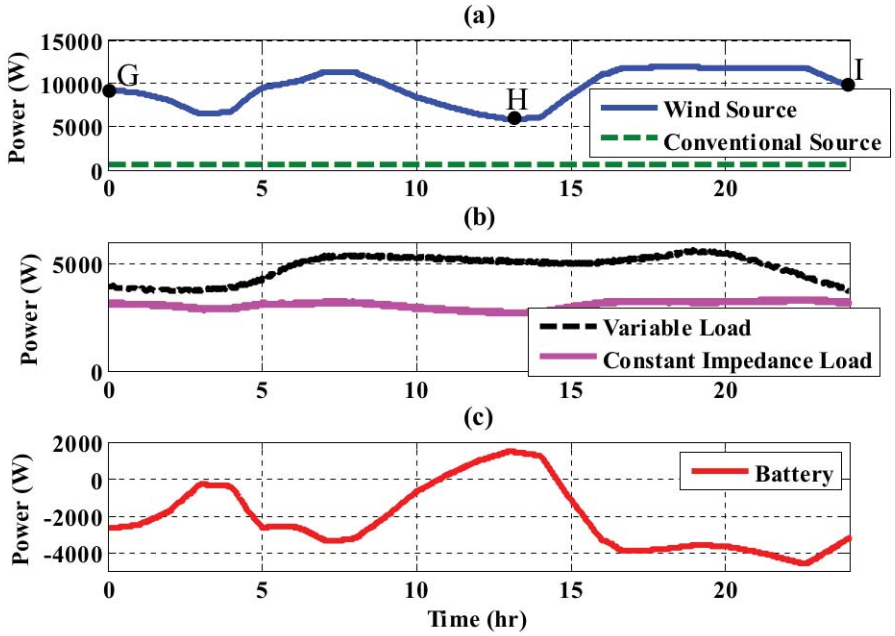

Figure 6.8: Simulation results using optimal high dimension droop control: (a) power supplied by each source, (b) power consumed by each load, and (c) power supplied by the battery.

A comparison of the amount of unused energy for each case is shown in Table 6.1. Using high dimension droop control (a plane) decreases the unused energy by almost 75% compared to traditional linear droop control. Using the optimized droop surface for the Wind Source decreases the unused energy by an additional 94 %.

The bus voltage during each of the simulations is shown in Fig. 6.10. When high dimension droop control is used, with both a plane and an optimal surface, the bus voltage varies more than in the traditional droop case. This is one trade-off that must be considered when choosing the droop surface. In all three cases, the bus voltage remains within $+/-$ 5% of

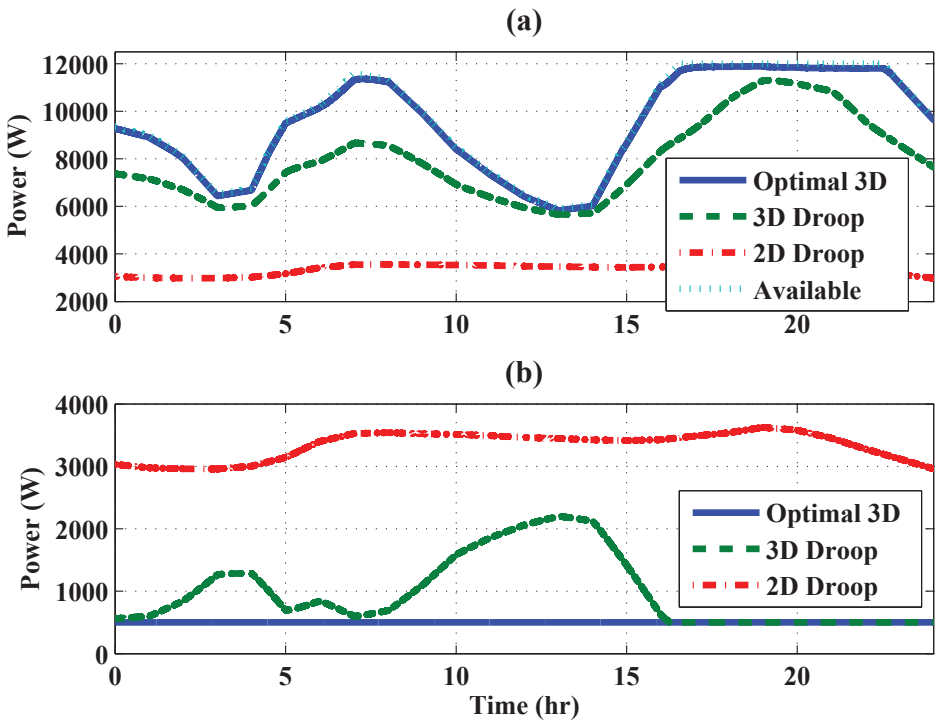

Figure 6.9: Power supplied from (a) wind source and (b) conventional source using 2D, 3D and optimal 3D droop. Power available from the wind is also shown.

the nominal 300 V.

6.2 Military Microgrid Example

This section demonstrates the use of optimal high dimension droop control in a military patrol base (PB) application. Load and source models for this type of microgrid will be presented first, followed by simulation and HIL results comparing traditional and multidimensional optimal droop control methods.

Table 6.1
Comparison of unused energy from the wind for three droop control methods, in full microgrid example.

Droop Control Strategy	Reference Current Equation	Unused Energy (W-hr)
Linear	$i_{ref1} = \frac{V_{ref} - V_{bus}}{R_d}$	149,770
Planar	$i_{ref1} = \frac{V_{ref} - V_{bus}}{R_{d1}} + \frac{v_w}{R_{d2}}$	39,792
Optimal Surface	$i_{ref1} = \frac{-V_{bus} + \sqrt{4\hat{P}(w)R_{1B} + V_{bus}^2}}{2R_{1B}}$	2,651

6.2.1 Load Modeling

In a military setting, the load on the microgrid is different than in a residential or commercial setting. A load model for a patrol base (PB) was developed with the help of an experienced member of the military, Mike Cook (personal communication, March-April 2014). First, three load tiers were identified to distinguish between loads that may be connected at a PB. Tier 1 includes loads that are critical to the mission, while Tier 2 includes loads that are important for extended operations. Tier 3 includes loads for improving quality of life and boosting moral. The loads in Tier 3 are important for maintaining the living conditions and overall attitudes for the PB members, however they could be disconnected during some time periods in order to ensure that Tier 1 and 2 loads are met. Table 6.2 lists some examples of equipment that might be included in each load tier.

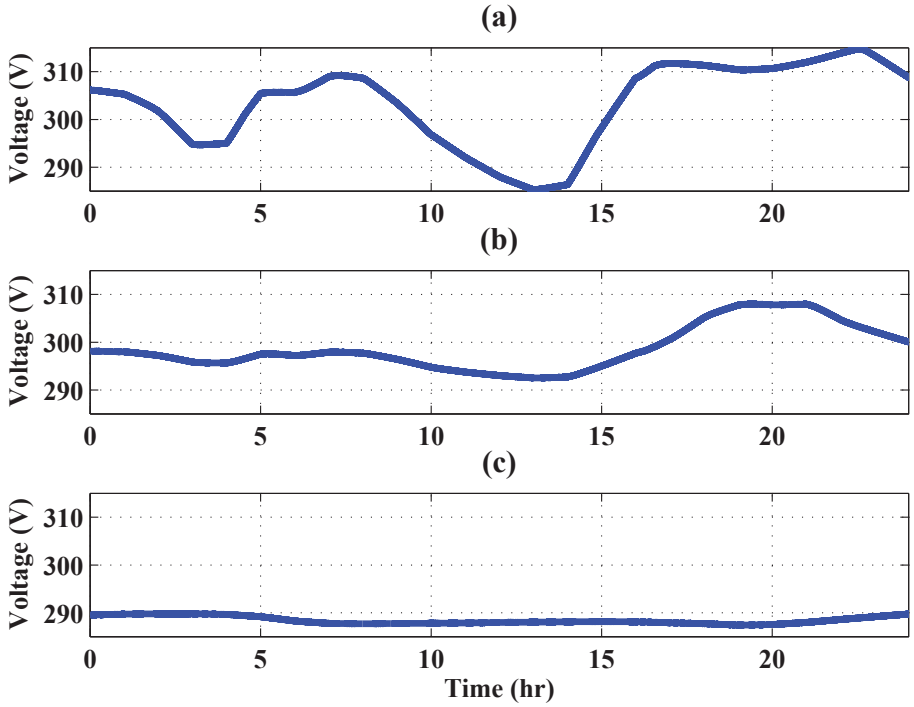

Figure 6.10: Microgrid bus voltage with (a) optimal high dimension droop control, (b) high dimension droop control, and (c) traditional droop control.

The amount of load needed in each tier varies based on time (day vs. night) as well as on activity (patrol vs. non-patrol). Table 6.3 shows the estimated load for a 20-40 person PB in each of these scenarios.

The estimates shown in Table 6.3 are for the total load used in each different type of scenario. The actual load is stochastic and will vary, so it was modeled using a compound Poisson process. A Poisson process is defined as

$$P[N(t) = k] = e^{-\lambda t} \frac{(\lambda t)^k}{k!} \tag{6.1}$$

where λ is the rate parameter. The Poisson process $N(t)$ is then implemented in a

Table 6.2
Equipment included in each load tier at a patrol base.

Load Tier	Equipment
Tier 1 (Mission Critical)	One to ten 80 W Panasonic Toughbooks Charging station for radios capable of recharging (30) 15 W radios One or two AC units One-Two TVs/projectors - monitors for the Blue Force Tracker Three to five 100 W bulbs (26 W CFL)
Tier 2 (Extended Operations)	Power tools and charging station if the platoon has vehicles ISR video feeds Portable lights powered via rechargeable battery pack One to three hotplates/coffee pots
Tier 3 (Morale Boosting)	One to three personal electronic devices (iPod, laptop, camera, etc.) 30-80 gallon hot water heater Three to five additional AC/heater units for berthing One to three flat panel TVs or projectors

Table 6.3
Amount of load in each tier based on time and activity.

Load Tier	Activity	Day	Night
Tier 1	Patrol	2-3 kW	2-3 KW
	Non-Patrol	1-2.5 kW	1-2.5 kW
Tier 2	Patrol	1-2 kW	1-2 KW
	Non-Patrol	2-3 kW	1-2 kW
Tier 3	Patrol	2-3 kW	2-3 KW
	Non-Patrol	0.5-1.5 kW	0.5-1 kW

compound Poisson process as

$$Y(t) = \sum_{i=1}^{N}(t)D_i \tag{6.2}$$

where D_i are independent and identically distributed (iid) random variables [97]. A compound Poisson process is an appropriate method for approximating the distribution of electrical loads, since they are discrete, independent random variables [98].

Table 6.4
Example patrol schedule.

Day 1 Patrol Schedule	
0725 - 0800	Squad 1
1110 - 1325	Squad 2
1610 - 1800	Squad 1
Night 1 Patrol Schedule	
1910 - 1955	Squad 1
2140 - 2225	Squad 2
2340 - 0050	Squad 1
0300 - 0400	Squad 2

Along with the load changing stochastically within each time and activity, the operation of the PB will also vary. In any combat environment, varying patrol patterns (route, length of patrol, time of departure, etc.) are used in order to limit the enemy's ability to execute a coordinated attack. Therefore, this load model also randomizes the number of patrols per day, their length, and the length of rest during both day and night. Some days may then include no patrols, to allow for debriefing or rest. Other days may include a high number of patrols, designed to limit the enemy's ability to operate. An example patrol schedule for two squads during one day and one night is shown in Table 6.4; the patrol schedule is randomized for other days and nights.

A load model incorporating all of these aspects was created using Matlab. Fig. 6.11 shows the load at a PB over one day, based on a changing patrol schedule and using a compound Poisson process to randomize the load. Each load tier is displayed in the figure. This load model is implemented in simulation and HIL in the following sections.

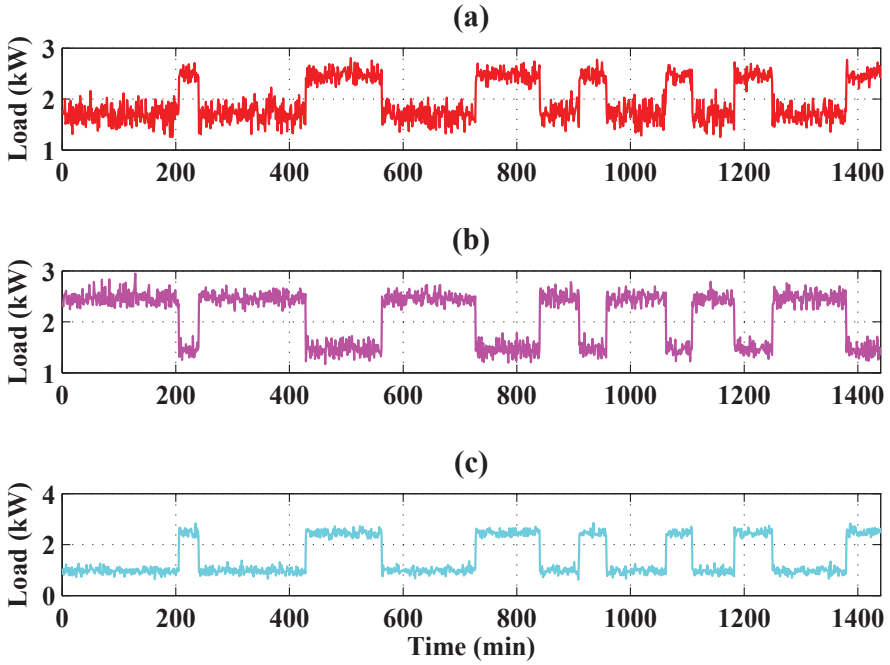

Figure 6.11: Stochastic load at a Patrol Base microgrid for (a) Tier 1, (b) Tier 2, and (c) Tier 3 loads.

6.2.2 Source Modeling

For a military application, it is likely that solar would be included as a renewable resource, instead of wind. Like wind resources, solar resources are intermittent and depend on weather conditions. The accurate prediction of solar irradiance is currently an important research area [99].

For military applications, portability is a key consideration [100], and the use of solar resources fits this requirement. Previous research has been completed on the inclusion of solar resources in military forward operating bases [101]. In this section, the proposed

optimal high dimension droop control will be applied with a solar resource; only applications with wind resources have been demonstrated in previous chapters.

Solar irradiance measurements are taken each minute by the National Renewable Energy Laboratory (NREL). These are recorded at their Golden, CO location and stored as part of the Baseline Measurement System (BMS). The data for June 1, 2012 is used in simulation and HIL in the following sections, and is shown in Fig. 6.12 [102].

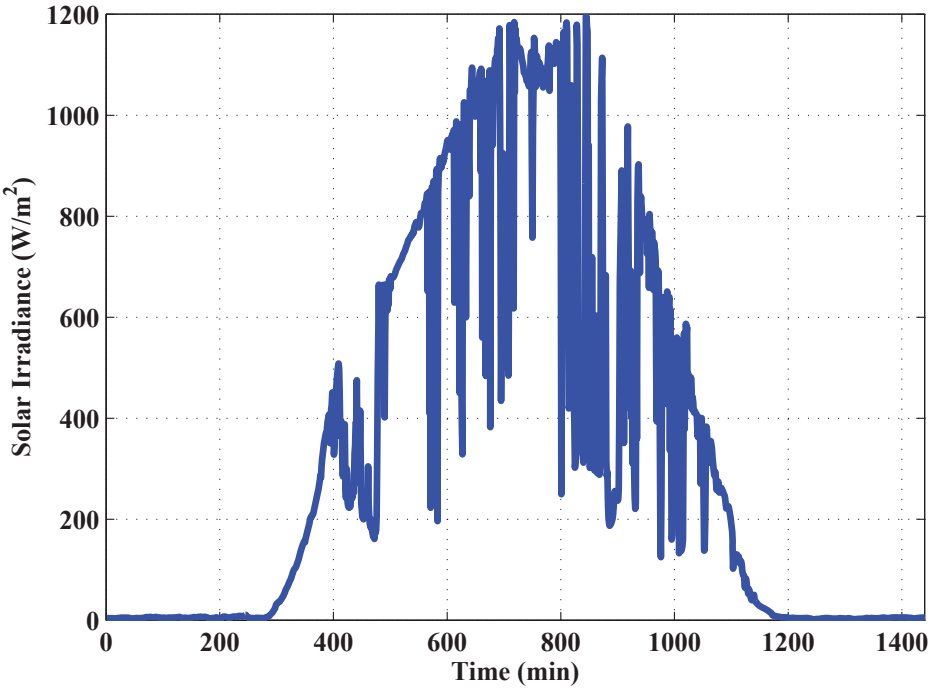

Figure 6.12: Solar irradiance measured each minute on June 1, 2012.

6.2.3 Simulation Results

The sample microgrid used in simulation for a PB is shown in Fig. 6.13. Three sources are included; one is a solar resource, one is a conventional resource such as a diesel generator, and one is an energy storage source such as a battery. In the simulation, these sources are modeled as variable voltage sources, and droop control is implemented for each. The numeric values used for this microgrid model are shown in Table 6.5.

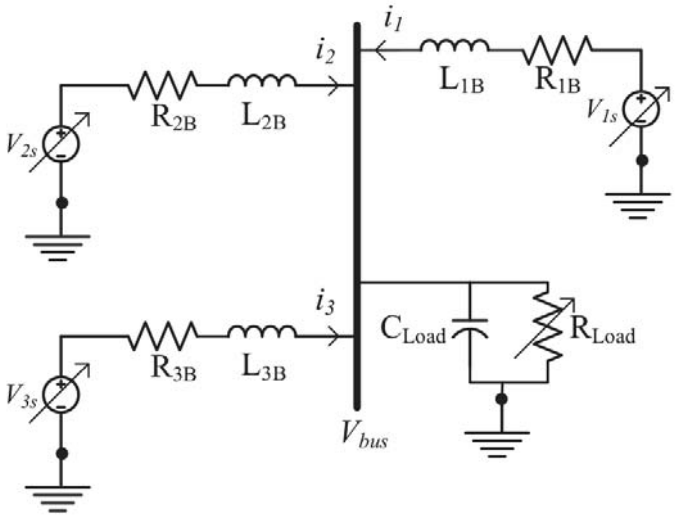

Figure 6.13: Example microgrid used in simulation for PB demonstration of droop control methods.

A simulation was completed to represent one full day at the PB. The power available from solar energy at each minute of the day is shown in Fig. 6.14a. The data described in the previous section is used, assuming that there are 4 square meters of solar panels available. The required load at each minute is shown in Fig. 6.14b, with the three load tiers described

Table 6.5
Patrol base microgrid parameter values.

Component	Value	Unit
R_{1B}	0.1	Ω
L_{1B}	1	mH
R_{2B}	0.2	Ω
L_{2B}	2	mH
R_{3B}	0.12	Ω
L_{3B}	1	mH
C_{load}	1	mF
k_p	1	
k_i	10	

above added together to form the total required load.

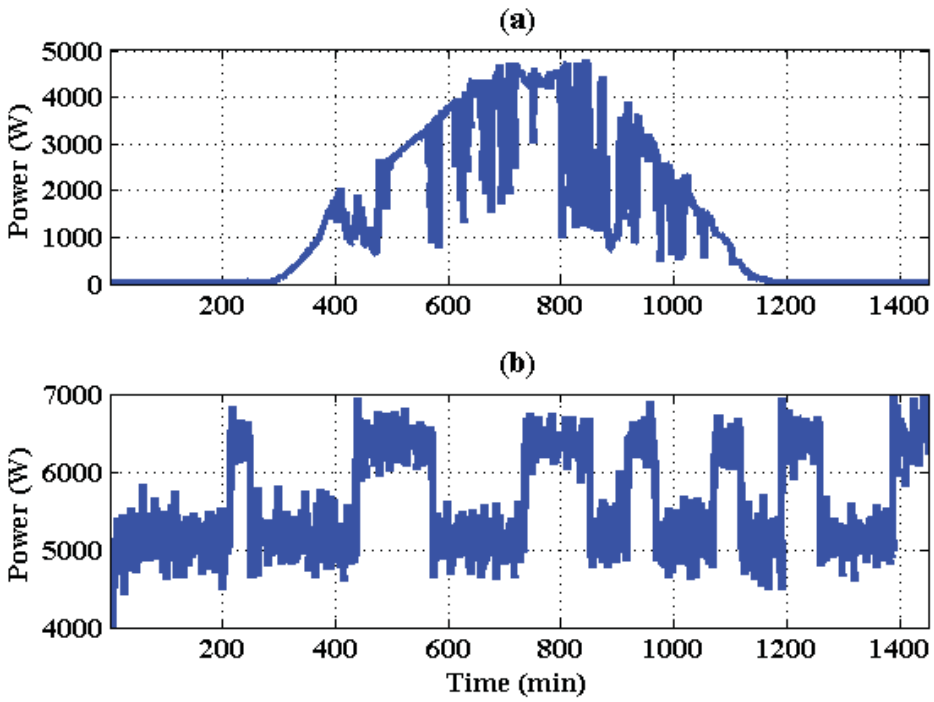

Figure 6.14: (a) Solar power available and (b) load profiles for simulated 1440 minute period.

The system was first simulated using traditional, linear droop control for each of the three

Table 6.6
Traditional droop control settings for PB simulation.

Source	V_{ref}	R_d
Solar	300	2.5
Conventional	300	0.4
Storage	295	1.0

sources, where the reference current is defined as

$$i_{ref} = \frac{V_{ref} - V_{bus}}{R_d} \tag{6.3}$$

The droop control settings for each of the three sources are shown in Table 6.6.

The power supplied by each of the three sources during the simulated one day period is shown in Fig. 6.15. When it is sunny during the day, the solar source operates with traditional droop control, and does not use all of the available power. The conventional source is required to meet most of the load demand. The storage source supplies and absorbs power throughout the day as the load changes.

The simulation was then repeated using optimal high dimension droop control for the solar resource. Its reference current is defined as

$$i^*_{ref1} = \frac{-V_{bus} + \sqrt{4\hat{P}(s)R_{1B} + V^2_{bus}}}{2R_{1B}} \tag{6.4}$$

where s is the solar irradiance in W/m^2 multiplied by the 4 m^2 of panels. The conventional and storage sources kept the same droop settings as in Table 6.6 for the second simulation.

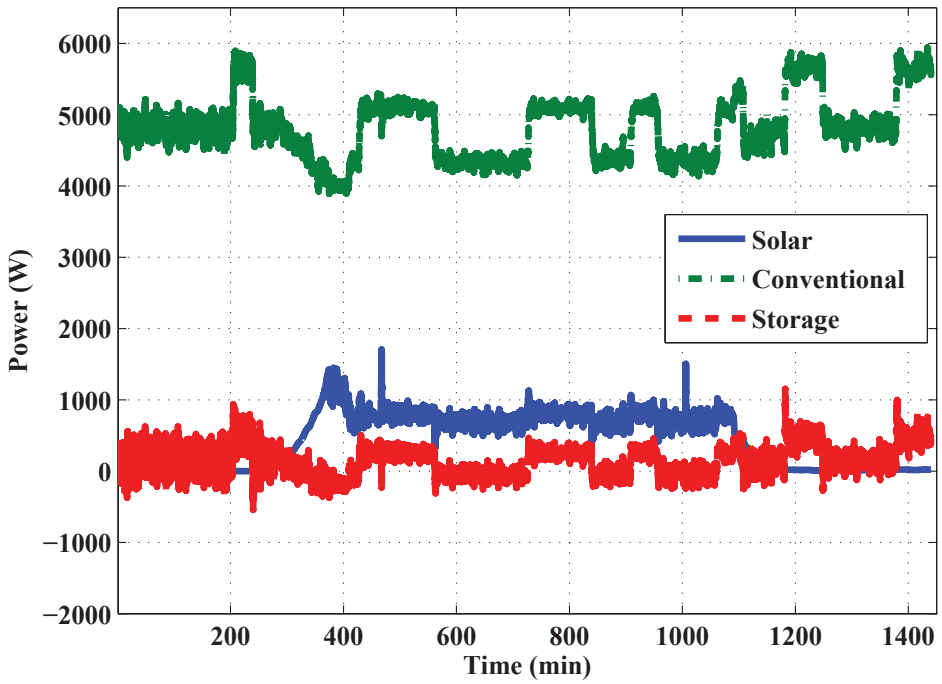

Figure 6.15: Power supplied by solar, conventional, and storage sources when traditional droop control is used.

The power supplied by each of the three sources during the simulated one day period is shown in Fig. 6.16. With optimal high dimension droop control, all of the available power from the solar resource is utilized. This means that the conventional source is required to provide less power to the system. The storage source charges during the sunny part of the day, and supplies power as need during the night.

A comparison of Figs. 6.15 and 6.16 shows that the use of traditional linear droop control limits the amount of power that can be utilized from the solar resource, while the use of optimal high dimension droop control allows all of the available power from that resource to be utilized. This also means that the conventional source is needed less, and the storage

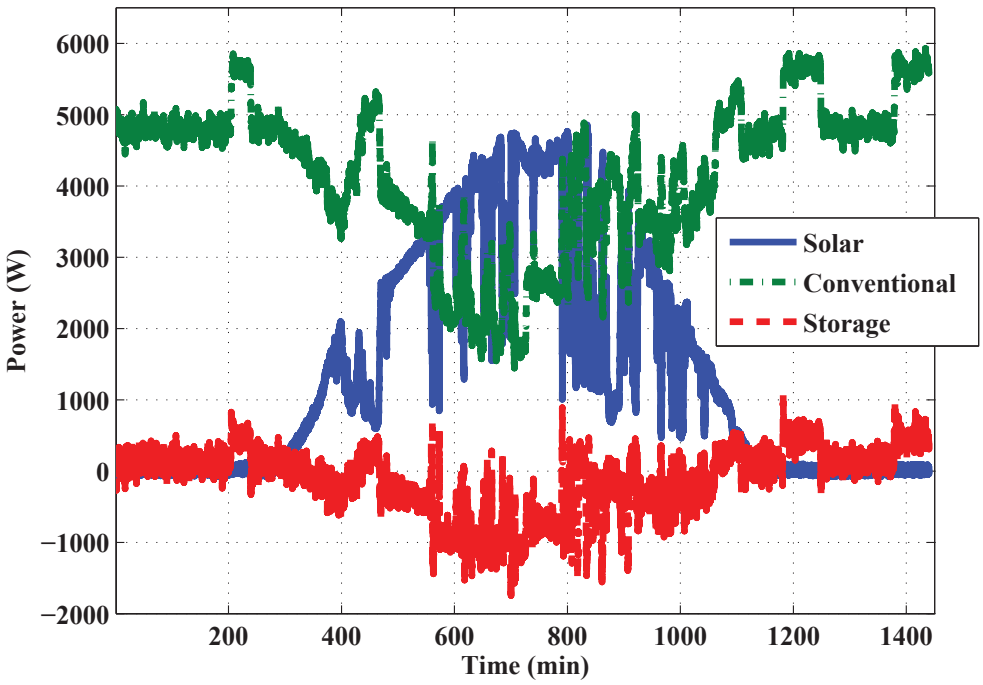

Figure 6.16: Power supplied by solar, conventional, and storage sources when optimal high dimension droop control is used.

source is able to charge during times of high irradiance, and use that stored energy during cloudy periods or at night.

The bus voltage during each of the two simulations is shown in Fig. 6.17. While the bus voltage varies more when optimal high dimension droop control is used, it stays well within a bound of 5% around the reference value of 300 V.

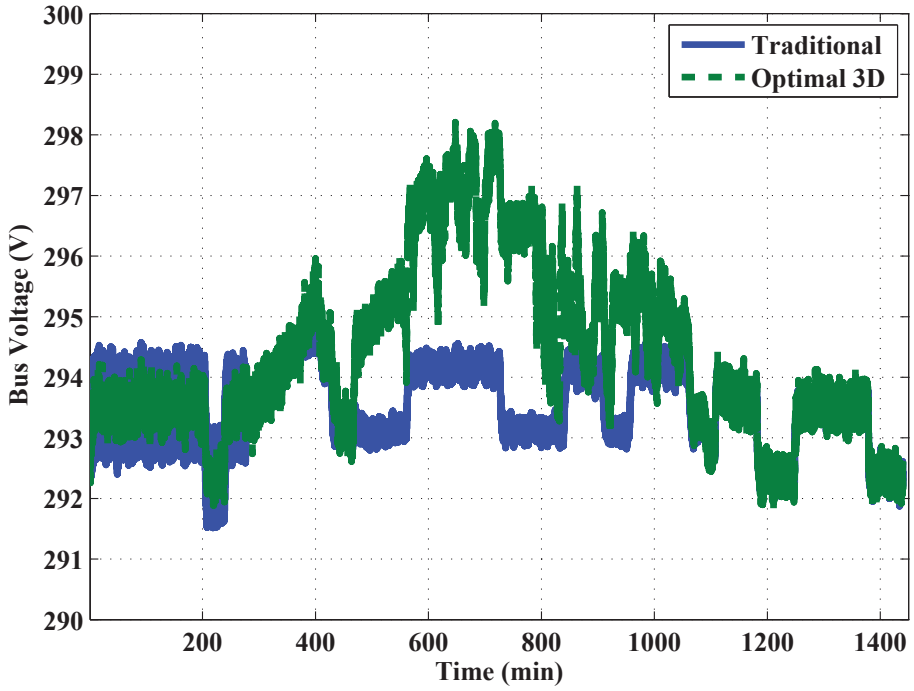

Figure 6.17: Bus voltage using traditional vs. optimal high dimension droop control.

6.2.4 Hardware-in-the-Loop Results

In order to validate the simulation results presented in the previous section, the example microgrid shown in Fig. 6.18 was implemented using a hardware-in-the-loop (HIL) system, as described in Ch. 3. This microgrid has the same topology as the one implemented in the simulation. However, for the HIL experiment, power electronics were included, along with parasitic inductances and capacitances. To represent the variable load, a controllable current source was included. This type of load is comparable to an inductive or motor load in an actual system.

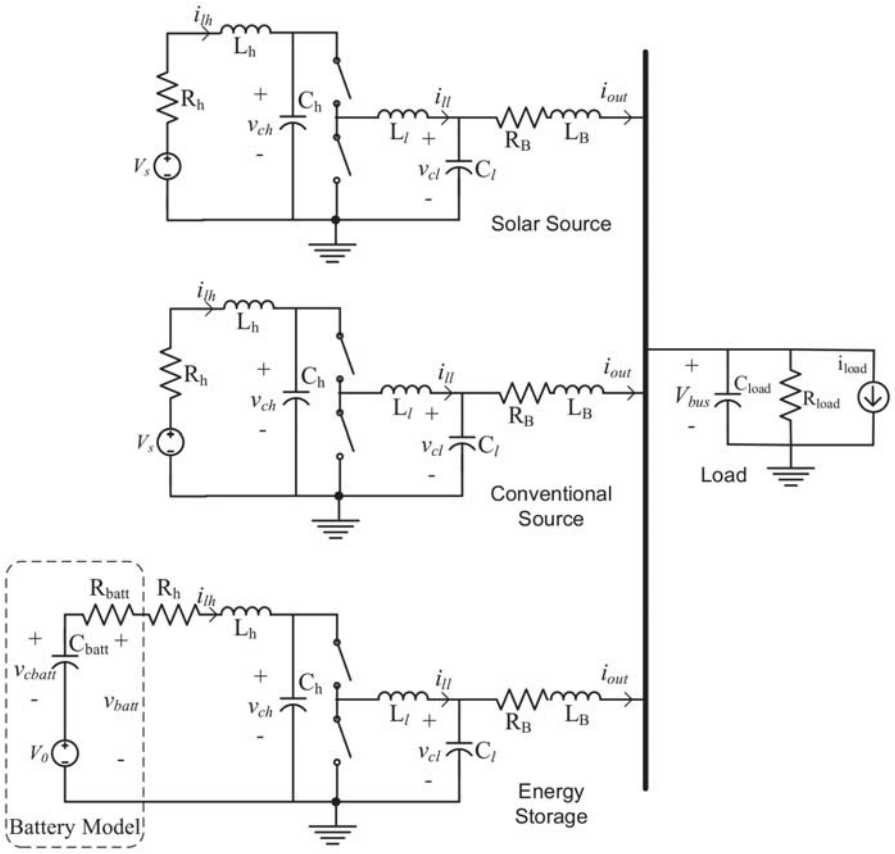

Figure 6.18: Example microgrid used in HIL for PB demonstration of droop control methods.

The system was implemented on a Typhoon HIL600 unit using distributed control through Texas Instruments F28335 DSP ContolCARDs. Each of the three sources is controlled using a separate TI card, using only local sensors. The circuit schematic used in the Typhoon software is shown in Fig. 6.19. The numeric parameter values are the same as those shown in Tables 4.1 and 4.3.

The controllers implemented for each of the three sources are shown in Figs. 6.20 - 6.22. Sources 2 and 3, representing a conventional and energy storage source, respectively, are

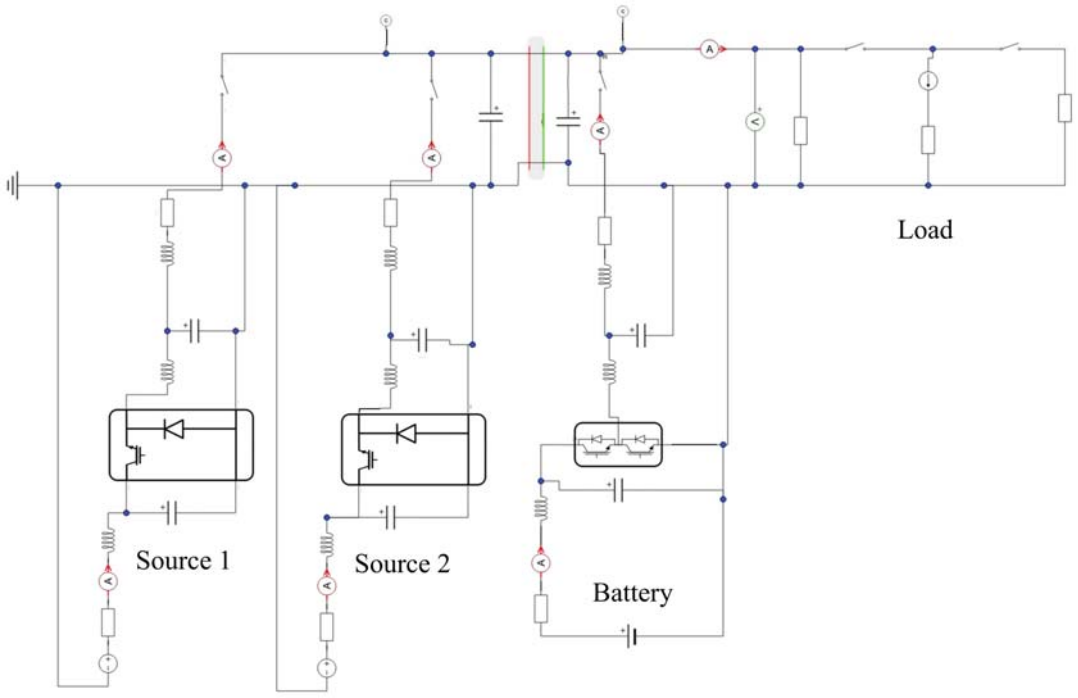

Figure 6.19: Hardware-in-the-loop schematic for PB microgrid example.

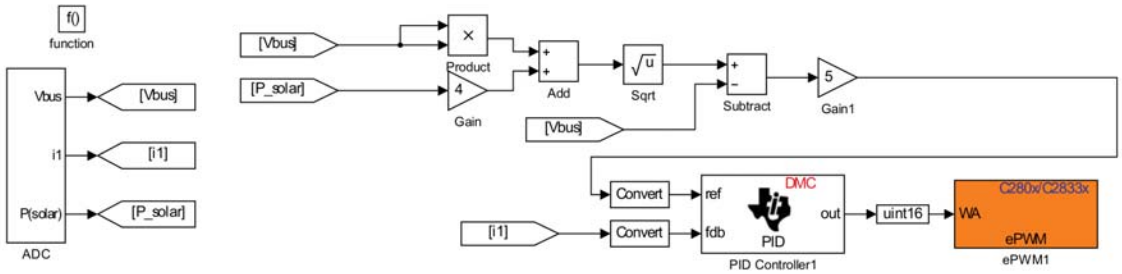

Figure 6.20: HIL controller for Source 1 (solar) - optimal high dimension droop.

controlled using traditional linear droop control. Source 1, representing a solar source, is controlled using optimal high dimension droop control as in (6.4).

Due to the limitations of the HIL system, a short overall time period was used, and the per-minute solar and load information was scaled. The profiles for power available from

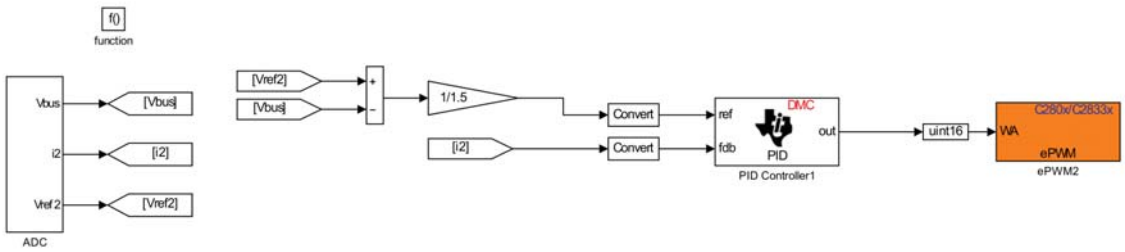

Figure 6.21: HIL controller for Source 2 (conventional) - traditional droop.

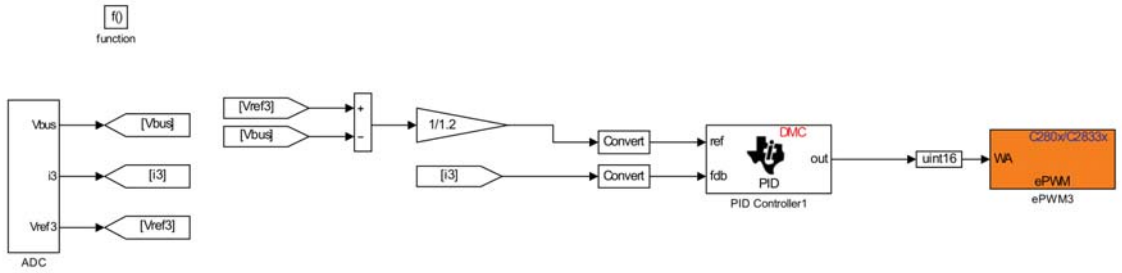

Figure 6.22: HIL controller for Source 3 (storage) - traditional droop.

the solar resource and required load current are shown in Fig. 6.23. The solar irradiance data is taken from the NREL BMS measurements from June 1, 2012, starting at 11:00 am.

The results of implementing these profiles in the HIL system are shown in Fig. 6.24. The bus voltage is shown, along with the current supplied from each of the three sources - all three use the same zero point on the oscilloscope trace. As the power available from the sun and the required load change, the conventional and storage sources change their output based on traditional linear droop control. Source 1 changes its output based on optimal high dimension droop control, where the reference current is determined by (6.4).

In order to verify that the proposed controller is operating as desired, data from the oscilloscope trace in Fig. 6.24 was imported and plotted using MATLAB. The bus voltage

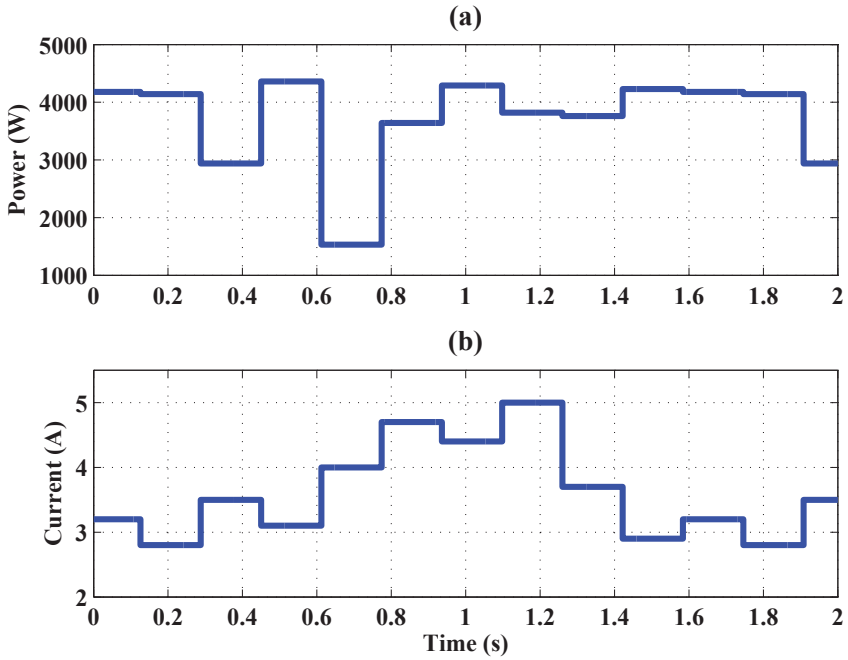

Figure 6.23: (a) Solar power available and (b) load profiles for HIL implementation.

and solar power available were used in (6.4) to calculate the reference current that Source 1 should be supplying. This reference current is plotted with the actual Source 1 current in Fig. 6.25. The source output does match the desired reference value calculated using optimal high dimension droop control.

6.3 Sensitivity Analysis

In the optimal high dimension droop control method presented in this dissertation, the optimal reference current depends on the changing bus voltage, and the reference power, which may be a function of another variable such as wind speed or solar irradiance. The

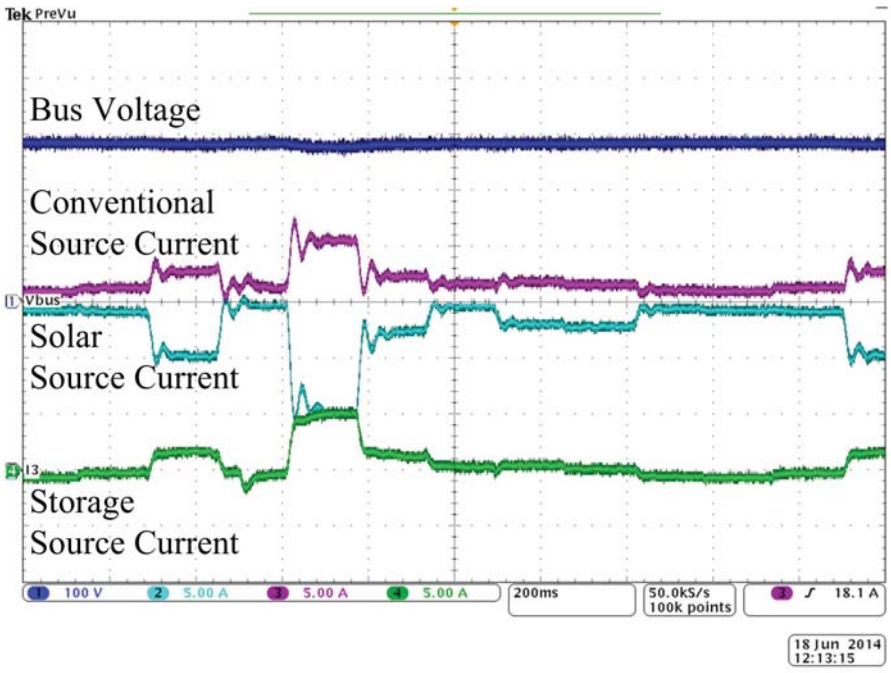

Figure 6.24: Hardware-in-the-loop results with optimal high dimension droop control: Ch1 Bus Voltage; Ch2 Source 1 Current; Ch3 Source 2 Current; Ch4 Source 3 Current.

optimal reference current also depends on R_{1B}, the line resistance which connects the source to the dc bus. The reference power $\hat{P}$ is a value chosen by the control designer based on the scenario. However, the bus voltage is measured continuously while the microgrid is operating, and there may be some small errors in its measurement. The value of R_{1B} is constant, but there may also be some error in the actual resistance included in the system. This section will present the results of a sensitivity analysis on the constant value of R_{1B}, and the measured value of V_{bus}.

One method for evaluating the sensitivity of a model to a given parameter is to find the partial derivative of the control equation with respect to that parameter [103]. Another is to

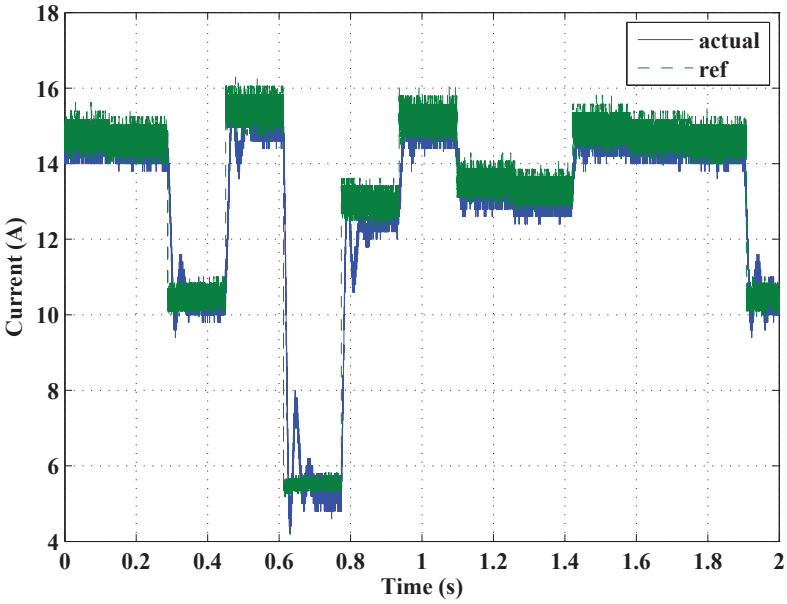

Figure 6.25: Reference and actual current supplied by solar resource using optimal high dimension droop control.

find the ratio of the actual value given perfect information, and the reference value based on the model parameters [104]. Both of these approaches will be demonstrated here. The optimal relationship for reference current is repeated:

$$i^*_{ref1} = \frac{-V_{bus} + \sqrt{4\hat{P}R_{1B} + V^2_{bus}}}{2R_{1B}} \tag{6.5}$$

6.3.1 Sensitivity in R_{1B}

The partial derivative of (6.5) with respect to R_{1B} is

$$\delta_{R_{1B}} i^*_{ref1} = \frac{V_{bus} + \frac{2\hat{P}R_{1B}+V_{bus}^2}{\sqrt{4\hat{P}R_{1B}+V_{bus}^2}}}{2R_{1B}^2}. \tag{6.6}$$

Choosing reasonable values for $\hat{P}$ of 2000 W, V_{bus} of 295 V, and R_{1B} of 0.1 Ω, the resulting value of (6.6) is -0.154.

A ratio was then calculated to compare the reference current based on the actual resistance value to the reference current based on an assumption of an 0.1 Ω resistance. The result is plotted in Fig. 6.26 over a range of resistances from +/- 50% from the nominal value. This result shows that even if the line resistance used to calculate the reference current differs within +/- 50% from the actual line resistance, the impact on reference current is less than +/- 0.1%.

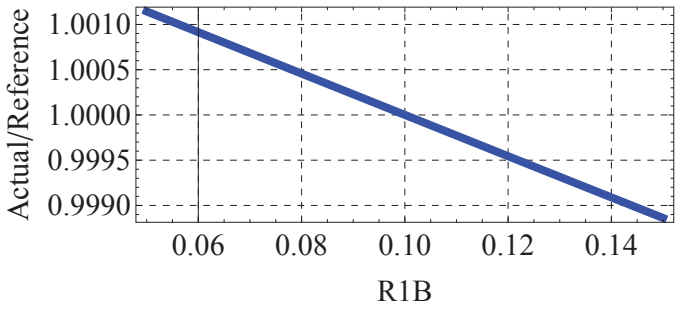

Figure 6.26: Ratio of actual to ideal reference current with respect to line resistance.

6.3.2 Sensitivity in V_{bus}

The partial derivative of (6.5) with respect to R_{1B} is

$$\delta_{V_{bus}} i^*_{ref1} = \frac{-1 + \frac{V_{bus}}{\sqrt{4\hat{P}R_{1B}+V^2_{bus}}}}{2R_{1B}}. \tag{6.7}$$

Choosing reasonable values for $\hat{P}$ of 2000 W, V_{bus} of 295 V, and R_{1B} of 0.1 Ω, the resulting value of (6.7) is -0.0228.

A ratio was then calculated to compare the reference current based on the actual bus voltage to the reference current based on an assumption of a bus voltage measurement of 295 V. The result is plotted in Fig. 6.27 over a range of bus voltages from +/- 1% from the nominal value. This result shows that even if the measured bus voltage used in the controller differs within +/- 1% from the actual bus voltage, the impact on reference current is also less than +/- 1%.

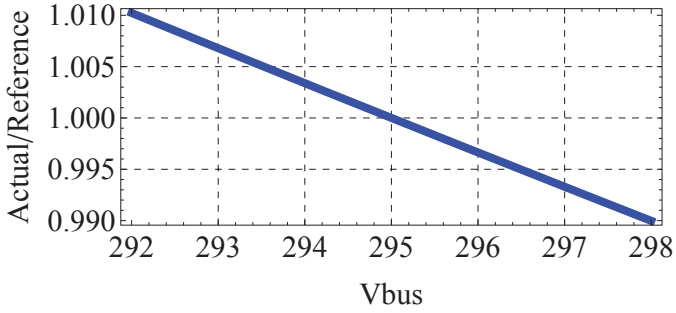

Figure 6.27: Ratio of actual to ideal reference current with respect to measured bus voltage.

The parameter sensitivity analysis presented in this section demonstrates that small errors in bus voltage measurement, and large errors in line resistance value, have a minimal effect on the calculated reference current for optimal high dimension droop control.

Chapter 7

Conclusions

7.1 Summary of Accomplishments

There are two significant contributions from this work. The first was presented in Ch. 4, where a method for high dimension droop control was proposed and demonstrated. Choosing a droop control relationship where the reference current depends on more than one variable is a novel concept. The expansion of traditional linear droop control to three dimensions was demonstrated, where a plane in three dimensions is used instead of a line in two dimensions to implement droop control. The third dimension was chosen as wind speed, and the results presented in Ch. 4 show that the use of high dimension droop control with wind resources allows much more of the available wind power to be utilized. With the

improved control system, the benefits of droop control are maintained.

The second contribution is the method for optimizing the droop control relationship to meet a given objective, presented in Ch. 5. This method was first demonstrated in two dimensions, where the objective was to maintain a constant output power from the source. It was then applied again with wind resources, where the desired output power varies as a function of the wind speed. The droop control reference current then depends on both the bus voltage and wind speed, and the equation for an optimal surface can be found. The use of optimal high dimension droop control was demonstrated in two and three dimensions, using both simulation and hardware-in-the-loop experiments.

The proposed control method was then implemented in two applications in Ch 6. First, optimal high dimension droop control was implemented in a simulation of a residential size microgrid containing two sources and an energy storage device. Optimal high dimension droop control was then implemented with a solar resource in a military patrol base microgrid scenario. Simulation and hardware-in-the-loop results were presented to show the operation of the system over a one day period, using load and solar data measured each minute.

Optimal high dimension droop control applied with renewable resources allows the variability of the resource to be included in the droop control relationship. The benefits of traditional droop control are maintained, including having a simple control system that does not require a communication link between system components. This lack of dependence

on communication is important for system reliability, especially for microgrids in remote residential or military situations.

7.2 Recommendations for Future Work

This dissertation has presented a method for determining an optimal droop control relationship in multiple dimensions to meet a given objective. This method has been demonstrated in various microgrid example cases with both wind and solar resources, with the objective of utilizing all of the renewable power that is available. Optimal high dimension droop control may also be useful with other types of sources. For example, with a conventional resource such as a diesel generator, the third dimension may be the cost of fuel. As the price goes up, the desired power from this resource might go down, and a droop control surface could be found to meet this objective. For an energy storage device, the third dimension might be its current state of charge.

All of the control development and example microgrids in this dissertation have been dc. For future work, it would be beneficial to apply these optimal high dimension droop control methods in an ac system, where the reference power for each source is related to the system frequency. It would also be interesting to consider higher dimension droop control, where the reference depends on three or more variables instead of the traditional one, or the two variables presented in this dissertation.

References

[1] Y. Wang, Z. Wu, and Z. Li, "Research on wind energy distributed generation in microgrid," in *International Conference on Power System Technology*, pp. 1–6, 2010.

[2] K. Nagim and L. Wei-Jen, "Micro grid integration opportunities and challenges," in *IEEE Power Engineering Society General Meeting*, pp. 1–6, 2007.

[3] R. Lasseter and P. Paigi, "Microgrid: a conceptual solution," in *IEEE Power Electronics Specialists Conference*, vol. 6, pp. 4285–4290, 2004.

[4] T. S. Ustun, C. Ozansoy, and A. Zayegh, "Recent developments in microgrids and example cases around the world - a review," *Renewable and Sustainable Energy Reviews*, vol. 15, no. 8, pp. 4030–4041, 2011.

[5] F. Blaabjerg, Z. Chen, and S. Kjaer, "Power electronics as efficient interface in dispersed power generation systems," *IEEE Transactions on Power Electronics*, vol. 19, no. 5, pp. 1184–1194, 2004.

[6] F. Katiraei, M. R. Iravani, and P. W. Lehn, "Micro-grid autonomous operation during and subsequent to islanding process," *IEEE Transactions on Power Delivery*, vol. 20, no. 1, pp. 248–257, 2005.

[7] I. Chung, W. Liu, D. Cartes, E. Collins, and S. Moon, "Control methods of inverter-interfaced distributed generators in a microgrid system," *IEEE Transactions on Industry Applications*, vol. 46, no. 3, pp. 1078–1088, 2010.

[8] D. Salomonsson, L. der, and A. Sannino, "Protection of low-voltage dc microgrids," *IEEE Transactions on Power Delivery*, vol. 24, no. 3, pp. 1045–1053, 2009.

[9] P. Karlsson and J. Svensson, "Dc bus voltage control for a distributed power system," *IEEE Transactions on Power Electronics*, vol. 18, no. 6, pp. 1405–1412, 2003.

[10] L. Xu and D. Chen, "Control and operation of a dc microgrid with variable generation and energy storage," *IEEE Transactions on Power Delivery*, vol. 26, no. 4, pp. 2513–2522, 2011.

[11] N. W. A. Lidula and A. D. Rajapakse, "Microgrids research: a review of experimental microgrids and test systems," *Renewable and Sustainable Energy Reviews*, vol. 15, no. 1, pp. 186–202, 2011.

[12] B. K. Johnson, R. H. Lasseter, F. L. Alvarado, and R. Adapa, "Expandable multiterminal dc systems based on voltage droop," *IEEE Transactions on Power Delivery*, vol. 8, no. 4, pp. 1926–1932, 1993.

[13] R. Ma, H. Chen, Y. Huang, and W. Meng, "Smart grid communication: its challenges and opportunities," *IEEE Transactions on Smart Grid*, vol. 4, no. 1, pp. 36–46, 2013.

[14] K. Moslehi and R. Kumar, "A reliability perspective of the smart grid," *IEEE Transactions on Smart Grid*, vol. 1, no. 1, pp. 57–64, 2010.

[15] J. Zhou, Y. Chen, M. Huang, and Y. Tong, "Study on energy control strategies in microgrid-modeling and simulation," in *Asia-Pacific Power and Energy Engineering Conference (APPEEC)*, pp. 1–4, 2012.

[16] J. A. P. Lopes, C. L. Moreira, and A. G. Madureira, "Defining control strategies for microgrids islanded operation," *IEEE Transactions on Power Systems*, vol. 21, no. 2, pp. 916–924, 2006.

[17] P. Piagi and R. H. Lasseter, "Autonomous control of microgrids," in *IEEE Power Engineering Society (PES) General Meeting*, 2006.

[18] J. Kim, J. M. Guerrero, P. Rodriguez, R. Teodorescu, and K. Nam, "Mode adaptive droop control with virtual output impedances for an inverter-based flexible ac microgrid," *IEEE Transactions on Power Electronics*, vol. 26, no. 3, pp. 689–701, 2011.

[19] K. D. Brabandere, B. Bolsens, J. V. den Keybus, A. Woyte, J. Driesen, and R. Belmans, "A voltage and frequency droop control method for parallel inverters," *IEEE Transactions on Power Electronics*, vol. 22, no. 4, pp. 1107–1115, 2007.

[20] W. Yao, M. Chen, J. Matas, J. Guerrero, and Z. Qian, "Design and analysis of the droop control method for parallel inverters considering the impact of the complex impedance on the power sharing," *IEEE Transactions on Industrial Electronics*, vol. 58, no. 2, pp. 576–588, 2011.

[21] R. A. F. Ferreria, P. G. Barbosa, H. A. C. Braga, and A. A. Ferreira, "Analysis of non-linear adaptive voltage droop control method applied to a grid connected dc microgrid," in *Brazilian Power Electronics Conference (COBEP)*, pp. 1067–1074, 2013.

[22] T. M. Haileselassie and K. Uhlen, "Precise control of power flow in multiterminal vsc-hvdcs using dc voltage droop control," in *IEEE Power and Energy Society (PES) General Meeting*, pp. 1–9, 2012.

[23] F. Luo, Y. M. Lai, C. K. Tse, and K. H. Loo, "A triple-droop control scheme for inverter-based microgrids," in *IEEE Industrial Electronics Society Annual Conference*, pp. 3368–3375, 2012.

[24] J. Yaoqin, L. Dingkun, and P. Shengkui, "Improved droop control of parallel inverter system in standalone microgrid," in *IEEE International Conference on Power Electronics and ECCE Asia (ICPE and ECCE)*, pp. 1506–1513, 2011.

[25] E. Barklund, N. Pogaku, M. Prodanovic, C. Hernandez-Aramburo, and T. C. Green, "Energy management in autonomous microgrid using stability-constrained droop

control of inverters," *IEEE Transactions on Power Electronics*, vol. 23, no. 5, pp. 2346–2352, 2008.

[26] R. Majumder, B. Chaudhuri, A. Ghosh, R. Majumder, G. Ledwich, and F. Zare, "Improvement of stability and load sharing in an autonomous microgrid using supplementary droop control loop," *IEEE Transactions on Power Systems*, vol. 25, no. 2, pp. 796–808, 2010.

[27] Y. A. I. Mohamed and E. F. El-Saadany, "Adaptive decentralized droop controller to preserve power sharing stability of paralleled inverters in distributed generation microgrids," *IEEE Transactions on Power Electronics*, vol. 23, no. 6, pp. 2806–2816, 2008.

[28] M. Hassanzahraee and A. Bakhshai, "Transient droop control strategy for parallel operation of voltage source converters in an islanded mode microgrid," in *IEEE International Telecommunications Energy Conference (INTELEC)*, pp. 1–9, 2013.

[29] N. R. Chaudhuri and B. Chaudhuri, "Adaptive droop control for effective power sharing in multi-terminal dc (mtdc) grids," *IEEE Transactions on Power Systems*, vol. 28, no. 1, pp. 21–29, 2013.

[30] A. Nagliero, R. A. Mastromauro, D. Ricchiuto, M. Liserre, and N. Nitti, "Gain-scheduling-based droop control for universal operation of small wind turbine systems," in *IEEE International Symposium on Industrial Electronics*, pp. 1459–1464, 2011.

[31] S. Tian, X. Tong, and B. Ren, "The control strategy based on improved droop method of microgrid-connected inverters," in *IEEE International Conference on Electrical and Control Engineering (ICECE)*, pp. 5700–5703, 2010.

[32] J. M. Guerrero, N. Berbel, J. Matas, J. L. Sosa, and L. G. de Vicuna, "Droop control method with virtual output impedance for parallel operation of uninterruptible power supply systems in a microgrid," in *IEEE Applied Power Electronics Conference (APEC)*, pp. 1126–1132, 2007.

[33] M. Gao, Y. Zhang, C. Jin, M. Chen, and Z. Qian, "An improved droop control method for parallel operation of distributed generations in microgrid," in *IEEE Applied Power Electronics Conference (APEC)*, pp. 3016–3020, 2013.

[34] Y. Zhu, F. Zhuo, and H. Shi, "Accurate power sharing strategy for complex microgrid based on droop control method," in *IEEE ECCE Asia Downunder*, pp. 344–350, 2013.

[35] M. Savaghebi, A. Jalilian, J. C. Vasquez, and J. M. Guerrero, "Secondary control scheme for voltage unbalance compensation in an islanded droop-controlled microgrid," *IEEE Transactions on Smart Grid*, vol. 3, no. 2, pp. 797–807, 20142.

[36] M. Fazeli, G. M. Asher, C. Klumpner, Y. Liangzhong, and M. Bazargan, "Novel integration of wind generator-energy storage systems within microgrids," *IEEE Transactions on Smart Grid*, vol. 3, no. 2, pp. 728–737, 2012.

[37] B. H. Chowdhury, H. T. Ma, and N. Ardeshna, "The challenge of operating wind power plants within a microgrid framework," in *Power and Energy Conference at Illinois (PECI)*, pp. 93–98, 2010.

[38] K. Strunz, E. Abbasi, and D. N. Huu, "Dc microgrid for wind and solar power integration," *IEEE Journal of Emerging and Selected Topics in Power Electronics*, vol. 2, no. 1, pp. 115–126, 2014.

[39] M. Fazeli, G. M. Asher, C. Klumpner, S. Bozhko, L. Yao, and M. Bazargan, "Wind turbine-energy storage control system for delivering constant demand power shared by dfigs through droop characteristics," in *European Conference on Power Electronics and Applications (EPE)*, pp. 1–10, 2009.

[40] A. Junyent-Ferre, E. Prieto-Araujo, O. Gomis-Bellmunt, and F. Bianchi, "Voltage sag ridethrough of pmsg wind turbines using droop control stabilization," in *European Conference on Power Electronics and Applications (EPE)*, pp. 1–8, 2011.

[41] W. Wang, M. Barnes, and O. Marjanovic, "Droop control modelling and analysis of multi-terminal vsc-hvdc for offshore wind farms," in *IET International Conference on AC and DC Power Transmission (ACDC)*, pp. 1–6, 2012.

[42] A. S. Abdel-Khalik, A. M. Massoud, A. A. Elserougi, and S. Ahmed, "Optimum power transmission-based droop control design for multi-terminal hvdc of offshore wind farms," *IEEE Transactions on Power Systems*, vol. 28, no. 3, pp. 3401–3409, 2013.

[43] E. Prieto-Araujo, F. D. Bianchi, A. Junyent-Ferre, and O. Gomis-Bellmunt, "Methodology for droop control dynamic analysis of multiterminal vsc-hvdc grids for offshore wind farms," *IEEE Transactions on Power Delivery*, vol. 26, no. 4, pp. 2476–2485, 2011.

[44] K. V. Vidyanandan and N. Senroy, "Primary frequency regulation by deloaded wind turbines using variable droop," *IEEE Transactions on Power Systems*, vol. 28, no. 2, pp. 837–846, 2013.

[45] A. Buckspan, J. Aho, P. Fleming, Y. Jeong, and L. Pao, "Combining droop curve concepts with control systems for wind turbine active power control," in *IEEE Power Electrics and Machines in Wind Applications (PEMWA)*, pp. 1–8, 2012.

[46] G. Diaz, A. M. A. el Motaleb, and V. Mier, "On the capacity factor of distributed wind generation in droop-regulated microgrids," *IEEE Transactions on Power Systems*, vol. 28, no. 2, pp. 1738–1746, 2013.

[47] J. Chen, J. Chen, R. Chen, X. Zhang, and C. Gong, "Decoupling control of the non-grid-connected wind power system with the droop strategy based on a dc microgrid," in *World Non-Grid-Connected Wind Power and Energy Conference (WNWEC)*, pp. 1–6, 2009.

[48] T. Goya, E. Omina, Y. Kinjyo, T. Senjyu, A. Yona, N. Urasaki, and T. Funabashi, "Frequency control in isolated island by using parallel operated battery systems

applying h-infinity control theory based on droop characteristics," *IET Renewable Power Generation*, vol. 5, no. 2, pp. 160–166, 2011.

[49] L. Wu and D. Infield, "Investigation on the interaction between inertial response and droop control from variable speed wind turbines under changing wind conditions," in *International Universities Power Engineering Conference (UPEC)*, pp. 1–6, 2012.

[50] L. Corradini, A. Costabeber, P. Mattavelli, and S. Saggini, "Parameter-independent time-optimal digital control for point-of-load converters," *IEEE Transactions on Power Electronics*, vol. 24, no. 10, pp. 2235–2248, 2009.

[51] I. U. Nutkani, P. C. Loh, and F. Blaabjerg, "Cost-prioritized droop schemes for autonomous microgrids," in *IEEE Energy Conversion Congress and Exposition (ECCE)*, pp. 1021–1025, 2013.

[52] N. C. Ekneligoda and W. W. Weaver, "Optimal transient control of microgrids using a game theoretic approach," in *IEEE Energy Conversion Congress and Exposition (ECCE)*, pp. 935–942, 2011.

[53] W. W. Weaver, "Dynamic energy resource control of power electronics in local area power networks," *IEEE Transactions on Power Electronics*, vol. 26, no. 3, pp. 852–859, 2011.

[54] K. Yao, K. Lee, M. Xu, and F. C. Lee, "Optimal design of the active droop control method for the transient response," in *IEEE Applied Power Electronics Conference and Exposition (APEC)*, pp. 718–723, 2003.

[55] R. Eriksson, J. Beerten, M. Ghandhari, and R. Belmens, "Optimizing dc voltage droop settings for ac/dc system interactions," *IEEE Transactions on Power Delivery*, vol. 29, no. 1, pp. 362–369, 2014.

[56] E. Rokrok and M. E. H. Golshan, "Adaptive voltage droop scheme for voltage source converters in an islanded multibus microgrid," *IET Generation, Transmission and Distribution*, vol. 4, no. 5, pp. 562–578, 2010.

[57] B. Banerjee and W. W. Weaver, "Geometric manifold control of power electronics in dc microgrids," in *IEEE Workshop on Control and Modeling for Power Electronics (COMPEL)*, pp. 1–8, 2012.

[58] K. J. Bunker and W. W. Weaver, "Optimization of grid-connected wind and battery energy storage system," in *IEEE Power and Energy Conference at Illinois (PECI)*, pp. 1–6, 2014.

[59] T. Markvart, "Microgrids: Power systems for the 21st century?," *Refocus*, vol. 7, no. 4, pp. 44,46,48, 2006.

[60] S. Mizani and A. Yazdani, "Design and operation of a remote microgrid," in *IEEE Conference on Industrial Electronics (IECON)*, pp. 4299–4304, 2009.

[61] F. Katiraei and C. Abbey, "Diesel plant sizing and performance analysis of a remote wind-diesel microgrid," in *IEEE Power Engineering Society (PES) General Meeting*, pp. 1–8, 2007.

[62] R. Langella, G. Margiotta, D. Proto, and A. Testa, "Hybrid pv-diesel stand-along system sizing for remote microgrids," in *IEEE International Energy Conference and Exhibition (ENERGYCON)*, pp. 475–482, 2012.

[63] M. Arriaga, C. A. Canizares, and M. Kazerani, "Renewable energy alternatives for remote communities in northern ontario, canada," *IEEE Transactions on Sustainable Energy*, vol. 4, no. 3, pp. 661–670, 2013.

[64] C. Nayar, M. Tang, and W. Suponthana, "Wind/pv/diesel micro grid system implemented in remote islands in the republic of maldives," in *IEEE International Conference on Sustainable Energy Technologies (ICSET)*, pp. 1076–1080, 2008.

[65] L. D. Watson and J. W. Kimball, "Frequency regulation of a microgrid using solar power," in *IEEE Applied Power Electronics Conference and Exposition (APEC)*, pp. 321–326, 2011.

[66] K. J. Bunker and W. W. Weaver, "Microgrid frequency regulation using wind turbine controls," in *IEEE Power and Energy Conference at Illinois (PECI)*, pp. 1–6, 2014.

[67] P. Asmus, "Microgrids, virtual power plants and our distributed energy future," *The Electricity Journal*, vol. 23, no. 10, pp. 72–82, 2010.

[68] R. Majumder, "Some aspects of stability in microgrids," *IEEE Transactions on Power Systems*, vol. 28, no. 3, pp. 3243–3252, 2013.

[69] T. Dragicevic, J. Guerrero, J. C. Vasquez, and D. Skrlec, "Supervisory control of an adaptive-droop regulated dc microgrid with battery management capability," *IEEE Transactions on Power Electronics*, vol. 29, no. 2, pp. 695–706, 2014.

[70] H. Liu, Y. Chen, S. Li, and Y. Hou, "Improved droop control of isolated microgrid with virtual impedance," in *IEEE Power and Energy Society General Meeting (PES)*, pp. 1–5, 2013.

[71] M. D. Johnson and R. A. Ducey, "Overview of u.s. army microgrid efforts at fixed installations," in *IEEE Power and Energy Society (PES) General Meeting*, pp. 1–2, 2011.

[72] A. G. Skowronska-Kurec, S. T. Eick, and E. T. Kallio, "Demonstration of microgrid technology at a military installation," in *IEEE Power and Energy Society (PES) General Meeting*, 2012.

[73] United States Army Corps of Engineers, *Base camp development in the theater of operations*, 2009.

[74] T. J. Hartranft, F. Yeboah, D. Grady, and R. Ducey, "Proceedings of the 1st army installation energy security and independence conference," in *Army Installation Energy Security and Independence Conference*, pp. 1–28, 2007.

[75] E. Rosenthal, "U.s. military orders less dependence on fossil fuels," *http://www.nytimes.com/2010/10/05/science/earth/05fossil.html*, Oct 2010.

[76] D. S. Eady, S. B. Siegel, R. S. Bell, and S. H. Dicke, "Sustain the mission project: casualty factors for fuel and water resupply convoys," in *Army Environmental Policy Institute*, pp. 1–28, 2007.

[77] M. R. Vallem, D. Jensen, and J. Mitra, "Reliability evaluation and need based storage assessment for surety microgrids," in *North American Power Symposium (NAPS)*, pp. 29–33, 2006.

[78] J. Mitra and M. R. Vallem, "Determination of storage required to meet reliability guarantees on island-capable microgrids with intermittent sources," *IEEE Transactions on Power Systems*, vol. 27, no. 4, pp. 2360–2367, 2012.

[79] P. T. Krein, *Elements of Power Electronics*. New York, NY: Oxford University Press, first ed., 1998.

[80] P. T. Krein, J. Bentsman, R. M. Bass, and B. L. Lesieutre, "On the use of averaging for the analysis of power electronic systems," *IEEE Transactions on Power Electronics*, vol. 5, no. 2, pp. 182–190, 1990.

[81] Z. R. Ivanovic, E. M. Adzic, M. S. Vekic, S. U. Grabic, N. L. Celanovic, and V. A. Katic, "Hil evaluation of power flow control strategies for energy storage connected to smart grid under unbalanced conditions," *IEEE Transactions on Power Electronics*, vol. 27, pp. 4699–4710, Nov 2012.

[82] N. Yousefpoor, A. Azidehak, S. Bhattacharya, B. Parkhideh, I. Celanovic, and A. Genic, "Real-time hardware-in-the-loop simulation of convertible static

transmission controller for transmission grid management," in *IEEE Workshop on Control and Modeling for Power Electronics*, pp. 1–8, June 2013.

[83] Texas Instruments, "Tms320f28335 controlcard," *http://www.ti.com/tool/tmdscncd28335*, 2014.

[84] W. W. Weaver and G. G. Parker, "Real-time hardware-in-the-loop simulation for optimal dc microgrid control development," in *IEEE Workshop on Control and Modeling for Power Electronics (COMPEL)*, pp. 1–6, 2014.

[85] N. S. Nise, *Control Systems Engineering*. Hoboken, NJ: John Wiley & Sons, 2008.

[86] H. Zhou, T. Bhattacharya, D. Tran, T. S. Siew, and A. M. Khambadkone, "Composite energy storage system involving battery and ultracapacity with dynamic energy management in microgrid applications," *IEEE Transactions on Power Electronics*, vol. 26, no. 3, pp. 923–930, 2011.

[87] Q. Fu, L. Montoya, A. Solanki, A. Nasiri, V. Bhavaraju, T. Abdallah, and D. C. Yu, "Microgrid generation capacity design with renewables and energy storage addressing power quality and surety," *IEEE Transactions on Smart Grid*, vol. 3, no. 4, pp. 2019–2027, 2012.

[88] C. A. Hill, M. C. Such, D. Chen, J. Gonzalez, and W. M. Grady, "Battery energy storage for enabling integration of distributed solar power generation," *IEEE Transactions on Smart Grid*, vol. 3, no. 2, pp. 850–857, 2012.

[89] M. Lu, "Combining the wind power generation system with energy storage equipment," *IEEE Transactions on Industry Applications*, vol. 45, no. 6, pp. 2109–2115, 2009.

[90] United States Department of Energy, *FreedomCAR Battery Test Manual for Power-Assist Hybrid Electric Vehicles*, 2008.

[91] ISO New England, "Forecast system demand," *http://www.iso-ne.com*, April 2013.

[92] U.S. Dept. of the Interior, "The pacific network cooperative agricultural weather network," *http://www.usbr.gov/pn/agrimet/webaghrread.html*, April 2013.

[93] WePOWER, "Wepower falcon 12 kw vertical axis wind turbine," *http://www.sierrasolarsystems.com/files/wepowerFALCON12.pdf*, May 2013.

[94] A. P. Sage and C. C. White, *Optimum Systems Control*. Englewood Cliffs, NJ: Prentice-Hall, first ed., 2002.

[95] J. Nocedal and S. J. Wright, *Numerical Optimization*. New York, NY: Springer, 2006.

[96] K. J. Bunker and W. W. Weaver, "Optimal geometric control of dc microgrids," in *IEEE Workshop on Control and Modeling for Power Electronics (COMPEL)*, pp. 1–6, 2014.

[97] N. L. Bowers, H. U. Gerger, J. C. Hickman, D. A. Jones, and C. J. Nesbitt, *Actuarial Mathematics*. Society of Actuaries, 1997.

[98] Z. Hu and X. Wang, "A probabilistic load flow method considering branch outages," *IEEE Transactions on Power Systems*, vol. 21, no. 2, pp. 507–514, 2006.

[99] S. Salcedo-Sanz, C. Casanova-Mateo, J. Munoz-Mari, and G. Camps-Valls, "Prediction of daily global solar irradiation using temporal gaussian processes," *IEEE Geoscience and Remote Sensing Letters*, vol. 11, no. 11, pp. 1936–1940, 2014.

[100] K. M. Trautz, P. P. Jenkins, R. J. Walters, D. Scheiman, R. Hoheisel, R. Tatavarti, R. Chan, H. Miyamoto, J. G. J. Adams, V. C. Elarde, and J. Grimsley, "Mobile solar power," *IEEE Journal of Photovoltaics*, vol. 3, no. 1, pp. 535–541, 2013.

[101] J. Tyner, M. Coates, D. Holloway, K. Goldsmith, C. Daniels, T. Vranicar, J. Roling, D. Jensen, A. Mundy, and B. Peterson, "The design of a portable and deployable solar energy system for deployed military applications," in *IEEE Systems and Information Engineering Design Symposium*, pp. 50–53, 2011.

[102] National Renewable Energy Laboratory, "Solar radiation research laboratory historical data," *http://www.nrel.gov/midc/srrl_bms/*, June 2014.

[103] D. G. Cacuci, *Sensitivity and Uncertainty Analysis Theory, Volume I*. Boca Raton, FL: Chapman & Hall/CRC, first ed., 2003.

[104] R. Krishnan and A. S. Bharadwaj, "A review of parameter sensitivity and adaptation in indirect vector controlled induction motor drive systems," *IEEE Transactions on Power Electronics*, vol. 6, no. 4, pp. 695–703, 1991.

Appendix A

Simulation Materials for Military Patrol Base Example

A.1 MATLAB Script

This section includes the MATLAB script for simulating the military PB example using both traditional and optimal high dimension droop control.

```
%% Initialize workspace
clc
clear all;
close all;

%% Parameters and Initial Conditions

% Source 1
Vref_1   = 300;
Rdroop_1 = 2.5;
kp1      = 1;
```

```
ki1      = 10;
xo1      = 0;

L1       = 0.001;
R1       = 0.1;

% Source 2
Vref_2   = 300;
Rdroop_2 = 0.4;
kp2      = 0.01;
ki2      = 0.3;
xo2      = 0.1;

L2       = 0.002;
R2       = 0.2;

% Source 3
Vref_3   = 294;
Rdroop_3 = 1;

L3       = 0.001;
R3       = 0.1;

% Load
C       = 0.001;

% Find changing load from FOB model
[tier1,tier2,tier3] = FOBload;

% Sum three tiers, convert from kW to W
Pload = 1000*(tier1+tier2+tier3);

% Choose start and end time for simulation
starts = 1;
stops = 1450;

minute =starts:stops;

solar = importfile('20120601.csv',starts,stops);

load(1:9) = 4000;
load(10:1450) = Pload;

% initial conditions
i1_o   =0;
i2_o   =0;
vbus_o =0;
x0     =0.1;

%% Open simulink model
open('ThreeNode_17Jun.slx')
```

```
%% Simulate model
sim ('ThreeNode_17Jun.slx',[starts,stops])
    t    = ScopeData.time;
    i1   = ScopeData.signals(1).values;
    i2   = ScopeData.signals(2).values;
    iload= ScopeData.signals(3).values;
    i3   = ScopeData.signals(4).values;

    v1   = ScopeData1.signals(1).values;
    v2   = ScopeData1.signals(2).values;
    vbus = ScopeData1.signals(3).values;
    v3   = ScopeData1.signals(4).values;

    p1   = ScopeData2.signals(1).values;
    p2   = ScopeData2.signals(2).values;
    pload= ScopeData2.signals(3).values;
    p3   = ScopeData2.signals(4).values;

    pa   = ScopeData3.signals(3).values;

%% Open simulink model
open('ThreeNode_Opt_17Jun.slx')

%% Simulate model
sim ('ThreeNode_Opt_17Jun.slx',[starts,stops])
    ot    = ScopeData.time;
    oi1   = ScopeData.signals(1).values;
    oi2   = ScopeData.signals(2).values;
    oiload= ScopeData.signals(3).values;
    oi3   = ScopeData.signals(4).values;

    ov1   = ScopeData1.signals(1).values;
    ov2   = ScopeData1.signals(2).values;
    ovbus = ScopeData1.signals(3).values;
    ov3   = ScopeData1.signals(4).values;

    op1   = ScopeData2.signals(1).values;
    op2   = ScopeData2.signals(2).values;
    opload= ScopeData2.signals(3).values;
    op3   = ScopeData2.signals(4).values;

    owind = ScopeData3.signals(2).values;

    oiref = ScopeData4.signals(2).values;


%% Plot Simulation Results
m2 = length(t);
m1 = (length(t)/1440)*10;
```

```
om2 = length(ot);
om1 = (length(ot)/1440)*10;

% Plot source power for traditional droop
figure;
        plot(t(m1:m2)-10, p1(m1:m2), t(m1:m2)-10, p2(m1:m2), ...
            '-.', t(m1:m2)-10, p3(m1:m2), '--','LineWidth',3);
            ylabel('Power (W)');
            grid on
            legend('p_1','p_2','p_3')
            axis([starts stops -2000 6500])
            xlabel('Time (min)');

% Plot source power for optimal high dimension droop
figure;
        plot(ot(om1:om2)-10, op1(om1:om2), ot(om1:om2)-10, ...
            op2(om1:om2), '-.', ot(om1:om2)-10, ...
            op3(om1:om2), '--','LineWidth',3);
            ylabel('Power (W)');
            grid on
            legend('p_1','p_2','p_3')
            axis([starts stops -2000 6500])
            xlabel('Time (min)');

% Plot bus voltage for both simulations
figure;
        plot(t(m1:m2)-10, vbus(m1:m2), ot(om1:om2)-10, ...
            ovbus(om1:om2), '--','LineWidth',3);
            ylabel('Bus Voltage (V)');
            grid on
            legend('Traditional','Optimal 3D')
            axis([starts stops 290 300])
            xlabel('Time (min)');

% Plot solar and load power profiles
figure;
subplot(2,1,1)
    plot(minute,solar,'LineWidth',3)
    grid on
    ylabel('Power (W)')
    title('(a) Power Available from Solar Resource')
    axis([starts stops 0 5000])
subplot(2,1,2)
    plot(minute,load,'LineWidth',3)
    grid on
    ylabel('Power (W)')
    title('(b) Load Power')
    xlabel('Time (min)')
    axis([starts stops 4000 7000])

% Plot solar power available, and source 1 power for both simulations
```

```
figure;
plot(t,p1,ot,op1,minute,solar,'--','LineWidth',3)
    grid on
    ylabel('Power (W)')
    xlabel('Time (min)')
    axis([starts stops 0 5000])
```

A.2 Simulink Model

This section includes the MATLAB Simulink model for the military PB example using optimal high dimension droop control. The Simulink model using traditional droop control is very similar, but implements linear droop control for source 1, as it is implemented here for sources 2 and 3.

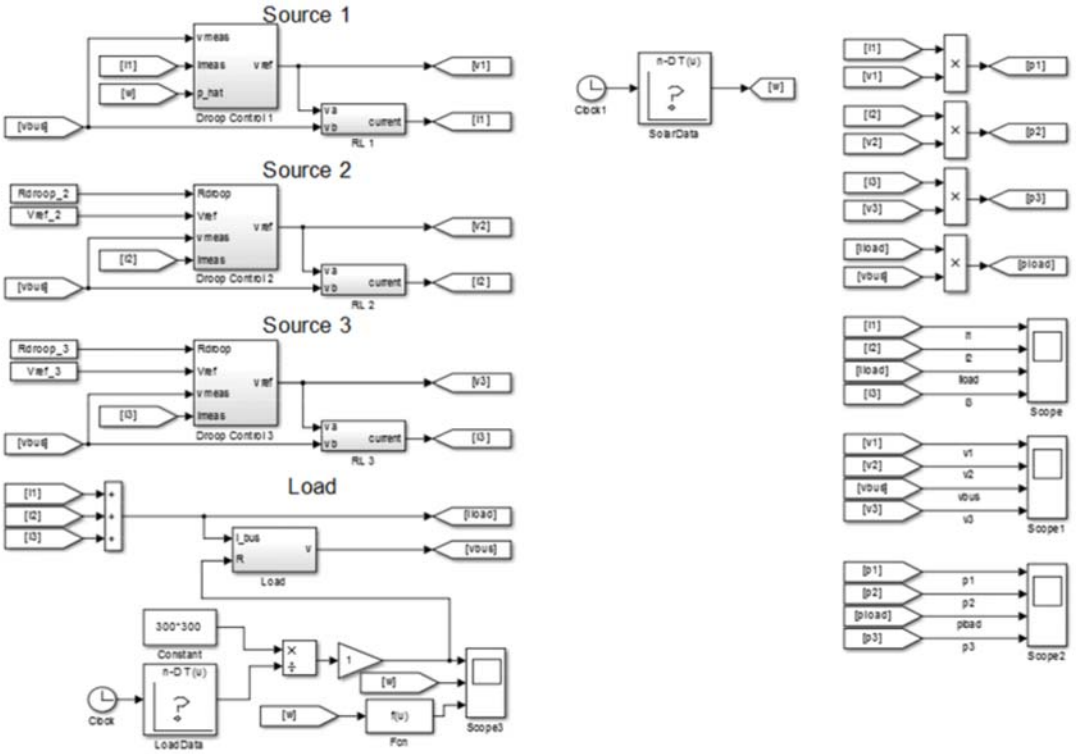

Figure A.1: Simulink model for military PB microgrid, implementing optimal high dimension droop control.